T.C

ISTANBUL AYDIN UNIVERSITY

INSTITUTE OF GRADUATE STUDIES

BALLISTIC MISSILE DEFENSE SYSTEMS

MASTER'S THESIS

Alfateh Mokhtar AHMED

Department of Electrical and Electronics Engineering

Electrical and Electronics Engineering Program

FEBRUARY, 2022

T.C

ISTANBUL AYDIN UNIVERSITY

INSTITUTE OF GRADUATE STUDIES

BALLISTIC MISSILE DEFENCE SYSTEM

MASTER'S THESIS

Alfateh Mokhtar AHMED

(Y1913.300031)

Department of Electrical and Electronics Engineering

Electrical and Electronics Engineering Program

Thesis Advisor: Assist. Prof. Dr. Necip Gökhan KASAPOĞLU

FEBRUARY, 2022

APPROVAL PAGE

DECLARATION

I hereby declare with respect that the study “Ballistic Missile Defense Systems Name”, which I submitted as a Master thesis, is written without any assistance in violation of scientific ethics and traditions in all the processes from the project phase to the conclusion of the thesis and that the works I have benefited are from those shown in the Bibliography. (20.03.2022)

Alfateh Mokhtar AHMED

FOREWORD

(أَلَمْ تَرَوْا أَنَّ اللَّهَ سَخَّرَ لَكُمْ مَا فِي السَّمَاوَاتِ وَمَا فِي الْأَرْضِ وَأَسْبَغَ عَلَيْكُمْ نِعَمَهُ ظَاهِرَةً وَبَاطِنَةً وَمِنَ النَّاسِ مَنْ يُجَادِلُ فِي اللَّهِ بِغَيْرِ عِلْمٍ وَلَا هُدًى وَلَا كِتَابٍ مُنِيرٍ) لقمان (20)

To my brothers, sisters and friends whom I have accompanied along the long path of my life and were the blessed spirits and the towering statures and the souls that have almost reached the apex of perfection.

إلى الرجال الذين إذا عاهدوا لم يغدروا لأنهم يعرفون أن «العهد كان مسؤولاً»

وإذا أعطوا ميثاقاً لم ينقضوا لأنهم يعرفون أنه «ميثاقاً غليظاً»

وإذا أخذوا قلباً لم يعبثوا به لأنهم يعرفون أن الله أمر أن «تؤدي الأمانات إلى أهلها»

To those men who don't betray their thrown pacts, as they honor their accountable pledges.

For those who don't rescind their own covenants, as they know it is a solemn commitment.

And for those who don't mess around with hearts that entrusted them, as they are aware that Allah commands to render trusts to whom they are destined.

To those whom I have accompanied in Bosnia, Turkey and in my beloved country Sudan.

I dedicate this humble work To my benevolent family, to the souls of my Mother & Father, to my brothers, sister and my relatives, for their endurance during my absence over the past years special thanks to Dr.Ahmet Salih Kansu for his continuous support over the past years, as well as to the Sudanese Military Institution.

To all those who lend their support during my study time Dr. Halit Eren, Mr. Osama Qutb, Mr. Yakup Çaymazoğlu, Mr. Muhannad F. Hassan, Mr. Abd Elrahman El Ashmawy and Mr. Hicham Gazi Ahmed, Allah SWT bless you all.

Special thanks to my mentor and advisor Professor. Dr.Necip Gökhan KASAPOĞLU, the great man who stood behind the success of this project,

Last but not least, to the golden man of all times, Dr. Elfatih Hassanein, may Allah SWT bless your soul wherever it lands.

Finally; to all those mentioned above, and the rest whom I apologized for not being mentioned here, your valuable efforts and competent services is well acknowledge and appreciated, may Allah SWT reward you all and help us to keep-up the path of goodness.

Blessings up on you all.

February, 2022 Alfateh Mokhtar AHMED

BALLISTIC MISSILE DEFENSE SYSTEMS

ABSTRACT

A successful Guidance, Navigation, and Control (GNC) system for ballistics defence system is critical to a target tracking scenario's success. This thesis applies a GNC system and compares it to state-of-the-art systems that are extensively used today. The work contains an autopilot, guiding law, target tracking law, and a dependable inertial navigation system capable of precisely operating an agile vehicle such as a UAV, missile, or other vehicle utilizing available sensor data. The GNC system is simulated using a non-linear generic missile model in a MATLAB/Simulink environment.

The control system is the first component of the GNC system to be examined. Two types of autopilots are contemplated: The commonly used three-loop autopilot is the initial design. The autopilot determines the ideal missile fin deflections to travel towards a target based on the guidance system's intended acceleration directives. The second configuration utilizes two decoupled autopilots for lateral and longitudinal control, with course and flight-path-angle serving as reference commands. Fin deflections are generated to achieve the required missile orientation using a Linear-Quadratic Regulator (LQR) based on the linearized generic missile model. By incorporating extra input from sideslip and angle-of-attack derivatives, performance and resilience features are increased.

The navigation system is the second component of the GNC system to be explored. Without trustworthy sensors and filters, other control loop subsystems will lose track of the vehicle's Position, Velocity, and Attitude (PVA). To achieve vehicle state convergence, a Multiplicative Extended Kalman Filter (MEKF) supported by Global Navigation Satellite Systems (GNSS) and gyro and acceleration biases is generated. The MEKF is distinguished from the regular Extended Kalman Filter (EKF) by the fact that it updates the Inertial Navigation System (INS) attitude calculations through quaternion multiplication, resulting in the inclusion of the

multiplicative property. When calculating guiding instructions in a target-tracking situation, it is critical to have information about the target's location, velocity, and, in certain circumstances, acceleration. Along with the INS-provided estimated missile states, a target-tracking Kalman Filter (KF) is used to monitor the relative states of the target and missile.

Finally, two guideline laws are compared to finalize the GNC design. The well-known Proportional Navigation (PN) rule is compared to a Line-Of-Sight (LOS) system with a course and flightpath-angle controlled autopilot. By assuming independent control of the horizontal and vertical planes, LOS guidance aims to steer the missile toward a vector connecting the launch platform and the predicted point of interception between the missile and target.

Simulink simulations of the GNC system provide encouraging results in both reference tracking for the autopilot and state estimation utilizing both KF designs.

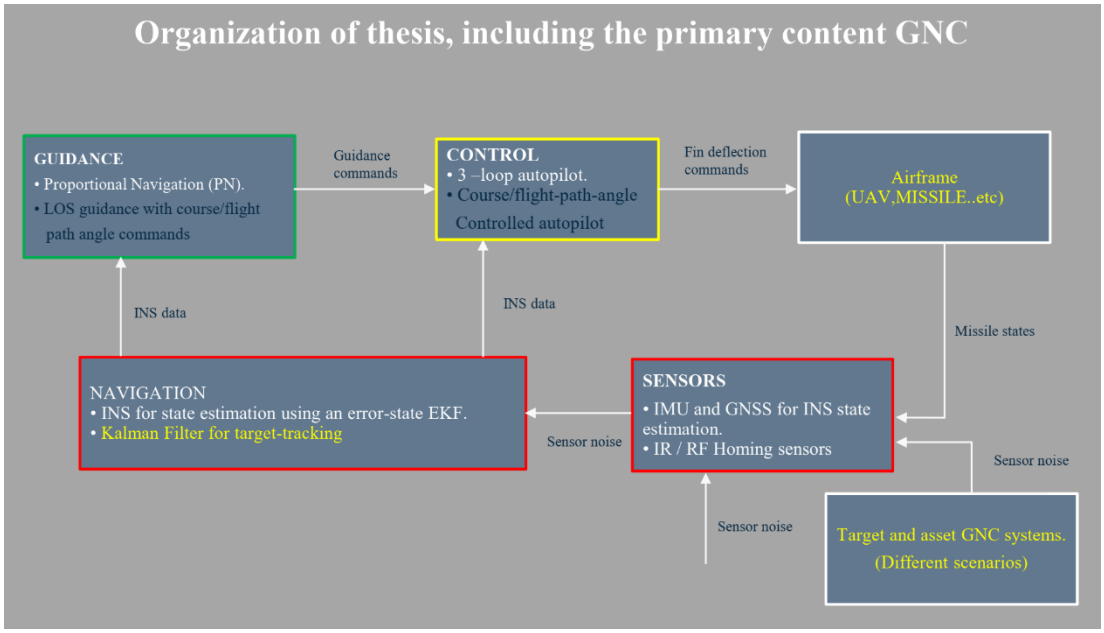

Figure 1 Organization of thesis, including the primary content Guidance, Navigation and Control (GNC)

Keywords: Ballistic Missiles trajectory Intercept Phases, The Phase Intercept, Kalman Filter, Line-Of-Sight, Guidance, Navigation and Control, Global Navigation Satellite Systems, Proportional Navigation.

BALİSTİK FÜZE SAVUNMA SİSTEMLERİ

ÖZET

Balistik savunma sistemi için başarılı bir Güdüm, Seyrüsefer ve Kontrol (GNC) sistemi, bir hedef izleme senaryosunun başarısı için kritik öneme sahiptir. Bu tezde bir GNC sistemini uygulanmakta ve önerilen sistem günümüzde yaygın olarak kullanılan son teknoloji sistemlerle karşılaştırmaktadır. Çalışma, bir otopilot, kılavuz yasa, hedef izleme yasası ve mevcut sensör verilerini kullanan bir İHA, füze veya diğer araçlar gibi çevik bir aracı hassas bir şekilde çalıştırabilen güvenilir bir atalet navigasyon sistemi içerir. GNC sistemi, MATLAB/Simulink ortamında doğrusal olmayan bir genel füze modeli kullanılarak simüle edilmektedir.

Kontrol sistemi, GNC sisteminin incelenecek ilk bileşenidir. İki tip otopilot göz önünde bulundurulur: Yaygın olarak kullanılan üç zamanlı otopilot ilk tasarımdır. otomatik pilot güdüm sisteminin amaçlanan hızlanma direktiflerine dayalı olarak bir hedefe doğru hareket etmek için ideal füze kanatçık sapmalarını belirler. İkinci konfigürasyon, yanal ve boylamsal kontrol için, rota ve uçuş yolu açısı referans komutları olarak hizmet veren iki özel otopilot kullanır. Doğrusallaştırılmış bir jenerik füze modeline dayalı bir Doğrusal-Kuadratik Düzenleyici (LQR) kullanılarak, gerekli füze yönelimini elde etmek için kanat sapmaları oluşturulur. Yan kayma ve hücum açısı türevlerinden ekstra girdi dahil edilerek performans ve esneklik artırılır.

Navigasyon sistemi, GNC sisteminin keşfedilecek ikinci bileşenidir. Güvenilir sensörler ve filtreler olmadan, diğer kontrol döngüsü alt sistemleri aracın Konumunu, Hızını ve Tutumunu (PVA) takip edemez. Araç durumu yakınsamasını sağlamak için, Küresel Navigasyon Uydu Sistemleri (GNSS) ve cayro ve hızlanma önyargıları tarafından desteklenen bir Çarpımsal Genişletilmiş Kalman Filtresi (MEKF) oluşturulur. MEKF, normal Genişletilmiş Kalman Filtresinden (EKF), Ataletsel Seyrüsefer Sistemi (INS) konum hesaplamalarını kuaterniyon çarpımı yoluyla güncellemesi ve çarpma özelliğinin dahil edilmesini sağlamasıyla ayırt edilir. Bir hedef izleme durumunda yol gösterici talimatları hesaplarken, hedefin konumu, hızı

ve belirli durumlarda ivmesi hakkında bilgi sahibi olmak çok önemlidir. INS tarafından sağlanan tahmini füze durumlarının yanı sıra, hedef ve füzenin göreceli durumlarını izlemek için bir hedef izleme Kalman Filtresi (KF) kullanılır.

Bu tezde GNC tasarımını tamamlamak için iki kılavuz yasa karşılaştırılır. İyi bilinen Orantılı Seyrüsefer (PN) kuralı, seyir ve uçuş yolu açısı kontrollü otomatik pilotlu bir Görüş Hattı (LOS) sistemiyle karşılaştırılır. Yatay ve dikey düzlemlerin bağımsız kontrolünü üstlenerek, LOS rehberliği, füzeyi fırlatma platformunu bağlayan bir vektöre ve füze ile hedef arasındaki öngörülen kesişme noktasına yönlendirmeyi amaçlar.

GNC sisteminin Simulink simülasyonları hem otopilot için referans izlemede hem de her iki KF tasarımını kullanan durum tahmininde başarılı sonuçlar sağlar.

Anahtar Kelimeler: Balistik Füzelerin Yörüngesini Kesişme Aşamaları, Faz Kesişimi, Kalman Filtresi, Görüş Hattı, Güdüm, Seyrüsefer ve Kontrol, Küresel Seyrüsefer Uydu Sistemleri, Oransal Seyrüsefer.

TABLE OF CONTENTS

LIST OF ABBREVIATIONS

BMD	Ballistic Missile Defense
CAD	Computer Aided Design.
CPA	Closest Point of Approach.
DOF	Degrees of Freedom.
ECI	Earth Centered Inertial.
EKF	Extended Kalman Filter.
FOG	Fiber Optic Gyros.
GNC	Guidance, Navigation and Control.
GNSS	Global Navigation Satellite Systems.
IMU	Inertial Measurement Unit.
INS	Inertial Navigation System.
KF	Kalman Filter.
LOS	Line-Of-Sight.
LQR	Linear-Quadratic Regulator.
MEKF	Multiplicative Extended Kalman Filter.
MEMS	Micro Electrical Mechanical Systems.
NED	North East Down.
PN	Proportional Navigation.
PVA	Position, Velocity and Attitude.
RMS	Root Mean Square.
TBMD	Theater Ballistic Missile Defense

LIST OF TABLES

LIST OF FIGURES

I. INTRODUCTION

The goal of this chapter is to offer context and insight into the conditions that led to the need for the formation of a BMD by examining the history of BMD and current national leadership activities that have impacted and will continue to influence the development of the BMDS. This is followed by a short explanation of why legacy systems are incapable of enabling future BMDS growth and why it is important to develop a new BMDS using a system-of-systems strategy.

A. Brief History of Ballistic Missiles Defence

Anti-weapons systems have been around nearly as long as offensive weapons systems. Due to its ability to carry some of the world's most deadly weapons, including nuclear-armed warheads, ballistic missiles have long been seen as one of the most severe dangers to a state's security. As a result, some governments have focused their efforts on developing ballistic missile defense systems, which are defenses against such weapons. However, during the Cold War, when both the US and the Soviet Union experimented with and deployed missile defense systems, both sides expressed concern that such systems might spark an uncontrolled weapons race between the two nations.

In reaction to German V-2 rocket assaults on civilian targets in France and England on September 8, 1944, the search for an anti-ballistic missile defense system started in earnest. Initially, the sole defense against these terror weapons was to find and destroy the launch locations, or to conquer enough land to keep the missiles out of reach of people in heavily populated regions such as big cities. The Germans, on the other hand, simply relocated these weapons to more safe locations and continued to employ them against targets within the operating range of the missile. By the conclusion of the war, around 3000 V-2s had been fired, the majority of which were aimed against London and Antwerp. While these weapons were ineffective tactically, they had far-reaching political and psychological consequences. The V-2 missiles were overpriced to build, the guidance system was imprecise, the missile itself was unstable, and the weapon was

delivered too late in the fight to have a meaningful impact on the result. On the other hand, the V2 was a forerunner of future warfare. With advancements in missile technology, weapons development that included all forms of WMD, and more efficient and cost-effective manufacturing of ballistic missiles, they became an enticing option of bolstering a country's military capabilities without bankrupting the economy. Throughout the Cold War, the threat of nuclear war posed by the exchange of Intercontinental Ballistic Missiles (ICBMs) between the US and the Soviet Union prompted the signing of many arms control treaties placing restrictions on the use of these weapons and their delivery vehicles. These treaties became a vehicle for delivering BMD, since neither side's technology had evolved enough to permit the establishment of a complete, interconnected system capable of countering such a threat. These Cold War-era systems were limited to tracking incoming warheads and attempting to destroy the reentry vehicles (RV) during the end atmospheric reentry phase with a nuclear defensive missile, such as Nike/Zeus in the US case, while also carrying out a nuclear retaliatory strike to prevent further launches. Throughout the Cold War, the notion of mutual assured destruction (MAD) outperformed any real defensive system as a deterrent. With the growth of technology, notably lasers and computers, the Reagan Administration committed to creating a space-based national ballistic missile defense system (BMDS) known as the Strategic Defense Initiative (SDI), dubbed the "Star Wars" program at times. While the 1972 ABM treaty allowed for the development of such a system, it prohibited its testing or deployment. These constraints eliminated the possibility that one side would obtain the advantage of self-defense, rendering the adversary's weaponry useless and so emboldening them to launch an initial offensive confident in their ability to withstand a counter ballistic missile assault. With the Soviet Union's breakup, the prospect of employing ballistic missiles increased. This is mostly due to the Cold War-era proliferation of Theater Ballistic Missiles (TBM) to Soviet client states, the subsequent transfer of technology by former Soviet governments, and the loss of Russia's power control over such client states in order to keep them in line. This is demonstrated by the proliferation of TBMs in Developing World countries such as Iraq and North Korea, which possess Soviet-made missiles and use the acquired technologies to develop indigenous TBMs such as the No Dong I, Taepo Dong I/II, and all SCUD variants that currently threaten the United States and its allies. The first substantial exposure to US forces to a TBM danger occurred during the Desert Storm Operation, when a Patriot missile successfully intercepted the first SCUD. Iraq conducted SCUD

attacks against targets in Saudi Arabia and Israel after the Coalition's air war's commencement. While tactically insignificant, the 88 SCUD missiles launched during the subsequent terror campaign came perilously close to pulling Israel into the conflict, threatening to destabilize the Coalition and alienate Arab nations. Following this campaign, a significant portion of the Department of Defense's focus shifted to countering the ballistic missile threat, resulting in the formation of the Ballistic Missile Defense Organization (BMDO), later renamed MDA, and the Joint Theater Air and Missile Defense Organization (JTAMDO), both of which are tasked with developing a BMDS.

B. Definition of Ballistic Missile Defense (BMD)

The MDA defines BMD as "the capacity to protect the United States, its allies, and friends' troops and territory against all classes and ranges of ballistic missile threats."

The missile flight phase divides the into three phases that correspond stages of a BM trajectory: Boost, Midcourse, and Terminal. Figure

C. Boost Phase

In spite of the fact that boost-phase defenses can intercept ballistic missiles of all ranges, including ICBMs, this phase is the most challenging to engage a missile. One to five minutes is the "window of opportunity" for an intercept. Although the missile's blazing and hot exhaust makes it simpler to recognize and track during the launch phase, interceptors and missile defense sensors must be near to the launch of the missile. Rapid reaction and interception may be possible even before countermeasures have been implemented due to early identification during the launch phase.

D. Midcourse Phase

The midcourse phase of flight occurs when the missile's fuel runs out and it begins to roll toward its target. There are multiple opportunities during this period, which may take up to twenty minutes, to destroy the incoming ballistic missile. Once

it's in the atmosphere, the heat will eat away at any debris that's left behind from the interception. After the intercept, any residual debris will burn up in the atmosphere.

The ground-based Midcourse Defense element was deployed in Alaska and California in order to safeguard the United States against a limited strike by rogue states. This system is only capable of intercepting medium and long-range ballistic missiles. Ships outfitted with interceptor missiles capable of intercepting short- to medium-range ballistic missiles are being used in the Aegis Missile Defense System, which has been tested against a medium-range missile and proved effective. The interceptors use hit-to-kill technology to find and destroy the enemy missile thanks to a complex network of sensors, radars, command, control, combat management, and communications components. Radars placed aboard Aegis cruisers and destroyers, as well as transportable X-band radars, are among the sensors and radars that can be deployed anywhere in the world. We've also built the Sea-Based X-band, the biggest X-band radar in the world, which is mounted on a floating platform and can travel across the seas of the globe with little obstructions. This radar differentiates between actual missiles and countermeasures that may be deployed in conjunction with an enemy missile.

E. Terminal Phase

The terminal phase of the missile is short and begins when it re-enters the atmosphere. It's the last opportunity to stop the warhead before it reaches its target. Because the target is so near, intercepting a warhead at this stage is very difficult and undesired. The Terminal High Altitude Area Defense (THAAD) missile, which is currently being delivered to the United States Army, the Aegis BMD Sea-Based Terminal Defense capability with the SM -2 Block IV missile, and the United States Army's PATRIOT Advanced Capability-3 (PAC -3) missile, which is currently deployed worldwide, are all examples of terminal phase interceptor elements. These mobile gadgets are designed to withstand missiles with a short-to-medium range.

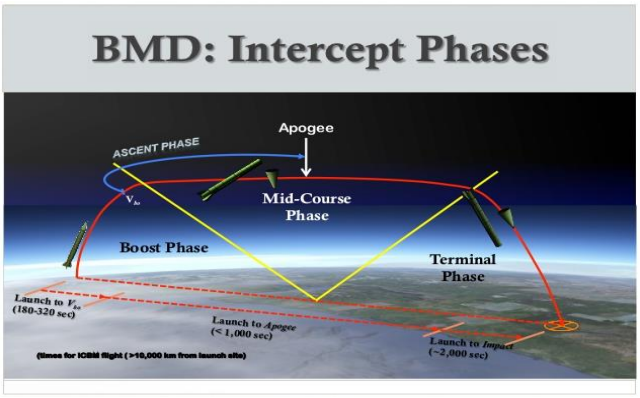

Figure 2 Ballistic Missiles Trajectory Intercept Phases.

The four major categories of ballistic missiles are as follows:

Ballistic missiles with a range of less than 1,000 kilometers (approximately 620 miles).

Ballistic missiles with a range of 1,000–3,000 kilometers (approximately 620-1,860 miles).

Intermediate-range ballistic missiles (IRBMs), which travel between 3,000 and 5,500 kilometers (1,860-3,410 miles), and intercontinental ballistic missiles (ICBMs), which go more than 5,500 kilometers.

Short- and medium-range ballistic missiles are referred to as "theatre" missiles, while intercontinental ballistic missiles or long-range ballistic missiles are referred to as "strategic" missiles.

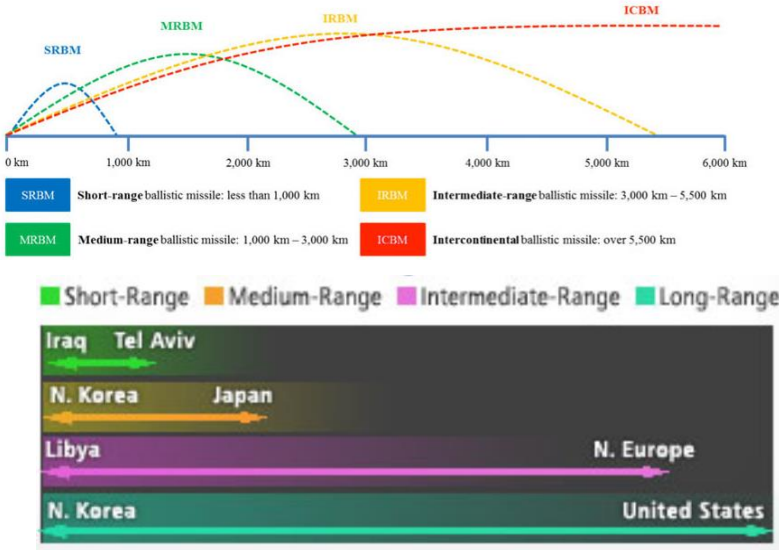

Figure 3 Missile Range and Comparison Distances Classifications.

II. DEFINITION OF THEATER BALLISTIC MISSILE DEFENSE (TBMD)

TBMD refers to the ability of the United States, its military partners, and friends to protect their soldiers, territory, and interests against ballistic missile threats operating in a specific geographical region. It refers to all missile types employed against short-range (SR), medium-range (MR), and intermediate-range (IR) targets within a defined region (500 km-3,500 km).

The ranges are shown in Figure 3, along with samples of each kind of missile.

A. Threat of the Ballistic Missile (BM)

Proliferation of BM has become an important concern in the last two decades. This scenario has emerged as a result of the former Soviet Union selling a major amount of its missile stockpiles and missile technology in an attempt to shore up its faltering economy. Apart from the former Soviet Union, rogue states such as North Korea continue to offer missiles and missile technology to almost anybody willing to pay for the knowledge or weapons. This readiness to sell missiles and technology for financial or political gain (or both) has resulted in the creation of a weapons industry unlike any other.

As a result of this flood of weapons becoming available to rogue states and the proliferation of missile technology from the former Soviet Union to states such as Iran and North Korea, the world has become less secure, and the Western world must step up its efforts to prevent the acquisition of missiles and missile technology.

B. Project Threat Definition

A ballistic missile (BM) is a weapon which has a predetermined trajectory that cannot be considerably changed after the fuel has been used (the trajectory is determined by ballistics laws). To travel great distances, BMs are often launched extremely high into the air or into space; for intercontinental missiles, a suborbital

spaceflight halfway through the mission reaches a height of 1,200 kilometers. Once in orbit, the missile enters freefall when further force is applied.

BMs are not new; countries have used them successfully in battle since World War II. Indeed, Adolf Hitler's Nazi party successfully deployed the V-2 Rocket as a terror weapon throughout the war, launching as many as 3,225 in battle, principally on Antwerp and London." The Iranians and Iraqis traded volleys of missiles during their almost decade-long conflict. Iraq's domestic copy of the Soviet-developed SCUD missile was recently employed against Israel and Saudi Arabia. The fundamental difference between modern weapons and their forefathers is in terms of precision. Today's weapons are highly accurate to within meters, whereas older weapons, specifically the V-2s used against Great Britain during World War II, had a Circular Error Probable (CEP) radius of 12 kilometers (as determined by accuracy analysis data based on the number of missiles launched, their intended targets, and the impact distance from the intended target). Numerous missiles are available on the global armaments market, but the BM is the most lethal of them all, owing to the catastrophic consequences of the different payloads this weapon is capable of delivering. While conventional payloads were effective in previous conflicts (the Gulf War, the Iran/Iraq War, and World War II, respectively), they caused relatively little physical damage in comparison to the psychological terror ballistic missiles inflicted on the populations they targeted, most notably Israel in the 1991 Gulf War.

III. BALLISTIC MISSILE DEFENSE

Unsurprisingly, the bulk of discussions on Ballistic Missile Defense (BMD) center on national missile defense, since this was the subject of both the ABM Treaty and the two earlier US missile defense debates in the late 1960s and early 1980s. Nonetheless, between 1994 and 2000, the financial emphasis was on theater-missile defense, with spending on NMD being two to three times what was spent on theater-missile defense.

This is because ballistic missile proliferation is mainly concerned with short- and medium-range missiles, which represent a threat to US soldiers stationed overseas and to US allies. Additionally, talks focused on the distinction between theater and national defense systems under the ABM Treaty, culminating in the 1997 TMD Demarcation Accords.

Despite growing interest in national missile defense, theatre-missile defense is vital since the threat exists, extended deterrence is likely to be less successful than homeland deterrence, and US conventional counterforce attacks on mobile theater-range missiles are ineffective. Thus, theater-missile defense reduces the risks associated with US regional participation and reassures US allies. As a consequence, several regional powers place a higher premium on US theater defenses than on US national defenses. For example, despite Beijing's fierce opposition to both, China is more concerned about US TMD cooperation with Taiwan than with NMD deployments in Alaska.

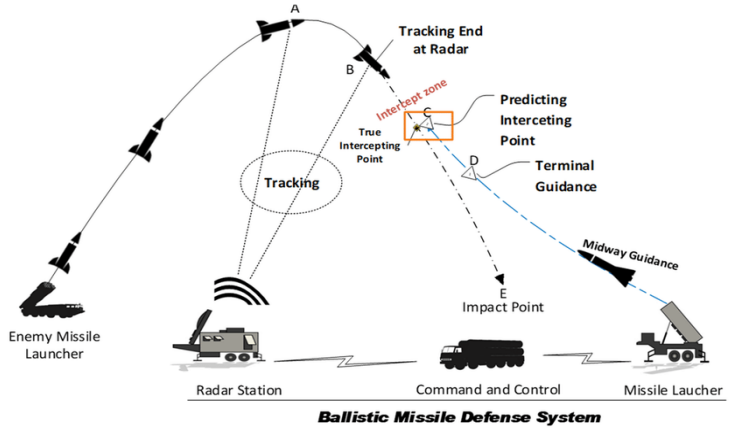

Figure 4 Ballistic Missile Defense System.

A. Interception of the Boost Phase

Concerns regarding the broad distribution of submunitions and the separation of decoys from real warheads delivered early in the midcourse phase led the investigation of intercepting TBMS during the boost phase. BPI would address this issue by destroying the adversary's ballistic missile during its initial launch phase, forcing the deadly payload and engagement debris to fall back on the aggressor. Due to the fact that boost phase defences stop a missile before to its payload being released, BPI seems to be the sole method of defending against submunitions. A benefit of the boost-phase defence is that at launch, the missile's rocket motors emit hot gases that are easy to detect; however, the engines only fire for a few minutes. The difficulty with BPI is detecting the launch of the missile, tracking it long enough to get a fix on its course, and then intercepting it. All of this must be accomplished in a short amount of time. The successful development of a BPI would significantly alleviate the load associated with relying exclusively on current terminal defences to fight TBMS.

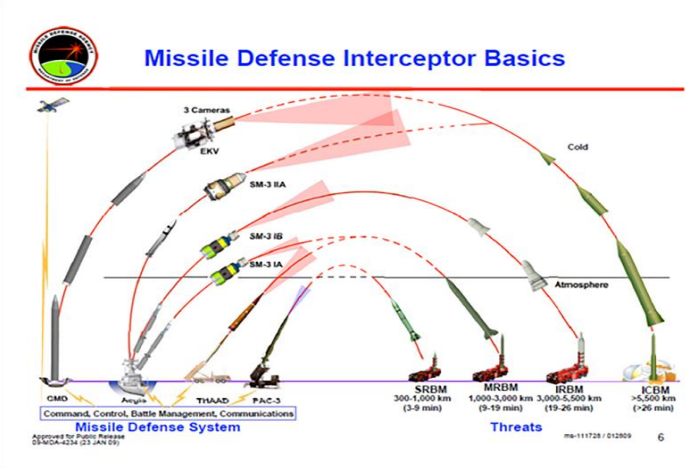

Figure 5 Missile Defence Interceptor Basics.

IV. TECHNIQUES AND PRACTICES FOR SENSOR FUSION

A. Tracking Fundamentals

An important foundational component of any approach of sensor fusion is the tracking mechanism associated with each of the sensors on the platform. Track start, track maintenance, drop track criteria, and false track management are all aspects of tracking. Data fusion depends on how the raw data is combined within the processors and mission computer, among other things. For the sake of this article, we'll be focusing on the algorithms required for track "maintenance" rather than the criteria for initiating or dropping tracks.

B. Sensors and Information Sources

1. Sensors

A successful layered defence employs a variety of sensors to identify and track threatening missiles as they fly. Satellites and a variety of land- and sea-based radars provide global sensor coverage.

In an ideal world, all potential threats and outcomes of an encounter could be assessed before the first shot is fired. Of course, the fineness of fusion information presented to decision-makers is limited by the sensors and data sources utilized as input. The kinds of Sensor are as varied as the platforms on which they are mounted. Radar units can be classified by their purpose, type, low/high frequency operation, scanning, and pulse repetition rate, among other criteria. Electronic Surveillance Measures systems differ in their ability to differentiate signal features, estimate angle of arrival, and identify signals. Sensors and sources supplied raw and preprocessed data to fusion systems, which process it in Sensor Fusion. Waltz and Llinas provide the following definitions.

- Sensors are devices that allow for the detection and quantification of physical phenomena. The word "remote sensing" refers to a sensor that detects a certain occurrence conveyed across a media, such as an ESM system.

- Sources refer to a variety of data sources, including observations, intercepted communications, or other data, a previous information as well as map data (terrain, roads, cities, lakes, and rivers), sea lanes, and air paths, like other archived data such as the OOB/EOB, the ATO/SPINS/ROE, and intelligence data.
- The term "connections" refers to the communication and interconnection between sensors and data sources, as well as the nodes that process the fusion of data.

2. Detection and sensors tracking

Detection and Follow-up Sensors detect the presence of signals and their characteristics. There is big difference between Sensors and tracking.

Sensor data: is signal processed to provide a measurement for the current time of measurement. *Tracking:* is the result of processing measurements to determine the current state of the target. The state estimation may include the kinematics and the properties of the target. Bar-Shalom defines measurements as "observations of the target that are often tainted by noise caused by the processing sensor or signal transmission medium." The properties of the measurement are dependent on the kind of sensor utilized. For instance, a three-dimensional radar would instantly calculate the target's range, azimuth, and elevation (relative to the sensor). A two-dimensional radar would determine the target's range and azimuth. Not only would a passive system, such as an ESM system, detect the direction of arrival (DOA), but also a variety of signal properties (such as signal strength, frequency, and pulse repetition frequency). The noise in the measurements is a result of process uncertainties, such as false alarm detection, signal jamming, additional targets, and deception/countermeasure detection. This article will outline the criteria for initiating and terminating a trace.

C. Algorithms for Tracking

1. The batch processing at the beginning

Many methods have already been used for this basic case of tracking a stationary object. The strategy is to collect a large number of hits on the target and then batch analyse the data to create a track. The more hits collected in batch processing, the better the response. However, as the number of hits increases, the computational requirements

also increase, making batch processing impractical for most surveillance systems. Each time a new measurement is taken, the previous measurements are used to calculate the current state, making batch processing very inefficient.

2. Methods of prediction-correction

A benefit of prediction-correction or recursive approaches is that state updates are completely dependent on the prior state and present measurement. Hutchins notes that although the simplest trackers are optimized for rectilinear motion (SLM), target accelerations may be accommodated by raising the gain of the philtre or the noise component in the state equations. The most sophisticated trackers are capable of adapting to rotational motion, considering numerous hypotheses for target motion, and filtering out noise. Combining tracker types enables the tracking of a large number of sensors, various targets, and data mapping.

a. Tracker Alpha-Beta

The simplest constant gain tracking algorithm is the alpha-beta tracker. Although the tracker performs poorly, it consumes relatively few computational resources. In this case, the equation to update the target position is established using a constant gain matrix. The alpha-beta tracker is applied in tracking systems that have access to status measurement updates and a state vector containing placement and velocities. The gain is preset to handle rectilinear or rotational movement. When the gain is increased to compensate for rotational motion within a target, performance suffers slightly for rectilinear movement. This is valid for a large number of the trackers discussed in the following sections. The alpha-beta gamma tracker is a variant of the alpha-beta method that incorporates accelerations into a single state vector.

b. Constant Gain Kalman Filter (CGKF)

The constant-gain Kalman filter (CGKF) is a shortened form of the Kalman filter. In instead of updating the covariance matrix every time a measurement is changed, the covariance is considered to be constant. It is possible to solve numerically the algebraic Riccati equation associated with the linear, time-invariant discrete time system if the covariance matrix approaches a constant value over time. In this example, the constant covariance and constant Kalman gain values may be calculated using MATLAB's dlge (discrete temporal linear quadratic estimation) function. As a result, the Kalman update

equations are solely dependent on the prior condition, the measurement, and the constant gain. Although the CGKF is not the best answer, it is not computationally intensive.

c. Kaplan Filter (KF)

The Kalman filter (KF) forms the base for much more sophisticated algorithms. The Kalman filter is an optimal resolution to the sequential least squares problem in the sense that it minimizes the least squares error. It is a sequential method in the sense that it requires only the last measurement and the last state estimate, as well as the associated covariance matrices. Although the Kalman filter is not very computationally intensive, it is not suitable for moving targets, clutter, or numerous targets. The filter can be modified to account for moving targets, but the solution will be less optimal. See the Results section for examples of this phenomenon.

d. Extended Kalman Filter (EKF)

The extended Kalman filter (EKF) is used when the coordinate mapping is non-linear. The EKF is particularly useful when the measurement method is nonlinear or when the target dynamics are nonlinear. According to Bar-Shalom, nonlinear transformations can introduce bias into the solution, the covariance calculation is not always accurate, and the EKF can diverge if the initial conditions are incorrect.

e. Interaction Multiple Models (IMM)

To forecast the present state of the target, the Tracker Interacting Multiple Models is employed. Models such as SLM (straight-line motion), left turn, and right turn may be employed if the target is predicted to move. Alternatively, multiple models can be used for turning speed or climb and descent. The number of models used depends on the application. Two models of IMM are employed in this study, with the sole difference between them being the noise term (one for SLM and one for rotational motion). Several equations of state are used to explain the many modes of operation of the IMM estimator. How likely is it that the target is in one of these modes is determined by a Markov transition matrix. Typically, these values are selected based on heuristics. When it comes to the two-model IMM applied in this work, the following likelihoods were chosen: (1) 10% probability of the target turning if it was in SLM mode at the time of measurement, and (2) 33% probability of the target returning to SLM mode if it was in a turn at the time of mensuration. Identical to the "soft switching" described in an Air Force Research Laboratory study, the model likelihoods are changed with every new

mensuration and the outcoming weighting factors are applied to calculate the status. That is, the tracker does not need a gating decision to work effectively. See chapter IV for a detailed explanation of the method.

V. ELEMENT OF BALLISTIC MISSILE DEFENSE SYSTEM

The Ballistic Missile Defense System (BMDS) is a sophisticated network of interconnected components and aiding activities. The combination of these numerous components provides a strong, coated defense capable of defeating an enemy missile in all stages of flight.

Ballistic missile trajectories are generally splitted into three stages of flight: boost, midcourse, and Terminal Phase. Every component is critical to building a strong system capable of defending against enemy missiles at any phase of flight.

A successful layered defence employs a variety of sensors to identify and track threatening missiles as they fly. Satellites and a variety of land- and sea-based radars provide global sensor covering.

A. Tracking and Identifying Targets

1. Long-Range Discrimination Radar (LRDR)

The Missile Defence Agency is committed to building and deploying the Long-Range Discrimination Radar (LRDR) as requested by Congress in Pecuniary Years 2014 and 2016. The LRDR will be a component of the United States' layered Missile Defence System (MDS), whose essential goal is to continuously and accurately monitor and discriminate missile threats to the US. Discrimination is an essential feature of missile defence because it provides data that allows lethal objects to be separated from debris and decoys in the vicinity of the lethal object. The LRDR integrates with the MDS command and control system and helps assess incoming threats so that MDS weapons can be more effectively activated to intercept them.

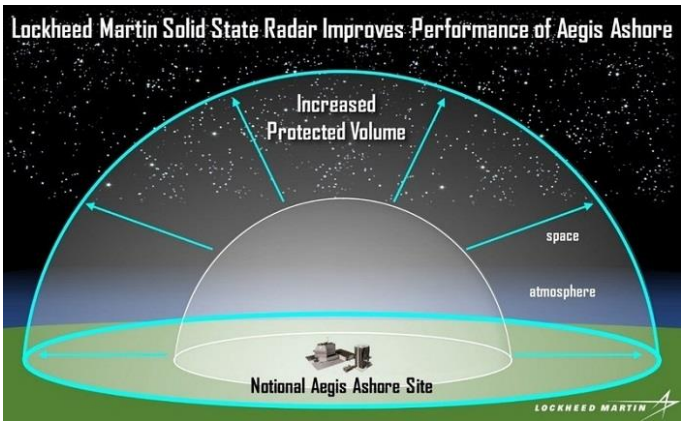

Figure 6 Long-Range Discrimination Radar (LRDR).

Figure 7 Long-Range Discrimination Radar (LRDR).

2. Homeland Defense Radar Hawaii (HDR-H)

The Pecuniary Year (FY) 2017 National Defense Authorization Act (NDAA) directs the Missile Defense Agency (MDA) to develop a strategy for procuring a discriminating radar or similar sensor for a site that would enhance homeland missile defense for the defense of Hawaii.

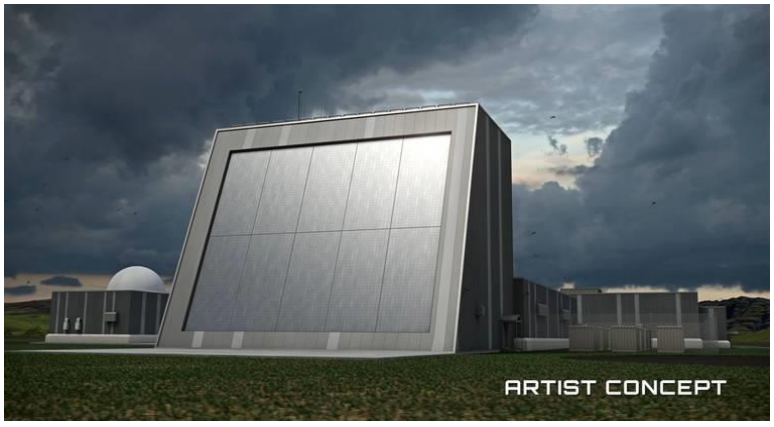

Figure 8 Homeland Defense Radar Hawaii (HDR-H).

3. Upgraded Early Warning Radars (UEWR)

Three Air Force early warning radars (UEWR) have been bettered and combined into the ballistic missile defense system. They are situated at Beale Air Force Base in California, RAF Fylingdales in the UK, and Thule Air Base in Greenland (BMDS). The enhancements updated the hardware and software to provide critical early warning, tracking, object categorization, and cueing data for the midcourse BMDS sensors. In FY14, the U.S. Air Force received all three UEWRs for sustainment. In FY12 and FY13, respectively, early warning radars in Clear, Alaska and Cape Cod, Massachusetts began upgrading UEWRs.

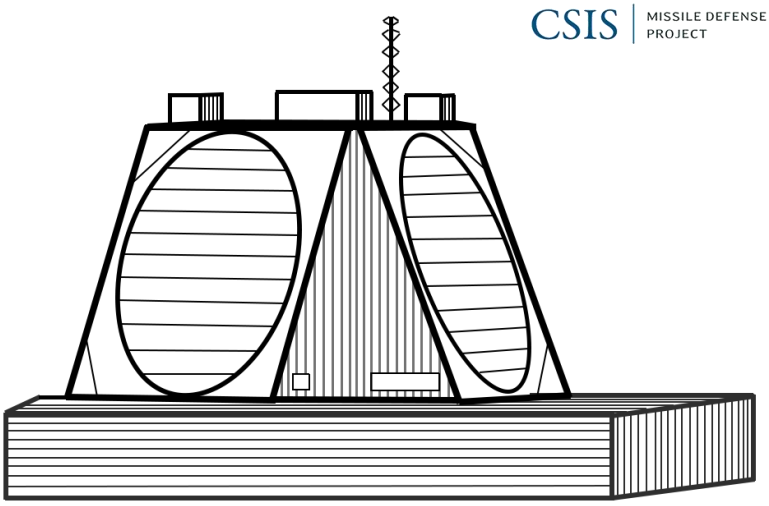

Figure 9 Upgraded Early Warning Radars (UEWR).

4. Cobra Dane Radar

The United States Air Force's COBRA DANE radar at Shemya, Alaska, has been modified for missile defense and incorporated into the Ballistic Missile Defense System (BMDS).

The upgrade increases the range of BMDS midcourse sensors by providing object detection, tracking and categorization data that can be used for cueing, launching interceptors and updating the course of interceptors whilst preserving the site's historical reconnaissance and space tracking missions. The Air Force is responsible for operating, maintaining and sustaining the COBRA DANE upgrade system.

Figure 10 The wideband phased-array Cobra Judy radar on the U.S. Naval ship Observation Island.

5. Army Navy/Transportable Radar Surveillance (AN /TPY 2)

The Army Navy/Transportable Radar Surveillance and Control Model 2, abbreviated AN/TPY-2, is a transportable X-band phased array radar intended primarily for ballistic missile defense. The AN/TPY-2 is capable of monitoring and identifying very small things across a great distance. This radar is crucial to the Ballistic Missile Defense System (BMDS) in forward-looking mode because it works as a forward-looking sensor for the system, recognizing ballistic missiles early in their flight and giving reliable tracking data for the system to employ. Multiple sensors offer overlapping sensor coverage, expanding the war or the fight range of the BMDS and making an adversary's penetration of the defensive system more difficult. The same radar, in terminal mode, provides observation, tracking, discriminating, and fire control for the Terminal High Altitude Area Defense (THAAD) missile system.

Figure 11 Army Navy/Transportable Radar Surveillance (AN /TPY 2).

6. Sea Bases X-band radar

Sea-based X-band radar (SBX) captures, tracks, and discriminates ballistic missile flight characteristics. The SBX extends the capabilities of the Ballistic Missile Defense System (BMDS) by allowing the Missile Defense Agency to undertake operational and realistic testing of the BMDS while also suppling combatant commanders with an operational capability.

Figure 12 Sea-based X-band radar.

7. Space Tracking and Surveillance System (STSS)

The Missile Defense Agency (MDA) is operating the Space Tracking and Surveillance System Demonstrators (STSS-D). The STSS-D constellation consists of two satellites orbiting at a distance of 1350 kilometers, with a 58-degree inclination and a 120-minute period. STSS-D, which acts as the experimental space layer for the BMD system, utilizes experimental sensors capable of detecting visible and infrared light (BMDS).

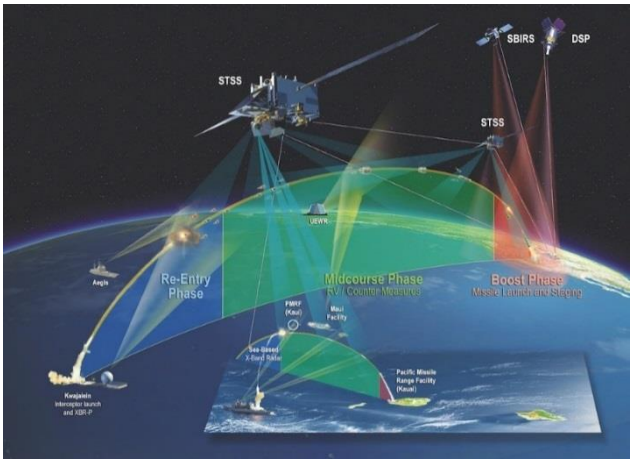

Figure 13 Space Tracking and Surveillance System (STSS).

8. Space bases Kill Assessment (SKA)

A network of tiny sensors installed aboard commercial satellites. Each sensor is equipped with three infrared detectors that record the energy signature of a collision amidst a ballistic missile and a Ballistic Missile Defense System interceptor.

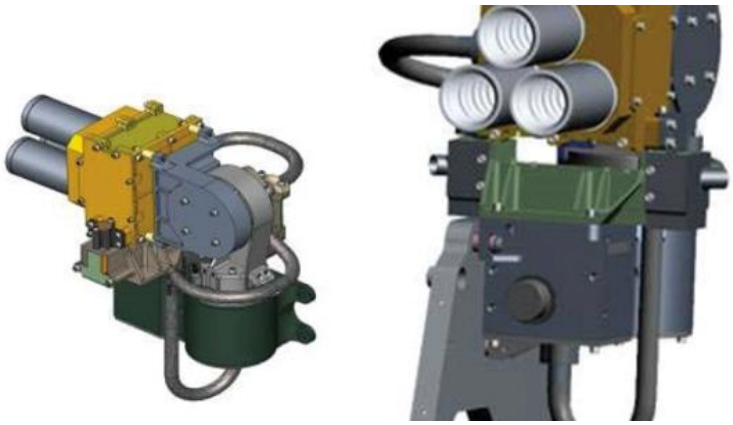

Figure 14 Space-based Kill Assessment (SKA).

9. Radar SPY -1

The SPY -1 radar is mounted on Aegis cruisers and destroyers as fraction of the initial missile defense capability. Existing S-band phased array radars are being upgraded to increase the system's capacity to monitor short, medium, and long-range interceptors.

Figure 15 Radar SPY -1.

10. Near Field Infrared Experiment (NFIRE)

The Missile Defense Agency (MDA) handles the Near Field Infrared Experiment (NFIRE) technology project out of the Missile Defense Space Development Center at Schriever Air Force Base in Colorado. The satellite's main mission is to gather data on near-field phenomenology for use in plume-to-hard body handover, navigation, guidance, and control algorithms, as well as end-game targeting algorithms for boost-

phase interceptor programs. This information is utilized by MDA to validate the models and simulations used to develop the guiding and homing algorithms. The secondary aim is to undertake proof-of-concept laser communication testing utilizing a commercial Laser Communications Terminal (LCT). The LCT will conduct these experiments with the assistance of the German Terra SAR-X satellite and optical ground equipment. These experiments illustrate the capabilities of low-Earth orbit satellite-to-satellite, satellite-to-aircraft, and satellite-to-ground communications by providing an extraordinarily high data rate at a cheap cost. Additionally, as compared to other modes of communication, LCT establishes a very secure communication channel with an extremely low possibility of eavesdropping.

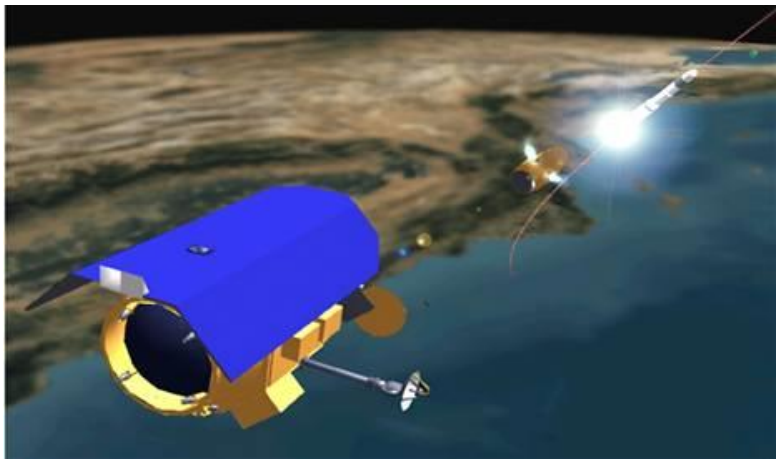

Figure 16 Near Field Infrared Experiment (NFIRE).

B. Boost Defense Segment

1. New technologies that may be available

As a result, the MDA wants to develop and test a wide range technology for intercepting and destroying ballistic missiles while their ascent phase of flight, enhancing targeting choices and resilience An important part of our strategy for reducing the risk of possible future attacks is a well-funded effort to develop improved missile defense systems.

2. Early interception

Early interception would enable us to intercept threatening missiles early in the battlespace. This maximizes our capability to employ "shoot-look-shoot" tactics, forces

countermeasures to be less efficient, minimizes the impact of debris, and reduces the number of interceptors required to repel a threat missile attack.

By using Unmanned Aerial Vehicles (UAVs) and space assets to supply ubiquitous sensor networks over the horizon, the effective range of existing Standard Missile-3 interceptors can be extended to the phase prior to a missile's apogee.

By firing an interceptor, evaluating the intercept attempt, and firing again if futile, Early Intercept can supply a prolonged engagement layer that evades wasted salvos.

Early Intercept capabilities are more attractive than midcourse weapons because of their mobility/transportability, the flexibility of UAV and space-based sensor support, and reduced Operation and Sustainment (O&S) costs. Forward-based AN /TPY-2 radars provide diplomatic difficulties and substantial operational and sustainment expenses, making the employment of existing Overhead Persistent Infrared (OPIR) and less costly Predator UAVs operations an attractive near-term alternative.

Figure 17 Unmanned Aerial Vehicles (UAVs).

C. Midcourse Defense Segment

1. Sea-Based Weapon Systems

The Missile Defense Agency's Missile Defense System (MDS) marine element is comprised of sea-based missile systems (MDA). The Aegis Ballistic Missile Defense (BMD) system, which is placed on US Navy destroyers and cruisers, supplements the Aegis Weapon System, the Standard Missile (SM), the Navy, and joint force command, control, and communications systems. Due to its scalability, Aegis BMD is also a critical component of Europe's Phased Adaptive Approach (EPAA) to missile defense.

a. Aegis BMD - Regional Defense Capability for Engagement

- The SM -3 is used to counter short to intermediate- range unitary and separating, midcourse- phase. ballistic missile threats, as well as short-range ballistic missile threats in the terminal phase with the SM-6.
- Each test improves the operational realism and complexity of targets and situations, as seen by Navy and Department of Defense testing assessors.
- In 2020, an Aegis-equipped destroyer successfully intercepted a simple target representative of the intercontinental ballistic missile (ICBM) threat using a SM -3 Block IIA missile, demonstrating how the system can be used in a layered missile defense architecture to strengthen the USA' missile defenses at home.

b. Homeland Defense - Aegis Ballistic Missile Defense Remote surveillance and tracking

- Aegis BMD ships conducting ballistic missile defense patrols detect and track ballistic missiles of all ranges, including intermediate range ballistic missiles, and transmit tracking data to the MDS. This capability shares tracking data with other missile defence sensors and provides fire control data to Midcourse Defense ground-based interceptors stationed at Fort Greely, Alaska, and Vandenberg Air Force Base, California, as well as to other MDS elements such as land-based launch units (Terminal High Altitude Area Defense, Patriot) and other Navy BMD ships.

c. Development

- The SM -3 Cooperative Development Programme was a joint effort between the United States and Japan to develop a 21-inch diameter variant of the SM -3, designated the SM -3 Block IIA, to defend against intermediate-range ballistic missile threats and provide robust regional ballistic missile defence. Deployment is scheduled to begin in 2021.

d. International Efforts

- The SM -3 Cooperative Development Programme was a joint U.S.-Japanese project to build the SM -3 Block IIA, a 21-inch diameter version of the SM -3 designed to defend against intermediate-range ballistic missile

threats and provide a robust regional defence against ballistic missiles. Deployment is scheduled for 2021.

- Japan has updated eight ships with Aegis BMD deployment capability.
- MDA's Sea-Based Weapon Systems Programme Office is in regular contact with maritime partners regarding missile defence cooperation, including commissioning support, testing, research, and information sharing.

e. Aegis Ashore

- Aegis Ashore is the land-based component of the Aegis BMD system. The deckhouse and launchers - which are virtually the same as the versions on U.S. Navy destroyers and cruisers - are equipped with Aegis BMD and SM -3.
- Under the EPAA phase II, the Aegis Ashore Station in Romania was certified as operational in 2016.
- The Aegis Ashore Missile Defence Test Complex at the Pacific Missile Range Facility in Kauai, Hawaii, is a test and evaluation facility used for Aegis Ashore development. It is scheduled for completion in fiscal year 2022 at the earliest.

f. Capabilities for the future

- Deploy ballistic missiles with greater range and complexity.
- Enhancement of terminal capacity against short and medium range ballistic missiles.
- Increased number of ships and missiles.
- Increased participation of maritime allies.
- Defense of hypersonic missiles in all phases of flight.

2. Ground-based Midcourse Defense (GMD)

For the security of the United States, Combatant Commanders are able to engage and destroy intermediate- and long-range ballistic missile threats in space using the Ballistic Missile Defense System's GMD component.

a. Overview

- GMD uses integrated communications networks, fire control systems, globally distributed sensors, and ground-based interceptors to identify, track, and destroy ballistic missile threats.
- The Exo-Atmospheric Kill Vehicle (EKV) is a sensor/propulsion system that uses the kinetic energy of a direct hit to kill the approaching target vehicle. This system has already been tested in a number of successful flight tests, including three with ground-based interceptors.

b. Details

- *Ground-based Midcourse Defense* is comprised of interceptors on the ground, as well as Ground logistical support and fire control systems.
- *The ground-based interceptor* is a solid-fuel booster carrying an EKV payload in many stages. Following launch, the missile carries the EKV to the target's projected orbital location. Once launched from the missile, the EKV approaches and destroys the target warhead using guidance data from ground logistical support and fire control system components, as well as on-board sensors. Outside of the Earth's atmosphere, the impact destroys the target warhead only by the kinetic force of direct contact.
- *Ground support and fire control systems* reformed of redundant fire control nodes, interceptor launchers, and a communications network. The GMD fire control (GFC) system collects data from satellites and ground-based radar sources and then Utilizes it to task and assist ground-based interceptors in intercepting target warheads. In addition, the GFC provides situational awareness data to the Command & Control, Battle Management, and Communications elements.

c. Deployment

- Ground-based interceptors are stationed at Fort Greely, Alaska, and Vandenberg Air Force Base, California. Currently, 44 interceptors are deployed.
- Fire control, battle management, planning, mission planning, and threat analysis are handled through an interface with two nodes at Fort Greely, Alaska, and Colorado Springs, Colorado, operated by humans. At Fort

Greely, Alaska, and Colorado Springs, Colorado, the system is controlled by soldiers from the 49th Missile Defense Battalion and the 100th Missile Defense Brigade.

- All GMD components interact via the GMD Communications Network, a secure data and voice communications system that uses satellite communications and fiber optic cables for long-haul communications.

Figure 18 Boeing Ground-Based Interceptor (GBI).

D. Terminal Defense Segment

1. Terminal High Altitude Area Defence (THAAD)

THAAD is an element of the Ballistic Missile Defense System (BMDS). It enables the BMDS to intercept and destroy ballistic missiles throughout their final phase of flight, whether within or outside the atmosphere.

a. Overview

- A land-based device capable of intercepting and destroying ballistic missiles both within and outside the atmosphere.
- Utilizes hit-to-kill technology to kinetically destroy the incoming warhead.
- High altitude intercept mitigates the effects of enemy weapons of mass destruction before they reach the ground.
- Highly effective against the ballistic threats.

b. Details

- *THAAD* batteries are rapidly deployable as they can be transported worldwide by air, land, and sea.
- *THAAD* battery consists of four main components:
- *Launcher:* truck-mounted, highly transportable, and storable interceptors can be launched and refilled quickly.

- *Interceptors:* Each launcher is equipped with eight interceptors.
- *Radar:* Army Navy/Transportable Radar Surveillance (AN /TPY-2) - The world's largest air-transportable X-band radar detects, tracks, and discriminates objects and provides interceptors with up-to-date tracking data.
- *Fire Control:* Serves as the communications and data management backbone for THAAD; interconnects THAAD components; connects THAAD to external command and control nodes and to the overall BMDS; prepares and executes intercept solutions.

c. Development

- State-of-the-art technology assures high standards and effective manufacturing and servicing.
- A inclusive program of ground and flight testing, quality affirmation, and design and development activities contributes to mission success.
- Significant THAAD program milestones include:
- Successfully intercepted 15 targets in 15 trials since program inception. The two most recent tests were conducted in July 2017.
- Continued element development to incrementally increase missile defense capabilities.

d. Field Deployment

- The U.S. Army has received and installed seven THAAD batteries.
- In August 2018, MDA delivered the 200th operational interceptor to the U.S. Army.

Arms Exports;

- The UAE as state has purchased and received two THAAD batteries (UAE).
- The UAE batteries are fully operational.

Figure 19 Terminal High Altitude Area Defense (THAAD).

2. PATRIOT Advanced Capability-3 (PAC -3)

The Patriot Defense System, which deploys Patriot Advanced Capability (PAC)-3 missiles, is the Ballistic Missile Defence System's most sophisticated hit-to-kill weapon system (BMDS). It is now operational and is being deployed by the US Army.

a. Overview

- A land-based element based on Patriot's proven air and missile defence infrastructure.
- The Army is responsible for the production and future development of the PAC -3. It is currently deployed in various theatres of operation around the world and conducts operations on a daily basis.
- The Missile Defence Agency will continue to be responsible for the interoperability and integration of the BMDS and PAC -3 systems.

b. Contributions to the Ballistic Missile Defence System

- As a lower echelon element in the defence of deployed U.S. forces and partners, supplies simultaneous air and missile defence abilities.
- Collaborates with THAAD to offer a layered defense against missile threats during the terminal phase of flight. These systems cooperate to counter the danger by establishing a layered defense against enemy missile threats through eye-level mission coordination, early warning track data, and situational awareness for battle management.

- Patriot contributes to the system's overall situational awareness by transmitting accurate cueing data to other components in the theater of operations while protecting system assets against short-range ballistic missiles, large-calibre missiles, and aerial threats.
- For homeland
- Patriot developed Upper-Tier Debris Mitigation to mitigate excessive radar exposure and probable missile fallout caused by upper-tier debris.

Figure 20 Patriot Advanced Capability-3 (PAC -3).

E. Command and Control, Battle Management and Communications (C2BMC)

Command and Control, Battle Management, and Communications (C2BMC) program is the integrating element of the Ballistic Missile Defense System (BMDS). It is a critical operational system that enables the President of the United States, the Secretary of Defense, and combatant commanders at the strategic, regional, and operational levels to plan ballistic missile defense operations collaboratively, collaboratively track the evolution of the battle, and dynamically control designated networked sensors and weapon systems to accomplish global and regional mission objectives.

Figure 21 Command and Control, Battle Management and Communications (C2BMC) in Kuwait.

Through a layered missile defense capabilities, the C2BMC responds optimally to threats of all ranges and phases of flight. C2BMC serves as a force multiplier, connecting, integrating, and synchronizing autonomous sensor and weapon systems and operations at the global and regional levels to maximize performance. C2BMC is a crucial component of all ground and air testing undertaken with the system for the purpose of validating and exercising all present and future BMDS capabilities.

Through its operational software and networks, the C2BMC program offers redundant connection and allows global force commanders to do field operations and maintenance. It delivers vital BMDS operating services via six product lines:

1. Ballistic Missile Defence Planner

- Enables forces to assess the effectiveness of various defence strategies.
- Supports three different planning approaches covering all phases of military operations: adaptive/deliberate, crisis-response, and dynamic planning.

2. Control and Command

- Provides situational awareness for force commanders by transforming comprehensive data into decision-relevant information.

- Ensures a consistent, integrated ballistic missile picture and communicates the status of the entire BMDS to the President and operational levels of command.
- Acts as a force multiplier in achieving integrated, layered ballistic missile defence through improved sensor resource management and mission coordination.
- Secure network connectivity for individual sensors and weapons components of the BMDS.
- Robust, high-availability connectivity for rapid and clear sharing of information across the global BMDS.

3. Simultaneous testing, training and operations

- Simultaneous Test, Train, and Operate - Enables commanders to maintain operational capability, conduct exercises, train, test, and rehearse operational scenarios while the system is in a deployed or "on alert" state.
- Enables combatant commanders to conduct dispersed, real-world operator-in-the-loop training for end-to-end missile defence.

4. International Cooperation

- Support the armed forces in creating international interfaces.
- Support international system development, test and policy agreements using MDA.

VI. MODERN MISSILE GUIDANCE

A successful Guidance, Navigation, and Control (GNC) system is critical to a target tracking scenario's success. This Chapter applies a GNC system and compares it to state-of-the-art systems that are extensively used today. The work contains an autopilot, guiding law, target tracking law, and a dependable inertial navigation system capable of precisely operating an agile vehicle such as a UAV, missile, or other vehicle utilizing available sensor data. The GNC system is simulated in this section using a non-linear generic missile model in a MATLAB/Simulink environment.

The control system is the first component of the GNC system to be examined. Two types of autopilots are contemplated: The commonly used three-loop autopilot is the initial design. The autopilot determines the ideal missile fin deflections to travel towards a target based on the guidance system's intended acceleration directives. The second configuration utilizes two decoupled autopilots for lateral and longitudinal control, with course and flight-path-angle serving as reference commands. Fin deflections are generated to achieve the required missile orientation using a Linear-Quadratic Regulator (LQR) based on the linearized generic missile model. By incorporating extra input from sideslip and angle-of-attack derivatives, performance and resilience features are increased.

The navigation system is the second component of the GNC system to be explored. Without trustworthy sensors and filters, other control loop subsystems will lose track of the vehicle's Position, Velocity, and Attitude (PVA). To achieve vehicle state convergence, a Multiplicative Extended Kalman Filter (MEKF) supported by Global Navigation Satellite Systems (GNSS) and gyro and acceleration biases is generated. The MEKF is distinguished from the regular Extended Kalman Filter (EKF) by the fact that it updates the Inertial Navigation System (INS) attitude calculations through quaternion multiplication, resulting in the inclusion of the multiplicative property. When calculating guiding instructions in a target-tracking situation, it is critical to have information about the target's location, velocity, and, in certain circumstances, acceleration. Along with the

INS-provided estimated missile states, a target-tracking Kalman Filter (KF) is used to monitor the relative states of the target and missile.

Finally, two guideline laws are compared to finalize the GNC design. The well-known Proportional Navigation (PN) rule is compared to a Line-Of-Sight (LOS) system with a course and flightpath-angle controlled autopilot. By assuming independent control of the horizontal and vertical planes, LOS guidance aims to steer the missile toward a vector connecting the launch platform and the predicted point of interception between the missile and target.

Simulink simulations of the GNC system provide encouraging results in both reference tracking for the autopilot and state estimation utilizing both KF designs.

A. Motivation

To intercept and negate the target, several functions must be performed. The goal of this thesis is to create a Guidance, Navigation, and Control (GNC) system for a tactical missile that uses a GNSS/IMU integrated navigation system for defensive reasons. All primary components of the GNC system will be explored in this thesis, and simulations for various target-tracking situations will be performed.

The following are the primary components of the GNC system:

1. Guidance

In order to properly track down and intercept a target, the guidance system is in charge of calculating key guidance orders. This may be done using a variety of techniques, but in this thesis, two alternative ways will be studied.

2. Navigation

It's critical to keep track of the missile's current PVA. The same may be said for keeping track of goal state data. In order to accomplish an engagement between the missile and the target, precise terminal position measurements are required. The navigation system is accountable for this. Without a strong inertial reference system for stabilizing target line-of-sight measurements and a good inertial reference system for stabilizing target line-of-sight measurements,

Compiling accurate missile guidance orders is challenging due to the difficulty of keeping track of one's own state information.

3. Control

While the guidance system is in charge of calculating guidance instructions, the control system is in charge of moving the missile actuators to ensure that these orders are carried out effectively. This is the equivalent of employing a strong and efficient autopilot to conduct fin deflections to modify the states of a missile.

VII. CONTROL SYSTEM

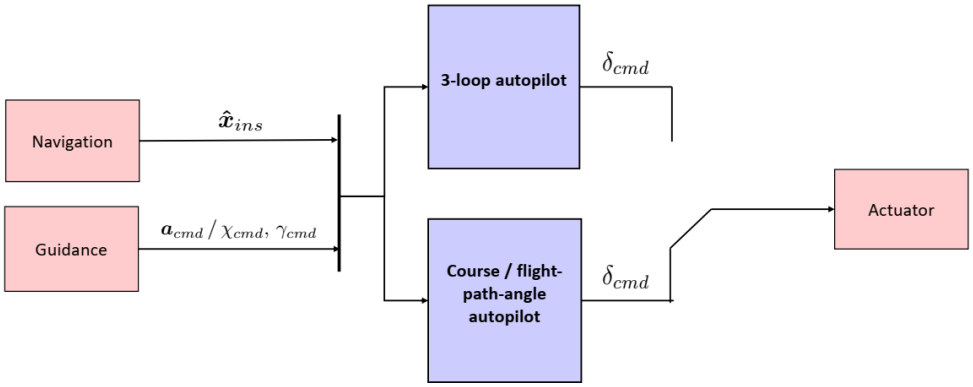

Figure 22 The autopilots compute desirable fin deflection orders using information from the INS and guiding commands. Two distinct designs will be contrasted in this thesis.

A. Introduction

The purpose of the missile autopilot's design is to provide a steady response to a given set of command inputs. Over the past 50 years, such autopilots have been effectively implemented, and the conventional three-loop autopilot has been the preferred design topology (Mracek & Ridgely, 2005). Due to the acceleration command input, a large number of the design issues given by the homing missile relate to the need to integrate the autopilot into the guidance loop without introducing heading inaccuracies during the terminal phase, as well as avoiding stability concerns (Horton, 1995). Typically, controllers are intended to function inside vast flight envelopes using gain scheduling (Mracek & Ridgely, 2005). This chapter will describe two distinct types of autopilots: the commonly used three-loop autopilot and one that is based on course and flight-pathangle command inputs.

B. Three-Loop Autopilot

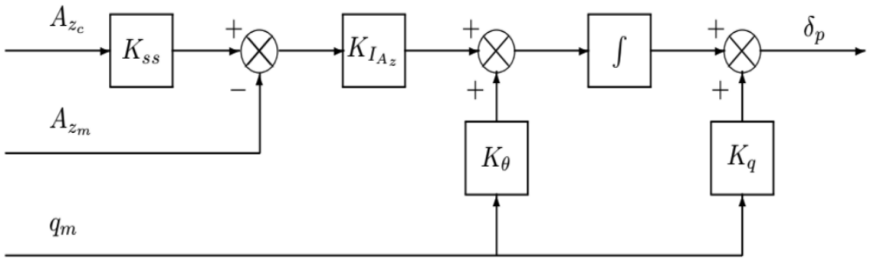

Figure 23 Pitch control with a classic three-loop topology. By applying the appropriate sign modifications, the same architecture may be employed for yaw control.

Source: Mracek and Ridgely, 2005

The traditional three-loop autopilot employs acceleration and angular rate feedback to generate the necessary fin deflections. There are various distinct typologies for generating the appropriate performance using the provided feedback amounts. Mracek and Ridgely (2005) investigated the resilience of numerous alternative topologies and determined that the conventional three-loop-autopilot has the greatest overall robustness features. According to Mracek and Ridgely (2005), the fundamental longitudinal dynamics are as follows:

$$\boldsymbol{x}^{\cdot} = \boldsymbol{Ax} + \boldsymbol{Bu}$$

Equation 1

$$\boldsymbol{y} = \boldsymbol{Cx} + \boldsymbol{Du}$$

Equation 2

Were

$$\boldsymbol{x} = \begin{bmatrix} \boldsymbol{\alpha} \\ \boldsymbol{q} \end{bmatrix} \boldsymbol{u} = \boldsymbol{\delta p} \boldsymbol{y} = \begin{bmatrix} \boldsymbol{A_{z_m}} \\ \boldsymbol{q_m} \end{bmatrix}$$

Equation 3

Figure 24 illustrates the conventional three-loop structure. Azc denotes the commanded acceleration, Azm is the measured linear acceleration, and q m denotes the measured angle of rotation around the perpendicular axis. These measurements are made with the use of an IMU. The same structure is suitable for pitch and yaw channel autopilots, provided that the feedback signals have the required sign changes (Mracek & Ridgely, 2005).

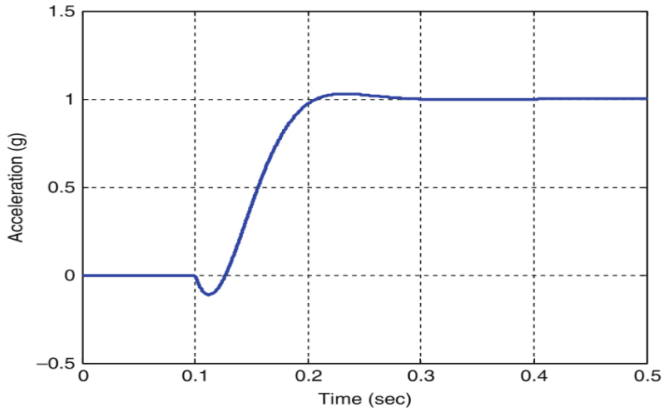

Figure 24 Acceleration response of the classical three-loop autopilot architecture when a step input is supplied.

Source: Mracek & Ridgely, 2005

It is worth noting that the architecture shown in figure 24 has an integrator. This stops the system from executing commands at an endless pace when it detects a step command on the input. However, this results in the system being non-minimum phase, which causes the missile to move in the opposite direction of the ordered direction before traveling in the requested direction, as seen by the step reaction in figure 25. This challenge may be addressed in a variety of ways other than via the use of classical designs, for example, through the use of Model Predictive Control (Sefastsson, 2016). This issue will be resolved when the course-controlled autopilot described in this thesis is implemented.

When various feedback typologies are used, the open-loop qualities will vary. This implies that despite identical closed loop answers, the various three-loop designs will exhibit varying degrees of resilience.

1. Course-commanded lateral autopilot

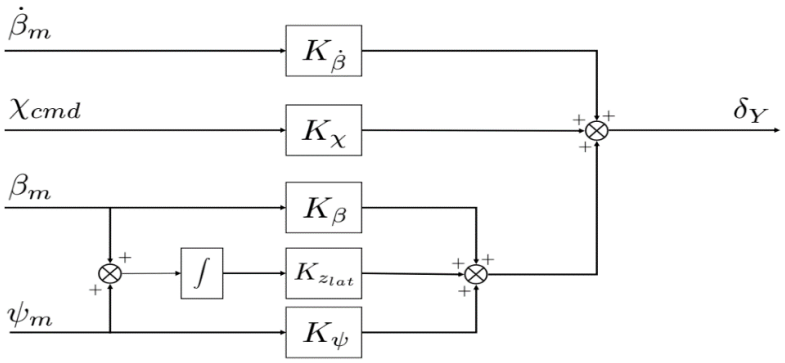

Figure 25 Autopilot with course control for lateral control.

A dependable autopilot architecture coupled with proper command structures is critical for the missile to execute as intended. This implies that distinct autopilot orders may be required at various stages, for example, at launch, mid-course, and when the missile approaches the target (C imen, 2011). Angle of attack and sideslip angle instructions may be favored for agile maneuvers and vertical launches, whereas flightpath-angle and course controls are sometimes employed during the launch phase.

Course and flight-path-angle command inputs are used in the autopilot system examined in this research. In contrast to the three-loop autopilot, the course and angle of the flight path may now be controlled directly, without the need of an extra outer-loop controller. This is shown in Figure 26, where χ_{cmd} signifies the commanded route and β_m and ψ_m signify the measured amounts. Notably, despite its design as a full-state feedback system, the optimum feedback control does not include input from the observed angular velocity r_m,.

Additionally, an extra input from $\dot{\beta}_m$ and, for the pitch channel $\dot{\alpha}_m$, provides an additional means of modifying the system's resilience features. The course-controlled design is able to alter these features through a tuneable parameter by incorporating extra data from$\dot{\beta}_m$. This provides a level of freedom in terms of robustness adjustment that is not available with the three-loop autopilot.

Due to the absence of a pure integrator in this autopilot architecture, the issue of minimum phase will not arise. When steps on reference inputs are handled, an extra reference model will be employed to inject saturation into the command rate.

Given a LOS vector with the necessary look-ahead distance, the LOS steering rule makes it simple to generate the correct course and flight path angle (Fossen, 2011). Due to the fact that the autopilot directly controls the route, the number of parameters required, and therefore the complexity of the autopilot, may be decreased in comparison to the standard three-loop autopilot.

When generating the longitudinal dynamics autopilot, the linearized equation for the yaw motion is taken into account. Because the autopilot's function is to regulate the course χ, it is required to supplement the model with another state. By adding a third state, ψ, the model becomes

$$\begin{bmatrix}\dot{\beta}\\ \dot{r}\\ \dot{\psi}\end{bmatrix} = \begin{bmatrix}-2.11 & -1 & 0\\ 423.97 & -1.44 & 0\\ 0 & 1 & 0\end{bmatrix}\begin{bmatrix}\beta\\ r\\ \psi\end{bmatrix} + \begin{bmatrix}0.39\\ 719.75\\ 0\end{bmatrix}\delta_Y$$

Equation 4

Since the relationship between the state vector and the course χ is

$$\chi = [1 \quad 0 \quad 1]\begin{bmatrix}\beta\\ r\\ \psi\end{bmatrix}_0^0$$

Equation 5

The C matrix related to the state-space model is simply written as

$$\boldsymbol{C} = [1 \quad 0 \quad 1]$$

Equation 6

When developing autopilots, the resilience qualities of the system must be considered in conjunction with the system's performance. Generally, the resilience features of the system will be enhanced at the price of the system's performance. It is desired to be able to design these qualities, and hence a new feedback term from $\dot{\beta}$ to χ_d with a gain $K_{\dot{\beta}}$ is introduced. This will represent a tuneable parameter in the linearized system's state space representation.

The system's enhanced input is expressed as

$$\delta_Y = \delta_Y' + K_{\dot{\beta}}\dot{\beta}$$

Equation 7

Such that (4.2) becomes

$$\begin{bmatrix}1 & 0 & 0\\ 0 & 1 & 0\\ 0 & 0 & 1\end{bmatrix}\begin{bmatrix}\dot{\beta}\\ \dot{r}\\ \dot{\psi}\end{bmatrix} = \begin{bmatrix}-2.11 & -1 & 0\\ 423.97 & -1.44 & 0\\ 0 & 1 & 0\end{bmatrix}\begin{bmatrix}\beta\\ r\\ \psi\end{bmatrix} + \begin{bmatrix}0.39\\ 719.75\\ 0\end{bmatrix}\delta_Y' + \begin{bmatrix}0.39K_{\dot{\beta}}\\ 719.75K_{\dot{\beta}}\\ 0\end{bmatrix}\dot{\beta}$$

Equation 8

The new feedback term is subtracted from the identity matrix on the left side

$$\begin{bmatrix}1-0.39K_{\dot{\beta}} & 0 & 0\\ -719.75K_{\dot{\beta}} & 1 & 0\\ 0 & 0 & 1\end{bmatrix}\begin{bmatrix}\dot{\beta}\\ \dot{r}\\ \dot{\psi}\end{bmatrix} = \begin{bmatrix}-2.11 & -1 & 0\\ 423.97 & -1.44 & 0\\ 0 & 1 & 0\end{bmatrix}\begin{bmatrix}\beta\\ r\\ \psi\end{bmatrix} + \begin{bmatrix}0.39\\ 719.75\\ 0\end{bmatrix}\delta_Y'$$

Equation 9

The left-hand matrix is inversed

$$\begin{bmatrix}\dot{\beta}\\ \dot{r}\\ \dot{\psi}\end{bmatrix} = \underbrace{\begin{bmatrix}1-0.39K_{\dot{\beta}} & 0 & 0\\ -719.75K_{\dot{\beta}} & 1 & 0\\ 0 & 0 & 1\end{bmatrix}^{-1}\begin{bmatrix}-2.11 & -1 & 0\\ 423.97 & -1.44 & 0\\ 0 & 1 & 0\end{bmatrix}}_{\boldsymbol{A}}\begin{bmatrix}\beta\\ r\\ \psi\end{bmatrix}$$

Equation 10

$$+\underbrace{\begin{bmatrix}1-0.39K_{\dot{\beta}} & 0 & 0\\ -719.75K_{\dot{\beta}} & 1 & 0\\ 0 & 0 & 1\end{bmatrix}^{-1}}_{\boldsymbol{B}}\begin{bmatrix}0.39\\ 719.75\\ 0\end{bmatrix}$$

Equation 11

This can be summarized by writing the system in state-space form, such that it becomes

$$\dot{x} = \boldsymbol{A}x + \boldsymbol{B}u$$

Equation 12

$$y = \boldsymbol{C}x + Du$$

Equation 13

were

$$x = \begin{bmatrix}\beta\\ r\\ \psi\end{bmatrix}\ u = \delta_Y\ y = \chi$$
$$\boldsymbol{C} = [1 \quad 0 \quad 1]\ D = 0$$

Equation 14

2. Since A and B are defined in (0.5c)

By examining the bode plot in figure 26, it is evident that the parameter $K_{\dot{\beta}}$ reduces the system's bandwidth, hence slowing it down. In many circumstances, it is preferable to attain the largest available bandwidth, since this improves the system's response time and performance (Balchen et al., 2004). While reaction speed and performance are critical for a missile, without a strong system, the missile would likely not function at all. As seen in Figure 27, feedback from $\dot{\beta}$ provides damping to the system, reducing step response oscillations. It is worth noting in Figure 26 that the feedback term $K_{\dot{\beta}}$ prevents the phase from falling below 180 degrees. This is a critical feature of robustness, since a gain crossover frequency near to the phase crossover frequency might cause the closed-loop system to become unstable.

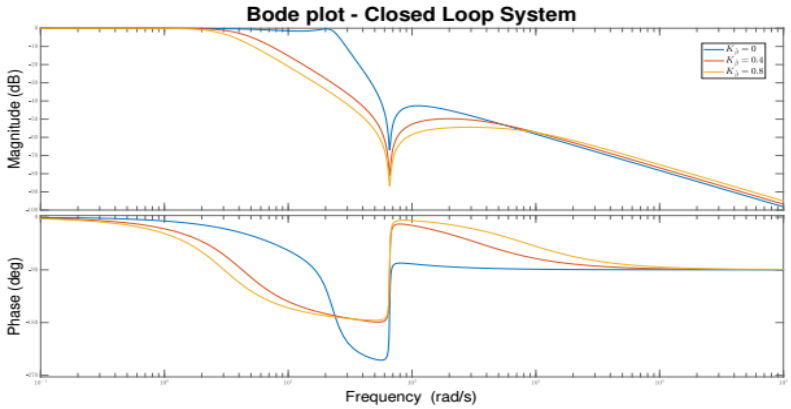

Figure 26 Bode plot of the closed-loop lateral autopilot for different values of $K_{\dot{\beta}}$.

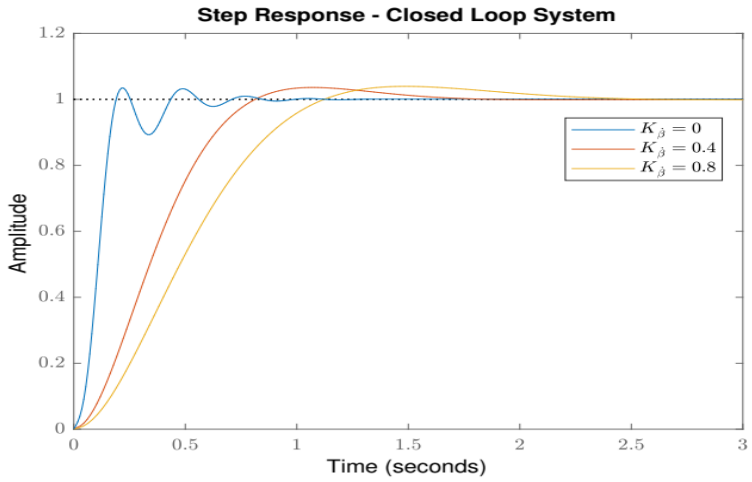

Figure 27 Step Response of the closed-loop lateral autopilot for different values of $K_{\dot{\beta}}$.

Different features of the system are shown in Table 1 for various values of $K_{\dot{\beta}}$. Stability.

3. Characteristics for various values of $K_{\dot{\beta}}$

Table 1 As seen, a resilient system is attained at the sacrifice of performance.

$K_{\dot{\beta}}$	Phase margin	Gain margin	Bandwidth	Closed loop stable?
-0.2	NaN	NaN	78.1	No
0.0	-0.3	0	24.37	No / Marginal
0.2	45.2	33.7	5.68	yes
0.4	33.5	41.3	4.15	yes
0.6	27.8	46.9	3.42	yes
0.8	24.3	52.5	2.98	yes
1.0	21.9	NaN	2.68	yes

$0 < K_{\dot{\beta}} \leq 0.4$ is used in further simulations.

C. Flight-Path Angle Commanded Longitudinal Autopilot

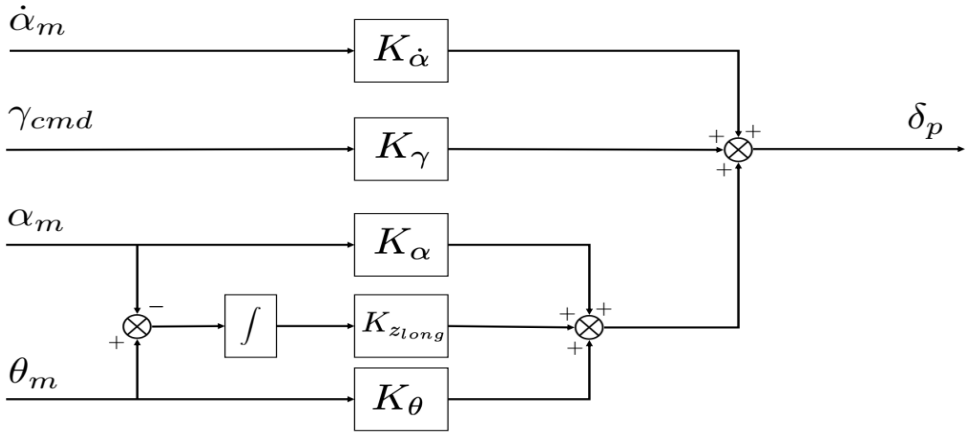

Figure 28 Longitudinal control using a flight-path angle-commanded autopilot.

This part develops the autopilot for longitudinal control. The topology is quite similar to that of the lateral control, as seen in figure 28.

When generating the longitudinal dynamics autopilot, the linearized equation for the yaw motion is taken into account. The autopilot's goal is to regulate the flight path angle γ, and as such, another state must be added to the model. The model becomes by adding θ as a third state.

$$\begin{bmatrix}\dot{\alpha}\\ \dot{q}\\ \dot{\theta}\end{bmatrix} = \begin{bmatrix}-0.07 & 1 & 0\\ -423.97 & -1.44 & 0\\ 0 & 1 & 0\end{bmatrix}\begin{bmatrix}\alpha\\ q\\ \theta\end{bmatrix} + \begin{bmatrix}0.39\\ 719.75\\ 0\end{bmatrix}\delta_p$$

Equation 15

Due to the fact that the connection between the state vector and the angle of the flight path γ is

$$\gamma = [1 \quad 0 \quad 1]\begin{bmatrix}\alpha\\ q\\ \theta\end{bmatrix}$$

Equation 16

The C matrix associated with the longitudinal state space model is denoted by the following notation:

$$\boldsymbol{C} = [1 \quad 0 \quad 1]$$

Equation 17

As with the lateral autopilot, it is desired to include a feedback term to optimize the system's performance.

$$\delta_P = \delta'_P + K_{\dot{\alpha}}\dot{\alpha}$$

Equation 18

Such that (0equation 16) becomes

$$\begin{bmatrix}1 & 0 & 0\\ 0 & 1 & 0\\ 0 & 0 & 1\end{bmatrix}\begin{bmatrix}\dot{\alpha}\\ \dot{q}\\ \dot{\theta}\end{bmatrix} = \begin{bmatrix}-0.07 & 1 & 0\\ -423.79 & -1.44 & 0\\ 0 & 1 & 0\end{bmatrix}\begin{bmatrix}\alpha\\ q\\ \theta\end{bmatrix}$$

Equation 19

$$+\begin{bmatrix}-0.39\\ -719.75\\ 0\end{bmatrix}\delta'_P + \begin{bmatrix}-0.39K_{\dot{\alpha}}\\ -719.75K_{\dot{\alpha}}\\ 0\end{bmatrix}$$

Equation 20

On the left, the new feedback term is subtracted from the identity matrix.

$$\begin{bmatrix}1+0.39K_{\dot{\alpha}} & 0 & 0\\ 719.75K_{\dot{\alpha}} & 1 & 0\\ 0 & 0 & 1\end{bmatrix}\begin{bmatrix}\dot{\alpha}\\ \dot{q}\\ \dot{\theta}\end{bmatrix} = \begin{bmatrix}-0.07 & 1 & 0\\ -423.79 & -1.44 & 0\\ 0 & 1 & 0\end{bmatrix}\begin{bmatrix}\alpha\\ q\\ \theta\end{bmatrix} + \begin{bmatrix}-0.39\\ -719.75\\ 0\end{bmatrix}\delta'_P$$

Equation 21

As with the lateral method, the left-hand matrix is inversed:

$$\begin{bmatrix}\dot{\alpha}\\ \dot{q}\\ \dot{\theta}\end{bmatrix} = \underbrace{\begin{bmatrix}1+0.39K_{\dot{\alpha}} & 0 & 0\\ 719.75K_{\dot{\alpha}} & 1 & 0\\ 0 & 0 & 1\end{bmatrix}^{-1}\begin{bmatrix}-0.07 & 1 & 0\\ -423.79 & -1.44 & 0\\ 0 & 1 & 0\end{bmatrix}}_{\boldsymbol{A}}\begin{bmatrix}\alpha\\ q\\ \theta\end{bmatrix}$$

Equation 22

$$+\underbrace{\begin{bmatrix}1+0.39K_{\dot{\alpha}} & 0 & 0\\ 719.75K_{\dot{\alpha}} & 1 & 0\\ 0 & 0 & 1\end{bmatrix}^{-1}\begin{bmatrix}-0.39\\ -719.75\\ 0\end{bmatrix}}_{\boldsymbol{B}}\delta'_P$$

Equation 23

This can be summarized by writing the system in the same form as (equation 15), such that

$$x = \begin{bmatrix}\alpha\\ q\\ \theta\end{bmatrix} u = \delta_p \quad y = \gamma$$

Equation 024

$$\boldsymbol{C} = [1 \quad 0 \quad 1]\ D = 1$$

Equation 25

While A and B are given in (equation 19).

VIII. NAVIGATION SYSTEM

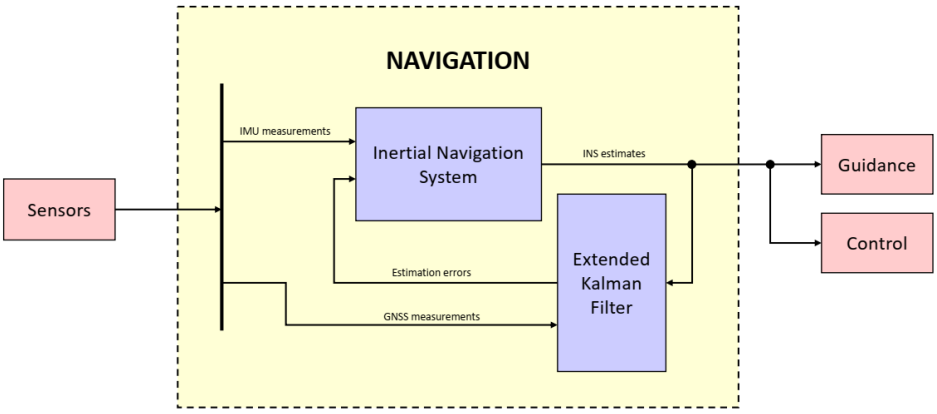

Figure 29 Navigation System.

A. Introduction

The navigation system is responsible for accurately estimating the status of the vehicle based on sensor data. In this chapter, an error-state Kalman Filter will be utilized to make error corrections in the navigation equations, providing more exact state estimations to the Guidance and Control systems. Because the INS estimates PVA by integrating sensor readings (see section 8.5), mistakes are inevitable because sensor measurements are only valid for a certain period of time. This is due to drift induced by imprecise measurements and biases. The navigation mechanism for estimating the interceptor status is shown in Figure 29.

It's worth noting that the frequency at which IMU and GNSS measurements are updated is often not the same. Due to the fact that an IMU works at a far higher frequency than a GNSS receiver, the INS system is capable of calculating estimates much more often than a straight Kalman Filter architecture, where the sampling rate is saturated depending on the GNSS update frequency.

Two distinct approaches to calculate the MEKF's measurement equations will be explained. The first method requires the inclusion of a Kalman Filter to calculate the specific-force reference, while the second method relies on estimate directly from sensor readings.

Additionally, a Kalman Filter will be developed to maintain track of the relative PVA between the interceptor and target. This is discussed in further detail in Section 8.8.

B. The Indirect Extended Kalman Filter Process

There are two well-known methods for implementing a Kalman filter. The direct and indirect Kalman filters are the two distinct techniques. Both approaches are based on a discrete-time state space model (Bryne and Fossen, 2016):

$$\boldsymbol{x}[k+1] = \boldsymbol{A}_d[k]\boldsymbol{x}[k] + \boldsymbol{B}_d\boldsymbol{u}[k] + \boldsymbol{E}_d\boldsymbol{w}[k]$$

Equation 26

$$\boldsymbol{y}[k] = \boldsymbol{C}[k]\boldsymbol{x}[k] + \boldsymbol{D}_d[k]\boldsymbol{u}[k] + \boldsymbol{\epsilon}[k]$$

Equation 27

(Where A_d B_d, and E_d denote the process model, $\boldsymbol{C}_d$, and $\boldsymbol{D}_d$ denote the measurement model, and E d and denote the process and measurement noise vectors, respectively.

The states of the indirect Kalman filter are expressed as error-states. After that, the filter may be used to determine the mistakes in terms of state and bias errors. This differs from the Kalman filter's direct approach in that the states of the filter represent the error dynamics rather than just the normal states. The error state-space model is expressed as follows:

$$\delta\dot{\boldsymbol{x}}[k+1] = \boldsymbol{A}_d[k]\delta\boldsymbol{x}[k] + \boldsymbol{E}_d\delta\boldsymbol{w}[k]$$

Equation 28

$$\delta\boldsymbol{y}[k] = \boldsymbol{H}_d[k]\delta\boldsymbol{x}[k]$$

Equation 29

where δ(.) denotes the error state.

When dealing with an indirect/error-state Kalman filter, we make a distinction between the true, nominal, and error-state states of the system, with the true state being the sum of the nominal and error-state states (Sola', 2017). The IMU measurement is a huge signal, but the incorrect state is considered a tiny signal. Integrating the high frequency IMU data yields the nominal state values. These dead-reckoning positional states do not account for noise and biases, and as a result, they will drift. Parallel to the nominal state integration, the indirect Kalman filter is employed to offer nominal state corrections. When more aiding measurements occur,

the mean of the error state is injected into the nominal state and then reset to zero. The processes for rectification are shown in (8.14). The $\oplus$ symbols denote the relevant compositions, which might be sums or quaternion products. Following that, the covariance matrix is changed to reflect this reset.

The indirect Kalman filter acts as seen in Figure 30 (Bryne and Fossen, 2016):

$$\hat{x}_{ins}[k]\& \leftarrow \hat{x}_{ins}[k] \oplus \delta\hat{x}^{+}[k]$$

Equation 30

$$\delta\hat{x}^{+}[k]\& \leftarrow 0$$

Equation 31

$$k\& \leftarrow k + 1$$

Equation 32

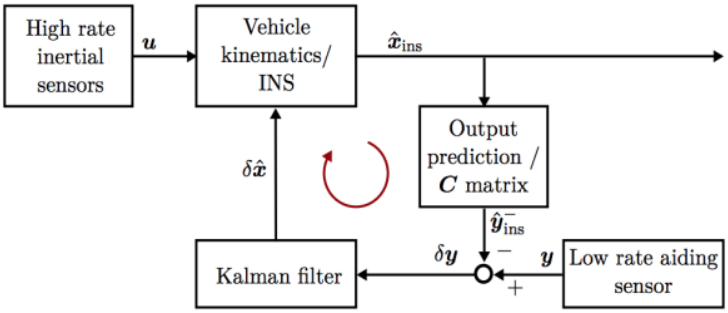

Figure 30 Indirect (feedback) Kalman filter for INS.

The estimation of $\delta\hat{\boldsymbol{x}}^{+}$is done every time step according to

$$\delta\hat{\boldsymbol{x}}^{+}[k] = \delta\hat{\boldsymbol{x}}^{-}[k] + \boldsymbol{K}[k]\big(\delta y[k] - \boldsymbol{h}(\delta\hat{\boldsymbol{x}}^{-}[k])\big)$$

Equation 33

while the Kalman gain and co-variance updates are calculated as

$$\boldsymbol{K}[k] = \hat{\boldsymbol{P}}^{-}[k]\boldsymbol{H}_d^{T}[k]\big(\boldsymbol{H}_d[k]\hat{\boldsymbol{P}}^{-}[k]\boldsymbol{H}_d^{T}[k] + \boldsymbol{R}_d[k]\big)^{-1}$$

Equation 34

$$\hat{\boldsymbol{P}}^{+}[k] = (\boldsymbol{I} - \boldsymbol{K}[k]\boldsymbol{H}_d[k])\hat{\boldsymbol{P}}^{-}[k](\boldsymbol{I} - \boldsymbol{K}[k]\boldsymbol{H}_d[k])^{T} + \boldsymbol{K}[k]\boldsymbol{R}[k]\boldsymbol{K}^{T}[k]$$

Equation 35

$$\hat{\boldsymbol{P}}^{-}[k+1] = \boldsymbol{H}_d[k]\hat{\boldsymbol{P}}^{+}[k]\boldsymbol{H}_d^{+}[k] + \boldsymbol{E}_d[k]\boldsymbol{Q}_d[k]\boldsymbol{E}_d[k]^{T}$$

Equation 36

where

$\boldsymbol{K}$ is the Kalman gain

$\delta\hat{\boldsymbol{x}}^{-}, \delta\hat{\boldsymbol{x}}^{+}$ are the priori and apostriori error measurements

$\boldsymbol{Q}_d, \boldsymbol{R}_d$ is the co-variance matrices for process and measurement noise, and

$\hat{\boldsymbol{P}}^{-}, \hat{\boldsymbol{P}}^{+}$ are the apriori and apostriori co-variance matrix estimates.

Due to the fact that the error δxˆ+[k] is reset prior to the arrival of a fresh measurement, the last term of (0.15) is superfluous and may be reduced to

$$\delta\boldsymbol{x}\hat{} + [k] \;=\; \delta\boldsymbol{x}\hat{} - [k] \;+\; \boldsymbol{K}[k]\delta y[k]$$

Equation 37

C. Sensors

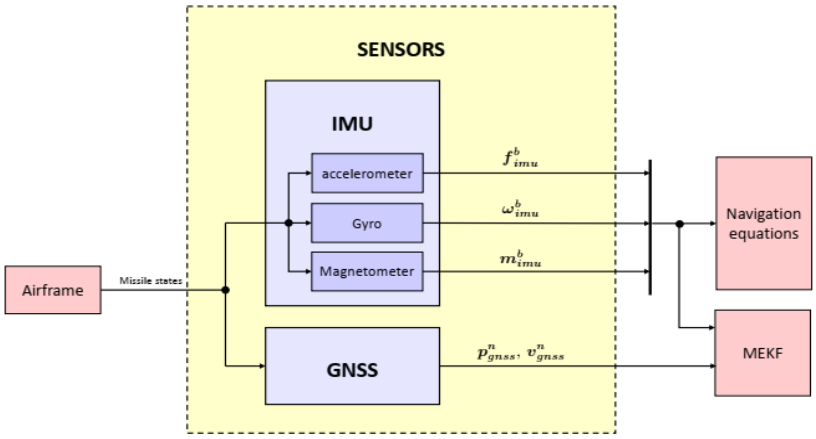

Figure 31 Sensors in relation to the rest of the control system.

A rigid body's state may be determined using a variety of sensors, most often accelerometer and gyroscope measurements. Three accelerometers, three gyroscopes, and three magnetometers comprise the IMU. The IMU measurements will offer estimates for acceleration and angular rates, which will be integrated to get the rigid body's PVA. This results in dead-reckoning position and attitude estimations that may be erroneous as a result of sensor noise and bias contamination. To evaluate the biases, assistive approaches based on GNSS location and velocity data, magnetometer readings, and relative force calculation are employed.

1. Rate Gyro Measurement

For some time, ring laser gyros and Fiber Optic Gyros (FOG) have been employed, and are projected to become the norm for high-precision strap-down inertial systems (Fossen, 2011). Micro Electrical Mechanical Systems (MEMS) have

traditionally been assumed to be employed in low- to moderate-cost applications. This assumption, however, has been challenged by modern MEMS systems like as the UTC Aerospace Systems TITAN® MEMS IMU, which rivals the performance of a FOG (UTC Aerospace Systems, 2017). The TITAN® MEMS IMU delivers the sensor parameters utilized in simulations with their associated properties. Assuming that the sensors are positioned with a tiny misalignment error in the body frame origin, the gyro output may be written as (Fossen, 2011) as

$$\boldsymbol{\omega}_{imu}^{b} \approx \boldsymbol{\omega}_{b/n}^{b} + \boldsymbol{b}_{ars}^{b} + \boldsymbol{\omega}_{ars}^{b}$$

Equation 38

where $b_{ars}^{b} = \begin{bmatrix} b_{ars,\phi}^{b} & b_{ars,\theta}^{b} & b_{ars,\psi}^{b} \end{bmatrix}^{T}$ is the unknown bias modeled as a Wiener process.

$$\dot{b}_{ars}^{b} = \omega_{b,ars}$$

Equation 39

and $\boldsymbol{\omega}_{ars}^{b}$ is Gaussian white noise.

By deploying a proof mass suspended from the sensor, the relative movement of the mass may be utilized to determine the sensor's acceleration. The displacement of the acceleration transducers may be simply translated to acceleration using a simple force balancing analysis:

$$m\ddot{x} + k\dot{x} = ky(t)$$

Equation 40

where x is the proof mass's inertial position and $y(t)$is the sensor housing's inertial position.

Accelerometers determine the particular force acting on the vehicle's body structure. The measured acceleration is consequently the casing's overall acceleration, less the force of gravity dragging the casing toward the earth's core. Accelerometer readings may be expressed mathematically as follows (Beard and McLain, 2013) (Fossen, 2011):

$$\boldsymbol{f}_{imu}^{b} = \begin{pmatrix} a_x \\ a_y \\ a_z \end{pmatrix} = \frac{d\boldsymbol{v}}{d_{tb}} + \omega_{b/i}^{b} \times \boldsymbol{v} - \boldsymbol{R}_{n}^{b} \begin{pmatrix} o \\ o \\ g \end{pmatrix} + \boldsymbol{b}_{acc}^{b} + \boldsymbol{\omega}_{acc}^{b} \quad 0.22$$

Equation 41

Where $\boldsymbol{\omega}_{b/i}$ is is the angular rotation in body-frame with respect to the inertial frame.

$b_{acc}^{b} = \begin{bmatrix} b_{acc,x}^{b} & b_{acc,y}^{b} & b_{acc,z}^{b} \end{bmatrix}^{T}$ is the unknown bias modeled as a Wiener process.

$$\dot{\boldsymbol{b}}_{acc}^{b} = \boldsymbol{\omega}_{b,acc}$$

Equation 42

and $\boldsymbol{\omega}_{acc}^{b}$ is Gaussian white noise. For local navigation, the NED frame can be assumed inertial, which gives

$$\boldsymbol{\omega}_{b/i}^{b} \approx \boldsymbol{\omega}_{b/n}^{b}$$

$$a_x = \dot{u} + qw - rv + g\,sin\,\theta + b_{acc,x} + \omega_{acc,x}$$

$$a_y = \dot{v} + ru - pw - gcos\,\theta sin\,\phi + b_{acc,y} + \omega_{acc,y}$$

Equation 43

$$a_z = \dot{w} + pv - qu - gcos\,\theta cos\,\phi + b_{acc,z} + \omega_{acc,z}$$

Equation 44

From (0equation 43) it is seen that the accelerometer measures linear acceleration, Coriolis acceleration and gravitational acceleration.

2. Magnetometer Measurement

The last section of the IMU measurements is made with the assistance of a cluster of three magnetometers. The earth's magnetic field may be likened to that of a simple bar magnet. Originating from the South Pole and extending to the North Pole, the magnetic field varies in intensity and direction over the Earth's surface (Fossen, 2011).

The magnetic field is unique on a global scale. The magnetic field in the horizontal plane is well-known and may be readily calculated online. The magnetic field at Berkeley, California is roughly [1] $m^n = [22494.35\ 5372.67\ 42301.72]^T$. By installing the magnetometers orthogonal to the body axis and aligned with them, the magnetometer readings may be translated to the horizontal plane in accordance with (Fossen, 2011)

[1] Magnetic separation apparatus and magnetic separation method, and wastewater treatment apparatus and wastewater treatment method. (2016, April 1). Retrieved January 3, 2022, from https://www.scirp.org/journal/paperinformation.aspx?paperid=100239

$$\boldsymbol{m}_{imu}^{b} = \boldsymbol{R}_{n}^{b}\boldsymbol{m}^{n} + \boldsymbol{b}_{mag}^{b} + \boldsymbol{w}_{mag}^{b}$$

Equation 45

where $\boldsymbol{m}^{n} = [m_N \quad m_E \quad mD]$ represents the magnetometer measurements.

$b_{\text{mag}}^{b} = \left[b_{\text{mag},x}^{b}\ b_{\text{mag},y}^{b}\ b_{\text{mag},z}^{b}\right]^{T}$ is the unknown bias modeled as a Wiener process

$$\dot{\boldsymbol{b}}_{\text{mag}}^{b} = \boldsymbol{\omega}_{b,\text{mag}}$$

Equation 46

and $\boldsymbol{\omega}_{\text{mag}}^{b}$ is Gaussian white noise.

3. Global Navigation Satellite System

The GNSS system, which utilizes space satellites to determine location and navigation, is extensively employed in both civil and military purposes according to (Zhang et-al., 2017). While the INS gives quick, high-precision PVA estimations for a brief period of time, they will drift over time due to sensor bias and noise. By integrating GNSS readings, very precise location assistance will be provided, avoiding estimates from drifting over time. The receiver's velocity may also be determined using carrier phase Doppler measurements with a standard deviation of 0.01 to 0.05 m/s (Beard and McLain, 2013).

Nowadays, the majority of GPS receivers are updated at a rate of 1 Hz. Position and velocity updates may be received at a frequency of as low as 0.1 Hz for certain low-speed applications, while sampling rates of up to 10 Hz are often required for high-speed navigation (Salih et-al., 2013). Trimble® Serial Embedded GPS Receiver (SEGR) is a series of Embedded GPS Receiver (EGR) that is optimized for airborne and other high-precision applications. According to their datasheet (Trimble, 2012), they can achieve an assist rate of 1-50 Hz.

D. Attitude Model

Due to the assumption that the attitude is unknown, it must be approximated using an attitude estimator. Due to the fact that there are other ways to describe the attitude, a comparison between Euler angles and the Hamilton quaternion follows. When Euler angles are used, the three parameters describe the attitude.

$$\boldsymbol{\Theta} = [\phi \quad \theta \quad \psi]^T$$

Equation 47

The matrix representation of the attitude yields (Fossen, 2011)

$$\boldsymbol{R}_b^n(\boldsymbol{\Theta}_{nb}) = \begin{bmatrix} c\psi c\theta & -s\psi c\phi + c\psi s\theta s\phi & s\psi s\phi + c\psi c\phi s\theta \\ s\psi c\theta & c\psi c\phi + s\phi s\theta s\psi & -c\psi s + \phi + s\theta s\psi c\phi \\ -s\theta & c\theta s\phi & c\theta c\phi \end{bmatrix}$$

Equation 48

It follows that

$$\dot{\psi} = q\frac{\sin\phi}{\cos\theta} + r\frac{\cos\phi}{\cos\theta} \; 0.27$$

Equation 49

Furthermore, it is obvious that the pitch angle $\theta = 90$ degrees indicates a singularity, providing only limited stability to an observer utilizing Euler angles.

The four-parameter quaternion attitude representation $\boldsymbol{q} = [\eta \quad \epsilon_1 \quad \epsilon_2 \quad \epsilon_3]^T$is singularity-free and capable of achieving near-global or semi-global stability (M.Innocenti and D.Fragopoulos, 2004). As a result, quaternions are used to describe the system's attitude.

The error terms in extended Kalman filtering issues may be addressed additively, i.e. $\boldsymbol{q} = \hat{\boldsymbol{q}} + \delta\boldsymbol{q}$ (Crassidis et al., 2007). This widely used technique results in a non-unique parameterization of the attitude in the filter state vector. However, combining two-unit quaternions does not result in the formation of a new unit quaternion, an issue that is often resolved by numerous renormalizations (Maley, 2013). An elegant method is to generate the injection term for the approximation of the actual state using the quaternion product of the estimated quaternion $\hat{\boldsymbol{q}}$ and the erroneous quaternion $\delta\boldsymbol{q}$:

$$\boldsymbol{q} = \hat{\boldsymbol{q}} \otimes \delta\boldsymbol{q} \;\Leftrightarrow\; \delta\boldsymbol{q} = \hat{\boldsymbol{q}}^{-1} \otimes \boldsymbol{q}$$

Equation 50

$$\boldsymbol{R}_b^n(\boldsymbol{q}) \; = \boldsymbol{R}_b^n(\hat{\boldsymbol{q}} \otimes \delta\boldsymbol{q}) = \boldsymbol{R}_{\hat{b}}^n(\hat{\boldsymbol{q}})\boldsymbol{R}_{\hat{b}}^{\hat{b}}(\boldsymbol{\delta q})$$

Equation 51

Where$\{\hat{b}\}$ denotes the approximate body-frame. Another advantage of utilizing error quaternion multiplication is that the number of terms required for parametrization is decreased from four to three, since η can be readily obtained by taking $\eta = \sqrt{1 - \epsilon^T\epsilon}$ when $q = [\eta \quad \epsilon_1 \quad \epsilon_2 \quad \epsilon_3]^T$is a unit quaternion.

The time derivative of the error $\delta \boldsymbol{q}$ is found by differentiating (equation 50)

$$\boldsymbol{\delta \dot{q}} = \begin{bmatrix} \boldsymbol{\delta \dot{\eta}} \\ \boldsymbol{\delta \dot{\epsilon}} \end{bmatrix} = \boldsymbol{\hat{q}^{-1}} \otimes \boldsymbol{\dot{q}}$$

Equation 52

$$= \frac{\mathbf{1}}{\mathbf{2}} \boldsymbol{\hat{q}^{-1}} \otimes \boldsymbol{q} \otimes \begin{bmatrix} \mathbf{0} \\ \boldsymbol{w^b_{b/n}} \end{bmatrix}$$

Equation 53

$$= \frac{1}{2} \boldsymbol{\delta q} \otimes \begin{bmatrix} 0 \\ \boldsymbol{w^b_{b/n}} \end{bmatrix}$$

Equation 54

The vector part $\delta \dot{\epsilon}$ is then written as

$$\delta \dot{\boldsymbol{\epsilon}} = \frac{1}{2} \left[\boldsymbol{I}_{3x3} \sqrt{1 - \delta \epsilon^T \delta \boldsymbol{\epsilon}} + \boldsymbol{S}(\delta \epsilon) \right] \boldsymbol{\omega^b_{b/n}}$$

Equation 55

E. Inertial Navigations Systems Equations

Three accelerometers, three angular rate sensors, and three magnetometers are supposed to be mounted on the vehicle.

The sensor models are supplemented with Gaussian white noise and time-varying biases, resulting in the IMU measurements given in (equation 46) and equation (45):

$$\boldsymbol{f^b_{imu}} = (\boldsymbol{R^n_b})^T \boldsymbol{f^b_n} + \boldsymbol{b^b_{acc}} + \boldsymbol{w^b_{acc}}$$

Equation 56

$$\boldsymbol{\omega^b_{imu}} = \boldsymbol{\omega^b_{b/n}} + \boldsymbol{b^b_{ars}} + \boldsymbol{\omega^b_{ars}}$$

Equation 57

Where $\boldsymbol{f^b_n}$ is the true specific force and $\boldsymbol{\omega^b_{b/n}}$ is the true angular rate.

$\boldsymbol{b^b_*}$ is the unknown bias modeled as a Wiener process

$$\dot{b}^b_* = \omega_{b,*}$$

Equation 58

When ω_* is Gaussian white noise.

To solve the sensors measurements for the true specific force and angular rate we give

$$\boldsymbol{f}_b^n = \boldsymbol{R}_b^n\left(\boldsymbol{f}_{imu}^b - \boldsymbol{b}_{acc}^b - \boldsymbol{w}_{acc}^b\right)$$

Equation 59

$$\boldsymbol{\omega}_{b/n}^b = \boldsymbol{\omega}_{imu}^b - \boldsymbol{b}_{ars}^b - \boldsymbol{\omega}_{ars}^b$$

Equation 60

The INS sensors estimates are defined as

$$\boldsymbol{f}_{ins}^n = \boldsymbol{R}_b^n(\hat{\boldsymbol{q}})\left(\boldsymbol{f}_{imu}^b - \boldsymbol{b}_{ins,acc}^b\right)$$

Equation 61

$$\boldsymbol{\omega}_{ins}^b = \boldsymbol{\omega}_{imu}^b - \boldsymbol{b}_{ins,ars}^b$$

Equation 62

Jay (2008) provides the strap-down navigation equations with quaternion representation for the attitude in the inertial frame:

$$\begin{aligned}\dot{\boldsymbol{p}}_{b/n}^n &= \boldsymbol{v}^n{}_{b/n}\\ \dot{\boldsymbol{v}}_{b/n}^n &= \boldsymbol{f}_b^n + \boldsymbol{g}^n\\ \dot{\boldsymbol{q}} &= \tfrac{1}{2}\boldsymbol{q} \otimes \begin{bmatrix}0\\ \boldsymbol{\omega}_{b/n}^b\end{bmatrix}\end{aligned}$$

Equation 63

By inserting (equation 61) into (equation 63) we obtain PVA estimates as well as bias estimates. The inertial navigation equations yields

$$\begin{aligned}\dot{\boldsymbol{p}}_{ins}^n &= \boldsymbol{v}^n{}_{ins}\\ \dot{\boldsymbol{v}}_{ins}^n &= \boldsymbol{R}_b^n(\hat{\boldsymbol{q}})\left(\boldsymbol{f}_{imu}^b - \boldsymbol{b}_{ins,acc}^b\right) + \boldsymbol{g}^n\\ \dot{\boldsymbol{q}}_{ins} &= \tfrac{1}{2}\boldsymbol{q}_{ins} \otimes \begin{bmatrix}0\\ \omega_{imu}^b - b_{ins,ars}^b\end{bmatrix}\\ \dot{\boldsymbol{b}}_{ins,ars}^b &= 0\\ \dot{\boldsymbol{b}}_{ins,acc}^b &= 0\end{aligned}$$

Equation 64

F. Error-State Equations

There will be error propagation between the INS estimations and the real states as a result of modeling flaws, sensor drift, and noise. To ensure that the system functions well, the error between these two states must be evaluated and adjusted. This is the portion where the EKF discussed in Section (equation 34). will be applied.

The error-state equations between the true states and the INS readings are defined as follows:

$$\begin{aligned}\delta \boldsymbol{p}_{b/n}^{n} &= \boldsymbol{p}_{b/n}^{n} - \boldsymbol{p}_{ins} \\ \delta \boldsymbol{v}_{b/n}^{n} &= \boldsymbol{v}_{b/n}^{n} - \boldsymbol{v}_{ins} \\ \boldsymbol{q} &= \boldsymbol{q}_{ins} \otimes \delta \boldsymbol{q} \\ \delta \boldsymbol{b}_{ars} &= \boldsymbol{b}_{ars} - \boldsymbol{b}_{ins,ars} \\ \delta \boldsymbol{b}_{acc} &= \boldsymbol{b}_{acc} - \boldsymbol{b}_{ins,acc}\end{aligned}$$

Equation 65

Due to the fact that the error state equations contain the quaternion multiplicative component $\otimes$ for quaternion estimation, the filter is referred to as the multiplicative extended Kalman filter MEKF.

1. Gibbs Vector

There are numerous methods for parametrizing the quaternion, including the usage of Euler angles and the Hamilton quaternion, which are discussed in Section (equation 67). The Gibbs vector will be utilized to parametrize the quaternion error in the MEKF. Markley (2008) specifies the Gibbs vector as

$$\boldsymbol{g}_{\text{gibbs}} = \frac{\delta \epsilon}{\delta \eta}$$

Equation 66

By scaling the Gibbs vector by two, the variance is expressed in radians squared, which is identical to angle errors in first-order terms. By establishing

$$\frac{\boldsymbol{a}_g}{2} = \frac{\delta \boldsymbol{\epsilon}}{\delta \eta}$$

Equation 67

Where $\boldsymbol{a}_g$ denotes a rotation such that

$$\boldsymbol{q} = \begin{bmatrix} \eta \\ \epsilon \end{bmatrix} = \begin{bmatrix} cos\frac{\phi}{2} \\ \boldsymbol{e} sin\frac{\phi}{2} \end{bmatrix}$$

Equation 68

$$\frac{\boldsymbol{a}_g}{2} = etan\frac{\phi}{2}$$

Equation 69

when e is a unit vector and ϕ denotes a rotational angle as stated in (equation 68) As seen in (equation 69), this parametrization assures that ϕ for small rotations, the size of a_g approximates (Markley, 2008).

From a_g, one can calculate the imaginary component $\boldsymbol{\epsilon}$ of the quaternion error as follows:

$$\boldsymbol{a}_g = 2\frac{\delta\boldsymbol{\epsilon}}{\delta\eta}$$
$$\boldsymbol{a}_g^2 = 4\frac{\delta\boldsymbol{\epsilon}^2}{\delta\eta^2} = 4\frac{\delta\boldsymbol{\epsilon}^2}{1-\delta\boldsymbol{\epsilon}^2}$$
$$\frac{\boldsymbol{a}_g^2}{4}(1-\delta\boldsymbol{\epsilon}^2) = \delta\boldsymbol{\epsilon}^2$$
$$\boldsymbol{a}_g^2 - \boldsymbol{a}_g^2\delta\boldsymbol{\epsilon}^2 - 4\delta\boldsymbol{\epsilon}^2 = 0$$
$$\delta\boldsymbol{\epsilon}^2\left[4+\boldsymbol{a}_g^2\right] = \boldsymbol{a}_g^2$$

Equation 70

Which at the end give

$$\delta\boldsymbol{\epsilon} = \sqrt{\frac{\boldsymbol{a}_g^2}{4+\boldsymbol{a}_g^2}} = \frac{\boldsymbol{a}_g}{\sqrt{4+\boldsymbol{a}_g^2}}$$

Equation 71

For now the quaternion c=error could be presented in term of a_g as:

$$\delta\boldsymbol{q}(\boldsymbol{a}_g) = \begin{bmatrix}\delta\eta\\ \delta\boldsymbol{\epsilon}\end{bmatrix} = \frac{1}{\sqrt{4+\boldsymbol{a}_g^2}}\begin{bmatrix}2\\ \boldsymbol{a}_g\end{bmatrix}$$

Equation 72

The Kalman filter equations are based on the discrete system explained in (equation 72). Consider the following model:

$$\delta\dot{x} = f(x,u) + Ew$$
$$\delta y = h(\delta x) + v$$

Equation 73

By defining

$$\delta x = \left[(\delta p^n)^T \quad (\delta v^n)^T \quad a_g^T \quad (\delta b_{ars})^T \quad (\delta b_{acc})^T\right]^T \quad 0.46$$

Equation 74

The system's non-linear equations will be derived.

The position error is denoted simply as

$$\delta\dot{p}_{b/n}^n = \delta v_{b/n}^n$$

Equation 75

The equations in Section equation 75, as well as the connection in (equation 74), are examined for the velocity error.

$$\begin{aligned}\delta\dot{v}_{b/n}^{n} = \;& \dot{v}_{b/n}^{n} - \dot{v}_{ins}^{n} \\ = \;& R(\dot{q})R\big(a_g\big)\big(f_{imu}^{b} - b_{ins,acc} - \delta b_{ins,acc} - w_{acc}\big) + g^{n} \\ & -R(\dot{q})\big(f_{imu}^{b} - b_{ins,acc}\big) - g^{n}\end{aligned}$$

Equation 76

By using $\boldsymbol{R}(\delta\epsilon) \approx \boldsymbol{I}_{3x3} + \boldsymbol{S}\big(\boldsymbol{a}_g\big)$, this can be approximated as

$$\begin{aligned}\approx \;& R(\dot{q})\Big(1 + S\big(a_g\big)\Big)\big(f_{imu}^{b} - b_{ins,acc} - \delta b_{ins,acc} - w_{acc}\big) \\ & -R(\hat{q})\big(f_{imu}^{b} - b_{ins,acc}\big) \\ = \;& -R(\hat{q})S\big(f_{imu}^{b} - b_{ins,acc} - \delta b_{ins,acc} - w_{acc}\big)a_g \\ & -R(\dot{q})\big(\delta b_{ins,acc} - w_{acc}\big)\end{aligned}$$

Equation 77

By substituting a_g in (equation 70), and by using (equation 71), the following expression for $\dot{a}_g$ is obtained:

$$\dot{a}_g = \Big(I_{3x3} + \frac{1}{4}a_g^{T}a_g\Big)\big(\omega_{b/n}^{b} - \omega_{ins}^{b}\big) - \frac{1}{2}S\big(\omega_{b/n}^{b} + \omega_{ins}^{b}\big)a_g$$

Equation 78

This expression is identical to the one in Markley (2008). Ignoring higher order terms, gives

$$\dot{a}_g \approx \big(\omega_{b/n}^{b} - \omega_{ins}^{b}\big) - \frac{1}{2}S\big(\omega_{b/n}^{b} + \omega_{ins}^{b}\big)a_g$$

Equation 79

From (equation 72) and (equation 73):

$$\begin{aligned}\omega_{b/n}^{b} &= \omega_{imu}^{b} - b_{ars}^{b} - w_{ars}^{b} \\ \omega_{ins}^{b} &= w_{imu}^{b} - b_{ins,ars}^{b}\end{aligned}$$

Equation 80

Which implies that

$$\begin{aligned}\omega_{b/n}^{b} + \omega_{ins}^{b} &= 2\omega_{imu}^{b} - b_{ars} - b_{ins,ars} - w_{ars}^{b} \\ \omega_{b/n}^{b} - \omega_{ins}^{b} &= -\delta b_{ars} - w_{ars}^{b}\end{aligned}$$

Equation 81

By substituting (equation 81) into (equation 82), the expression for a_g can be written as

$$\begin{aligned}\dot{a}_g &\approx -\delta b_{ars} - w_{ars}^{b} - -\frac{1}{2}S\big(2\omega_{imu}^{b} - b_{ars} - b_{ins,ars} - w_{ars}^{b}\big)a_g \\ \dot{a}_g &\approx -S\big(\omega_{imu}^{b} - b_{ins,ars}\big)a_g - \delta b_{ars} - w_{ars} + \frac{1}{2}S(\delta b_{ars} + w_{ars})a_g\end{aligned}$$

Equation 82

The bias errors are modeled as first order Gauss-Markov processes, which are simply given by

$$\delta\dot{b}_{ars} = -\frac{1}{T_{ars}}\delta b_{ars} + w_{b,ars}$$
$$\delta\dot{b}_{acc} = -\frac{1}{T_{acc}}\delta b_{acc} + w_{b,acc}$$

Equation 83

G. Measurement Equations

The vector of measurement is defined as

$$y = \left[\left(p^n_{b/n}\right)^T \quad \left(v^n_{b/n}\right)^T \quad \left(f^b_{imu}\right)^T \quad \left(m^b_{imu}\right)^T\right]^T$$

Equation 84

While the equivalent INS estimations result in

$$y_{ins} = \left[\left(p^n_{ins}\right)^T \quad \left(v^n_{ins}\right)^T \quad \left(f^b_{ins}\right)^T \quad \left(m^b_{ins}\right)^T\right]^T$$

Equation 85

The error between the measured values and the expected values from the INS is stated in the measurement equations. It is possible to express it in terms of the error state δx as follows:

$$\delta y = y - y_{ins} = h(\delta x) + v$$

Equation 86

The errors in position and velocity are easily expressed as

$$p^n_{b/n} - p_{ins} = \delta p^n_{b/n}$$
$$v^n_{b/n} - v_{ins} = \delta v^n_{b/n}$$

Equation 87

While the equation for magnetometer measurement may be written as

$$\begin{aligned} m^b_{imu} - m^b_{ins} &= \left[R\left(a_g\right)^T R(\hat{q})^T - R(\hat{q})^T\right] m^n + w_{mag} + b^b_{mag} \\ &= \left[R\left(a_g\right)^T - I_{3x3}\right] R(\hat{q})^T m^n + w_{mag} + b^b_{mag} \\ &\approx -S\left(a_g\right) R(\hat{q})^T m^n + w_{mag} + b^b_{mag} \end{aligned}$$

Equation 88

These measurement equations may be summed together and stated in the manner specified in (equation 86) as

$$\delta y = \begin{bmatrix} p_{b/n}^n - p_{ins} \\ v_{b/n}^n - v_{ins} \\ f_{imu}^b - f_{ins}^b \\ m_{imu}^b - f_{ins}^b \end{bmatrix} = \underbrace{\begin{bmatrix} \delta p_{b/n}^n \\ \delta v_{b/n}^n \\ -S(a_g)R(\hat{q})^T f_{ins}^n \\ -S(a_g)R(\hat{q})^T m^n + w_{mag} \end{bmatrix}}_{h(\delta x)} + \underbrace{\begin{bmatrix} w_{pos} \\ w_{vel} \\ w_{acc} + b_{acc}^b \\ w_{mag} + b_{mag}^b \end{bmatrix}}_{v}$$

Equation 89

While p_{ins}^n, v_{ins}^n, and m_{ins}^b may all be found directly from the Navigation equations. The estimation of $\boldsymbol{f}_{\text{ins}}^{\boldsymbol{b}}$ in the measurement equations will be accomplished via the use of two distinct approaches described below.

1. Estimation of $\boldsymbol{f}_{\text{ins}}^{\boldsymbol{b}}$

Because of f_{ins}^n cannot be directly determined from the navigation equations, two distinct estimate approaches will be discussed. The first entails designing a KF to act as a fast differentiator and estimating f_{ins}^n from the INS output by integrating p_{ins}^n and v_{ins}^n. The second approach is based on a fictitious measurement, which involves the computation of angular velocity. Figure 32 illustrates the two distinct approaches.

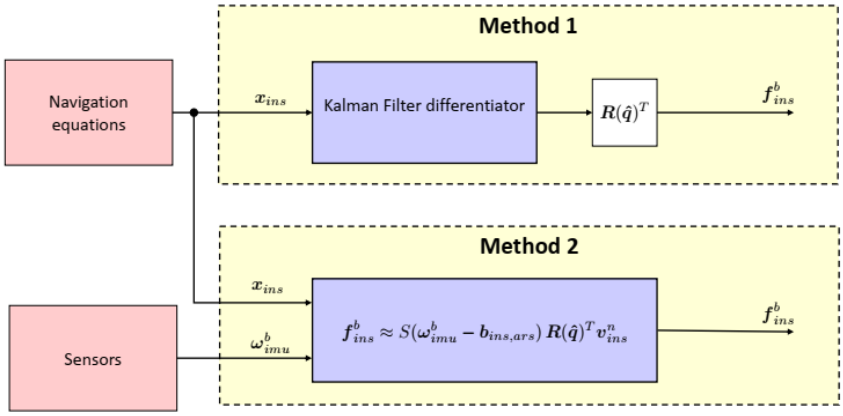

Figure 32 Illustrates two distinct ways for Estimation $\boldsymbol{f}_{\text{ins}}^{\boldsymbol{b}}$. The first technique integrates position and velocity using a rapid differentiator, while the second method employs fake measurements.

2. Method 1: The Kalman Filter differentiator

9-state KF will be used to estimate f_{ins}^n. The KF estimations f_{ins}^nusing the INS's location and velocity estimates p_{ins}^n and v_{ins}^n. In contrast to the KF outlined above, a straight linear KF is adequate.

For continuous time, the KF equations yield

$$\dot{\boldsymbol{x}} = \begin{bmatrix} \dot{\boldsymbol{p}}_{ins}^{n} \\ \dot{\boldsymbol{v}}_{ins}^{n} \\ \dot{\boldsymbol{f}}_{ins}^{n} \end{bmatrix} = \underbrace{\begin{bmatrix} 0 & \boldsymbol{I}_{3x3} & 0 \\ 0 & 0 & \boldsymbol{I}_{3x3} \\ 0 & 0 & 0 \end{bmatrix}}_{A} \begin{bmatrix} \boldsymbol{p}_{ins}^{n} \\ \boldsymbol{v}_{ins}^{n} \\ \boldsymbol{f}_{ins}^{n} \end{bmatrix} + \underbrace{\begin{bmatrix} 0_{3x1} \\ I_{3x1} \\ 0_{3x1} \end{bmatrix}}_{B} g^{n} + \underbrace{\begin{bmatrix} 0 \\ 0 \\ \boldsymbol{I}_{3x3} \end{bmatrix}}_{E} \boldsymbol{w}_{acc}$$

Equation 90

with measurements

$$y = \underbrace{\begin{bmatrix} \boldsymbol{I}_{3x3} & \boldsymbol{0}_{3x3} & \boldsymbol{0}_{3x3} \\ \boldsymbol{0}_{3x3} & \boldsymbol{I}_{3x3} & \boldsymbol{0}_{3x3} \end{bmatrix}}_{C} x + \begin{bmatrix} v_{pos} \\ v_{vel} \end{bmatrix}$$

Equation 91

Where v_* and w_* are white noise, $g^n = u = [0 \quad 0 \quad 9.81\ \mathrm{m/s^2}]^T$ is the typical acceleration of gravity on Earth.

The Kalman gain and co-variance updates are obtained by

$$\begin{aligned} \boldsymbol{K}[k] &= \hat{\boldsymbol{P}}^{- -}[k]\boldsymbol{C}_d^T[k]\left(\boldsymbol{C}_d[k]\hat{\boldsymbol{P}}^{-}[k]\boldsymbol{C}_d^T[k] + \boldsymbol{R}_d[k]\right)^{-1} \\ \hat{\boldsymbol{P}}^{+}[k] &= (\boldsymbol{I} - \boldsymbol{K}[k]\boldsymbol{C}_d[k])\hat{\boldsymbol{P}}^{-}[k](\boldsymbol{I} - \boldsymbol{K}[k]\boldsymbol{C}_d[k])^T + \boldsymbol{K}[k]\boldsymbol{R}[k]\boldsymbol{K}^T[k] \\ \hat{\boldsymbol{P}}^{- -}k+1] &= \boldsymbol{C}_d[k]\hat{\boldsymbol{P}}^{+}[k]\boldsymbol{C}_d^{+}[k] + \boldsymbol{E}_d[k]\boldsymbol{Q}_d[k]\boldsymbol{E}_d[k]^T \end{aligned}$$

Equation 92

The state corrections yields

$$\hat{\boldsymbol{x}}^{+}[k] = \hat{\boldsymbol{x}}^{-}[k] + \boldsymbol{K}[k](y[k] - \boldsymbol{C}_d\hat{\boldsymbol{x}}^{-}[k])$$

Equation 93

and finally, the predicted new states are as follows:

$$\hat{\boldsymbol{x}}^{-}[k+1] = \boldsymbol{A}_d\hat{\boldsymbol{x}}^{+}[k] + \boldsymbol{B}_d[k]\boldsymbol{u}[k]$$

Equation 94

The filter's performance can be seen in Figure 33, which demonstrates that the filter accurately monitors the real value of f_{ins}^{n}.

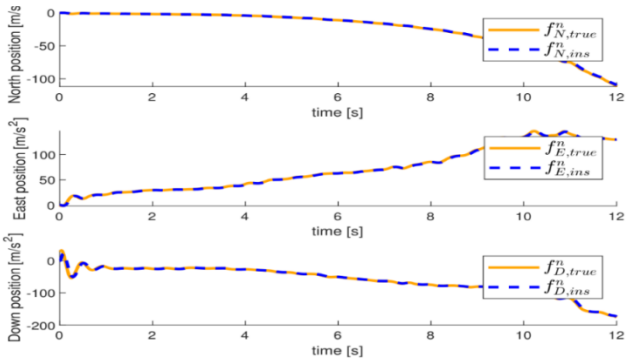

Figure 33 f_{ins}^{n}estimation using method 1.

For method 1, the accelerometer measurement equation is as follows:

$$\begin{aligned} \boldsymbol{f}_{imu}^{b} - \boldsymbol{f}_{ins}^{b} &= \left[\boldsymbol{R}\left(\boldsymbol{a}_g\right)^T \boldsymbol{R}(\hat{\boldsymbol{q}})^T - \boldsymbol{R}(\hat{\boldsymbol{q}})^T\right] \boldsymbol{f}_{ins}^{n} + \boldsymbol{w}_{acc} + \boldsymbol{b}_{acc}^{b} - \boldsymbol{b}_{acc,ins}^{b} \\ &= \left[\boldsymbol{R}\left(\boldsymbol{a}_g\right)^T - \boldsymbol{I}_{3x3}\right] \boldsymbol{R}(\hat{\boldsymbol{q}})^T \boldsymbol{f}_{ins}^{n} + \boldsymbol{w}_{acc} + \delta \boldsymbol{b}_{acc} \\ &\approx -\boldsymbol{S}\left(\boldsymbol{a}_g\right) \boldsymbol{R}(\hat{\boldsymbol{q}})^T \boldsymbol{f}_{ins}^{n} + \boldsymbol{w}_{acc} + \delta \boldsymbol{b}_{acc} \\ &= \boldsymbol{S}(\boldsymbol{R}(\hat{\boldsymbol{q}})^T \boldsymbol{f}_{ins}^{n}) \boldsymbol{a}_g + \boldsymbol{w}_{acc} + \delta \boldsymbol{b}_{acc} \end{aligned}$$

Equation 95

3. Method 2: Pseudo measurement

Rather than utilizing the differentiator given in the preceding section, the following equation may be used to estimate of $\boldsymbol{f}_{\text{ins}}^{b}$.

$$\begin{aligned} \boldsymbol{v}_{ins}^{n} &= \boldsymbol{R}(\hat{\boldsymbol{q}}) \boldsymbol{v}_{ins}^{b} \\ \boldsymbol{f}_{ins}^{b} = \dot{\boldsymbol{v}}_{ins}^{n} &= \dot{\boldsymbol{R}}(\hat{\boldsymbol{q}}) \boldsymbol{v}_{ins}^{b} + \boldsymbol{R}(\hat{\boldsymbol{q}}) \dot{\boldsymbol{v}}_{ins}^{b} \\ &= \boldsymbol{R}(\hat{\boldsymbol{q}}) \left[\dot{\boldsymbol{v}}_{ins}^{b} + S\left(\omega_{imu}^{b} - \boldsymbol{b}_{ins\,,\,ars}\right) \boldsymbol{v}_{ins}^{b}\right] \end{aligned}$$

Equation 96

By assuming that $\dot{\boldsymbol{v}}_{\text{ins}}^{b} << \boldsymbol{v}_{\text{ins}}^{b}$, the formula may be reduced further to

$$\dot{v}_{ins}^{n} \approx \boldsymbol{R}(\hat{\boldsymbol{q}}) S\left(\omega_{imu}^{b} - b_{ins,ars}\right) v_{ins}^{b}$$

Equation 97

This assumption may be incorrect during stages in which the interceptor makes rapid maneuvers. When (v _"ins " n) is much more than the real value of (f "ins " b), this measurement equation will exhibit oscillations.

The measurement equation for the second approach will be somewhat different. The accelerometer measurement equation for technique 2 produces the following results.

Rather than utilizing the differentiator given in the preceding section, the following equation may be used to estimate (f "ins " b).

This assumption may be incorrect during stages in which the interceptor makes rapid maneuvers. When $\dot{v}_{\text{ins}}^{n}$) is much more than the real value of $\boldsymbol{f}_{\text{ins}}^{b}$, this measurement equation will exhibit oscillations.

The measurement equation for the second approach will be somewhat different. The accelerometer measurement equation for technique 2 produces the following results.

$$\boldsymbol{f}^{b}_{\text{imu}} - \boldsymbol{f}^{b}_{\text{ins}} = \left[\boldsymbol{R}\left(\boldsymbol{a}_g\right)^{T}\boldsymbol{R}(\hat{\boldsymbol{q}})^{T} - \boldsymbol{R}(\hat{\boldsymbol{q}})^{T}\right]\boldsymbol{f}^{n}_{\text{ins}} + \boldsymbol{w}_{\text{acc}} + \boldsymbol{b}^{b}_{\text{acc}} - \boldsymbol{b}^{b}_{\text{acc , ins}}$$

Equation 98

$$\approx \left[\boldsymbol{R}\left(\boldsymbol{a}_g\right)^{T} - \boldsymbol{I}_{3x3}\right]\boldsymbol{R}(\hat{\boldsymbol{q}})^{T}\boldsymbol{R}(\hat{\boldsymbol{q}})S\left(\omega^{b}_{imu} - b_{ins,ars}\right)v^{b}_{ins} + w_{acc} + \delta b_{acc}$$

Equation 99

$$\approx S\left(\boldsymbol{\omega}^{b}_{imu} - \boldsymbol{b}_{ins,ars}\right)\boldsymbol{v}^{b}_{ins}\boldsymbol{a}_g + \boldsymbol{w}_{acc} + \delta\boldsymbol{b}_{acc}$$

Equation 100

4. Comparisons of Methods 1 and 2

The inaccuracies in state estimate are shown in Table 2 for the two distinct approaches mentioned in *Estimation of* $\boldsymbol{f}^{\boldsymbol{b}}_{ins}$ paragraph 8.7.1. The table demonstrates a reasonable degree of equivalence between the methodologies.

The second technique achieves a much smaller final attitude estimate error than the first method. This might be because the second approach directly incorporates the angular velocity into the measurement equation.

By contrast, the particular force provides no information regarding the yaw angle. Both the roll and pitch angles have an effect on the contribution of gravity to the particular force vector. On the other side, the yaw angle will remain constant. This will work against the first technique.

Additionally, the RMS values for the second technique are significantly larger, which is likely due to ocillations in the (f "ins " b) estimates induced by large values of $\dot{v}^{n}_{\text{ins}}$.

Figure 34 illustrates the mistake in bias calculations when two distinct approaches are used. The mistakes are calculated in accordance with.

Table 2 Two distinct estimation approaches f_{ins}^{b} are provided in subsections 2 and Estimation of f_{ins}^{b} for use in the MEKF measurement equation. The table summarizes the estimate errors for the various states.

	Attitude (deg)			Position (m)			Velocity (m/s)		
	roll	pitch	yaw	north	east	down	north	east	down
method 1									
max error	-0.93	-2.0	-2.3	-0.33	0.57	-0.88	-0.29	-0.38	-0.45
final error	0.17	-0.28	0.12	-0.33	0.57	-0.88	0.087	0.14	0.43
RMS	0.44	1.1	1.1	0.12	0.23	0.48	0.11	0.1	0.11
method 2									
max error	-0.87	-2.5	2.4	-0.34	0.59	-0.83	-0.29	-0.38	-0.45
final error	0.13	-0.2	9.3e−3	-0.34	0.59	-0.83	0.1	0.16	0.43
RMS	0.35	1.5	1.4	0.12	0.24	0.46	0.12	0.099	0.12

Where N is the number of bias samples and M denotes the dimension of the bias vector. Mequals three for both acceleration and gyro bias (roll, pitch, yaw).

For instance, $\boldsymbol{b}_{ars,ins}(2,35)$ represents the 35th bias sample used in the INS estimation of the pitch bias.

Take note of how the gyro bias converges more faster with approach 1 than with 2. This may be connected to the assumption made in (equation 94). When $\dot{v}_{ins}^{n}$, the measurement equation is wrong, causing the bias estimate to converge more slowly.

There is reason to suspect that this may also have an effect on the accuracy of state estimates. According to Table 2, the RMS values for the attitude error for method 2 are greater for pitch and yaw angles, but significantly lower for roll angles. The fact that procedure 2 consistently produces larger RMS values substantiates the above argument, since the second technique is more sensitive due to the huge values of $\dot{v}_{ins}^{n}$.

The first technique will be employed for the remainder of the simulations in this thesis, since it exhibits superior bias estimation performance.

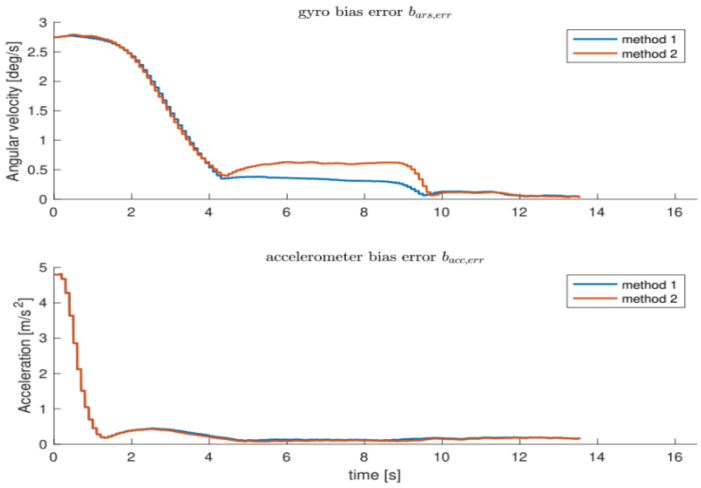

Figure 34 The inaccuracy in bias estimate using the two distinct approaches mentioned is compared.

H. Target Tracking

Inertial guidance systems may be adequate to direct ballistic missiles to a fixed-coordinate target, such as a predetermined location on the earth. The issue is that these algorithms are inadequate for steering toward moving objects with unknown coordinates, such as hostile cruise missiles or even other threats. When the target coordinates are unknown prior to the missile launch, real-time target detection and associated maneuvering modifications are necessary for interception. The three stages of a missile's flight are the boost, midcourse, and terminal. During the boost phase, onboard inertial guidance systems are often employed to compute an end-of-boost arrival location. Off-board target tracking techniques are often utilized throughout the midcourse phase of the missile's flight to generate the appropriate trajectory and move the missile closer to the target. When the missile approaches the goal, onboard sensors typically take control as the missile reaches terminal phase. The terminal phase may begin anywhere between tens of seconds and a few seconds before to intercept, depends on the missile capabilities and mission aim. Due to the possibility of residual errors during the boost and midcourse phases, the terminal phase is used to decrease the interceptor's ultimate distance from the target to a set value (Paluboo, 2010).

J. Homing Systems

There are Three broad categories of homing systems exist:

1. Passive Homing Systems

A passive system is intended to detect natural emanations or radiation such as heat, light, and sound waves via measurement. Thus, the passive system is based on determining the angular orientation of the target relative to the missile by analyzing the properties of the target's radiation. Passive systems do not offer information on the target range or closing velocity, which is a drawback since certain guiding approaches, such as PN, need this information. Infrared and radio-frequency seekers are also examples of passive systems Palumbo (2010).

2. Semiactive Homing Systems

While a passive system relies entirely on the target's generated signals, a semiactive system relies on a reflected wave emitted by a beam of light, laser, infrared, or radio frequency from an external source, such as a radar. Along with angular direction, semiactive systems may offer missile target closing velocity and angular direction to the target, which can aid overall guiding accuracy in specific cases. Due to the fact that the radiated signal is generated outside, the semiactive system has the benefit of requiring no extra size or weight on the missile. The Palumbo (2010). The lighting must be present at all times when the missile Siouris is in flight (2004).

3. Active Homing Systems

In an active system, the missile's on-board sensor illuminates and tracks the target. A benefit is that the active system may offer measurements of relative range, range rate, and angular orientation. Additional information may further increase the advice accuracy. Due to the fact that the missile contains the tracking technology, the active system comes at a significant cost in terms of increased power consumption and weight. This often limits the employment of active systems to the terminal phase of flight, when another method of guidance has delivered the missile within a short distance of the target Palumbo et al (2010c).

4. Filter for Target Tracking

By assuming a semiactive or active homing system, the measured quantities may be utilized to provide estimates of the missile's relative location to the target. As Palumbo et al. (2010b) demonstrate, relative location "data" may be derived using noisy LOS angle and relative range measurements between the interceptor and target (2010c).

Since a result, these observations must be filtered, and estimates of the relative velocity must be derived from these noisy pseudo-measurements of the relative position, as the PN-algorithm requires these measurements. Certain guiding rules additionally demand measurements of the target acceleration perpendicular to the missile target line of sight, which will be computed using the relative position data. To do this, a linear KF with nine states identical to the one described in *Estimation of* $\boldsymbol{f}_{ins}^{\boldsymbol{b}}$ Section will be employed. The stochastic continuous-time model produces the following results:

$$\begin{bmatrix} \dot{p}_r(t) \\ \dot{v}_r(t) \\ \dot{\boldsymbol{a}}_T(t) \end{bmatrix} = \begin{bmatrix} 0 & \boldsymbol{I}_{3x3} & 0 \\ 0 & 0 & \boldsymbol{I}_{3x3} \\ 0 & 0 & 0 \end{bmatrix} \begin{bmatrix} \boldsymbol{p}_r(t) \\ v_r(t) \\ \boldsymbol{a}_T(t) \end{bmatrix} + \begin{bmatrix} 0 \\ -\boldsymbol{1}_{3x1} \\ 0 \end{bmatrix} \boldsymbol{a}_I + \begin{bmatrix} 0 \\ 0 \\ \boldsymbol{I}_{3x3} \end{bmatrix} \boldsymbol{w}_{T,acc}$$

Equation 101

Based on measurements

$$y = [\boldsymbol{I}_{3x3} \quad 0 \quad 0] \begin{bmatrix} \boldsymbol{p}_r(t) \\ v_r(t) \\ \boldsymbol{a_T}(t) \end{bmatrix} + v_{r,pos}$$

Equation 102

The comparative position and velocity are p_r and v_r, respectively, while the interceptor's acceleration is a_I.white noise described as a wiener process is $v_{r,pos}$.

The following model can be created through discretizing:

$$\begin{bmatrix} \dot{p}_r[k+1] \\ \dot{v}_r[k+1] \\ \dot{a}_T[k+1] \end{bmatrix} = \boldsymbol{I}_{9x9} + h \begin{bmatrix} 0 & \boldsymbol{I}_{3x3} & 0 \\ 0 & 0 & \boldsymbol{I}_{3x3} \\ 0 & 0 & 0 \end{bmatrix} \begin{bmatrix} \boldsymbol{p}_r[k] \\ v_r[k] \\ \boldsymbol{a_T}[k] \end{bmatrix} + h \begin{bmatrix} 0 \\ -\boldsymbol{1}_{3x1} \\ 0 \end{bmatrix} \boldsymbol{a}_I + h \begin{bmatrix} 0 \\ 0 \\ \boldsymbol{I}_{3x3} \end{bmatrix} \boldsymbol{w}_{T,acc}$$

Equation 103

The Kalman gain, covariance and new state updates are computed as explained befor.

For initialization of the filter, four position samples $\{\boldsymbol{p}_m(1), \boldsymbol{p}_m(2), \boldsymbol{p}_m(3), \boldsymbol{p}_m(4)\}$ are acquired, so that the starting values may be calculated as (Palumbo et al., 2010c)

$$\begin{aligned} \hat{\boldsymbol{p}}_r[0] &= \sum_{i=1}^{4} \frac{\boldsymbol{p}_m(i)}{4} \\ \hat{\boldsymbol{v}}_r[0] &= \frac{\boldsymbol{p}_m(4) - \boldsymbol{p}_m(3)}{\Delta t} \\ \hat{\boldsymbol{a}}_T[0] &= \frac{\hat{\boldsymbol{v}}_r[0]}{2\Delta t} - \frac{\boldsymbol{p}_m(2) - \boldsymbol{p}_m(1)}{2\Delta t^2} \end{aligned}$$

Equation 104

where Δt is the interval between position sample measurements.

IX. GUIDANCE SYSTEM

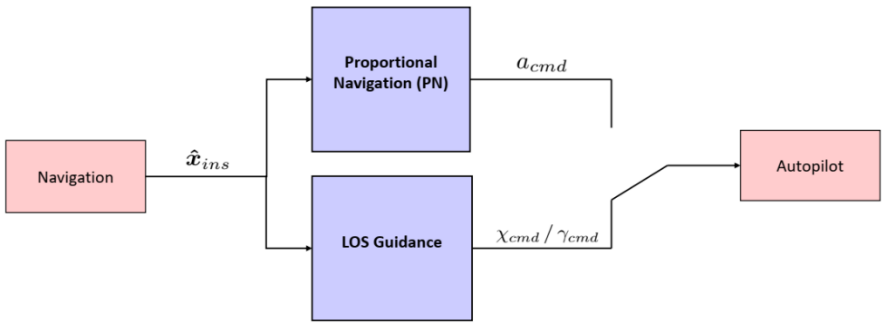

Figure 35 Two main guidance laws are applied.

A. Introduction

Two main guidance laws are applied in Figure 35. The first is a state-of-the-art proportional navigation law, whereas the second is a line-of-sight guiding law.

The guidance law is primarily what differentiates an unguided projectile from a guided missile. The guidance law's principal role is to create steering guidance orders in response to inputs regarding the missile and target. The guiding rules are often expressed in terms of the amount and direction of the normal acceleration that the missile must apply (NPTEL, 2012).

1. Sight Line (LOS)

The LOS vector is the basis for some of the most famous guiding rules (NPTEL, 2012). The objective is to maintain the missile on a line between the reference point and the target by guiding it on a LOS path. The vector between the waypoint/target and a reference point is defined as the line-of-sight vector. The reference point may be a ground-based control station, but if the missile's target tracker is onboard, the LOS vector will be the straight line between the missile and the target.

B. Proportional Navigation (PN)

Perhaps the most often employed guiding rule in contemporary missile guidance is proportional navigation. The guiding legislation is unrelated to navigation. The rather inaccurate moniker stems from the limited language of instruction literature during its formative years (NPTEL, 2012).

When the interceptor and target are on a collision path, there is no relative velocity between the two bodies perpendicular to their line of sight (LOS) vector. This indicates that the LOS rate is 0, yet the closing velocity is positive. This is the concept behind the PN law: if the LOS rate is greater than zero at any point in time, the guidance law should direct the autopilot to perform a fin deflection to cancel the LOS rate (NPTEL, 2012). Assuming a planar engagement, the commanded missile acceleration is defined as a (M c) (Palumbo et al., 2010a)

$$a_{M_c} = NV_c\dot{\lambda}$$

Equation 105

Where N is termed the navigation constant, V_c is the closing velocity and $\dot{\lambda}$ is the LOS rate in an inertial reference frame. For a three-dimensional instance, the LOS rate must simply be measured by two independent devices mutually perpendicular to the sensor boresight. Information regarding the LOS rate $\dot{\lambda}$ and closing velocity V_c are generated based on target sensor readings that are available. To achieve excellent estimations, a semi-active or active system with on-board sensors are essential. From (3), (4) and (6) in Palumbo et al. (2010a) (2010a)

$$\overline{\boldsymbol{v}} \triangleq \frac{\partial}{\partial t}\overline{\boldsymbol{r}} = \dot{R}\overline{\mathbf{1}}_{\boldsymbol{r}} + R\frac{\partial}{\partial t}\overline{\mathbf{1}}_{\boldsymbol{r}}$$
$$\overline{\boldsymbol{n}} \triangleq \frac{\partial}{\partial t}\overline{\mathbf{1}}_r$$
$$\overline{\mathbf{1}}_\omega \triangleq \overline{\mathbf{1}}_r \times \overline{\mathbf{1}}_n$$

Equation 106

where $\overline{\boldsymbol{v}}$ is the relative velocity, R is the distance, $\overline{\boldsymbol{r}}$ is the LOS vector between the missile and target. $\bar{n}$ is the LOS rate vector. $\overline{\mathbf{1}}_*$ is a unit vector. These vectors are all illustrated in figure 36 (Palumbo et al., 2010a).

By combining (equation 106) we could get:

$$\begin{aligned}\bar{\boldsymbol{v}} &= \dot{R}\bar{\mathbf{1}}_r + R|\bar{\boldsymbol{n}}|\bar{\mathbf{1}}_n \\ \bar{\mathbf{1}}_r \times \bar{\boldsymbol{v}} &= \dot{R}(\bar{\mathbf{1}}_r \times \bar{\mathbf{1}}_r) + R|\bar{\boldsymbol{n}}|(\bar{\mathbf{1}}_r \times \bar{\mathbf{1}}_n) \\ \bar{\mathbf{1}}_r \times \bar{\boldsymbol{v}} &= R|\bar{\boldsymbol{n}}|(\bar{\mathbf{1}}_r \times \bar{\mathbf{1}}_n) \\ \bar{\mathbf{1}}_r \times \bar{\boldsymbol{v}} &= R|\bar{\boldsymbol{n}}|\bar{\mathbf{1}}_w\end{aligned}$$

Equation 107

From equation 107 $\bar{\mathbf{1}}_\omega \triangleq \bar{\mathbf{1}}_r \times \bar{\mathbf{1}}_n$ can be rewritten as

$$\bar{\mathbf{1}}_w \times \bar{\mathbf{1}}_r = \bar{\mathbf{1}}_n$$

Equation 108

the LOS rate vector $\bar{n}$ yields

$$\bar{\boldsymbol{n}} = \dot{\lambda} = (\bar{\mathbf{1}}_r \times \bar{\boldsymbol{v}}) \times \frac{\bar{\mathbf{1}}_r}{R}$$

Equation 109

Finally, it follows from 6.5 that the range rate can be expressed as

$$\dot{R} = -V_c = \bar{\boldsymbol{v}} \cdot \bar{\mathbf{1}}_r$$

Equation 110

This shows how the required parameters for the PN law can be derived by the use of relative position and relative velocity measurements obtained from a semi-active or active seeker.

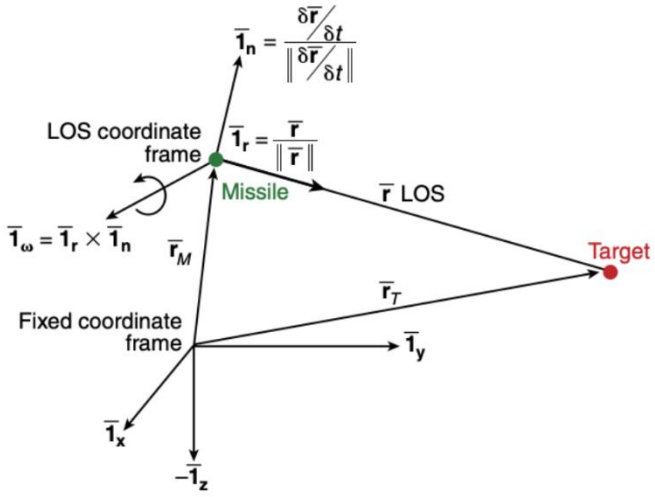

Figure 36 The LOS coordinate frame was utilized to derive the PN law.

C. LOS Guidance with Course and Flight-Path-Angle Commands

While the PN algorithm requires both relative position and velocity information, the course and flight-path-angle autopilot designs only on relative position information. This enables the employment of low-cost sensors on the ground, as well as monitoring threats farther away from the asset/interceptor than is feasible with on-board sensors.

It is very beneficial to make the software as basic as feasible in a real system. Using the autopilot in conjunction with the course and flight-path-angle instructions described in (chapter 4 control system section), an intuitive design based on trigonometric relationships is created. While the majority of conventional LOS guidance laws provide acceleration or angular velocity instructions (NPTEL, 2012), this guidance law generates direct commands for the desired course and flight path angle. The concept has a strong resemblance to the enclosure-based steering described in Section coming part for waypoint tracking.

In Proportional Navigation (PN) Section, it was shown how the PN law requires relative velocity information and generates acceleration orders rather than course and flight-path-angle commands for computing fin deflections. One benefit of this strategy is the ability to more easily manage the missile's turning rate. This makes the PN law more resistant to adversaries performing evasive and unexpected maneuvers, in comparison to a system that does not directly include velocity information into fin deflection command calculation. By switching from LOS to PN guiding law when the interceptor approaches the target, i.e. enters the terminal phase of the flight, the interceptor's likelihood of interception may be increased. Due to the fact that tracking accuracy diminishes as the target moves away from the control station, the likelihood is that the tracking is not accurate enough to result in an interception (Palumbo et al., 2010a). This issue might be prevented by switching to on-board sensors at the terminal phase.

1. Enclosure Based Steering for Waypoint Tracking

Numerous approaches for tracking paths and waypoints are based on LOS steering principles. The objective, while considering the vertical plane, is to appropriately give a value to to $\chi(t)$ in order to acquire sufficient steering control. One of these techniques is known as enclosure-based steering. By considering a

circle with sufficient large radius $R > 0$, enclosing $\boldsymbol{p^n} = [x, y]^T$, two intersections on the straight line between the last and next waypoint are obtained. The method computes desired course angle χ_d as

$$\chi_d(t) = atan\,2(y_{los} - y(t), x_{los} - x(t))$$

Equation 111

where

$$[[x_{los} - x(t)]^2 + [[y_{los} - y(t)]^2 = R^2$$

Equation 112

$$tan(\alpha_k) = \frac{y_{los} - y_k}{x_{los} - x_k} = constant$$

Equation 113

must be solved in order to get $\boldsymbol{p}_{\text{los}}^{n}$ Fossen (2011). A submarine travelling towards a waypoint employing enclosure-based steering is depicted in figure 37. This well-established technique for waypoint tracking reflects the essential principles for constructing the target tracking guiding law given below.

The LOS vector is often described in missile guidance as the straight line between a ground station and the target Fossen (2011). This is in contrast to Figure 37 (Fossen, 2011), which defines the LOS vector as the straight line between the marine vessel and the next waypoint. Additionally, the goal location is no longer fixed. The fundamental premise is to steer the missile in a straight route between the target/threat and the control point/launch station.

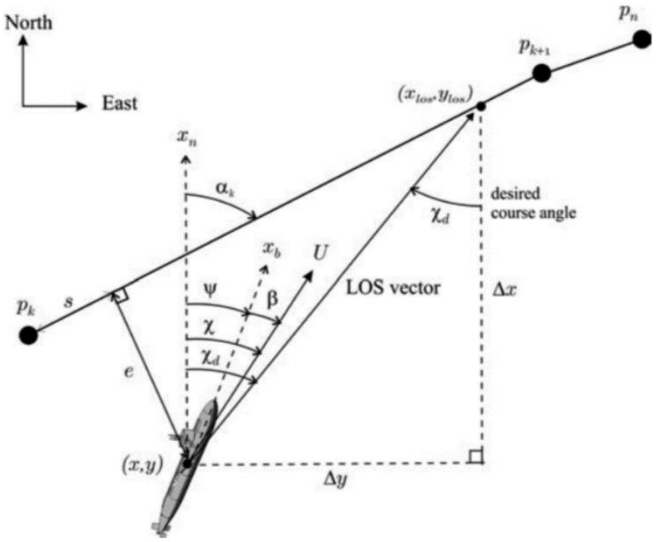

Figure 37 Encolsure based steering

LOS guidance tracking equations, like those for course and flight path angle-controlled autopilots, assume decoupling between the north/down and north/east planes. The trigonometric relationship between the launch platform, target, and interceptor is depicted in Figure 38. The interceptor's position is denoted pI = (xI, yI, zI), the threat position is pT = (xT , yT , zT) and the launch platform is pL = (xL, yL, zL). The interceptor's position decomposed in the north/east plane is given as $P_{I_{xy}}$.

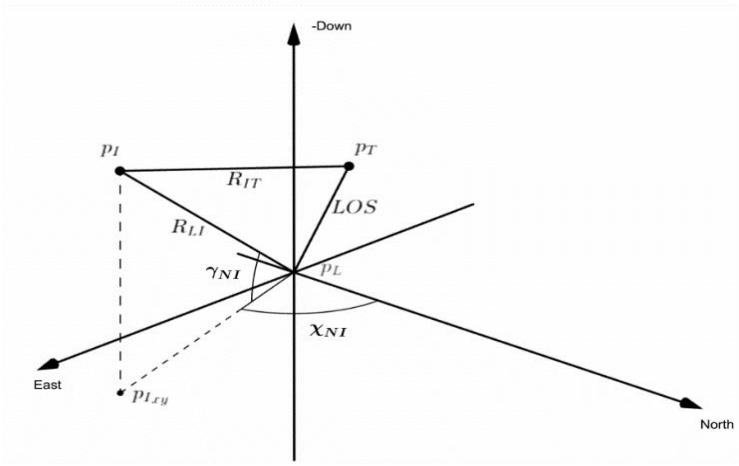

Figure 38 The guidance system decomposed in the horizontal plane.

2. Vertical Guidance System

The angles between north, threat and interception in the vertical plane are determined as

$$\begin{aligned} \gamma_{NT} &= sin^{-1}\left(\frac{z_T - z_L}{|p_T - p_L|}\right) \\ \gamma_{NI} &= sin^{-1}\left(\frac{z_I - z_L}{|p_I - p_L|}\right) \\ \theta_v &= \gamma_{NI} - \gamma_{NT} \end{aligned}$$

Equation 114

where $p_c = (x_c, y_c, z_c)$ is the vertical reference location in the vertical plane from which the commanded flight path angle is calculated. The vertical distance between both the launch platform and also the interceptor is

$$R_{LIv} = cos(\chi_{NI}) R_{LI}$$

Equation 115

whereas the interceptor's distance from the attacker is

$$R_{ITv} = \sqrt{(x_T - x_I)^2 + (z_T - z_I)^2}$$

Equation 116

Additionally, , e_v, r_v, and the required controlling flight path angle _c are determined as follows:

$$\begin{aligned} e_v &= sin(\theta_v) R_{LIv} \\ r_v &= \sqrt{R_{LIv}^2 - e_v^2} \\ |p_c - p_L| &= r_v + k_v \sqrt{R_{ITv}^2 - e_v^2} \\ z_c &= sin(\gamma_{NT}) |p_c - p_L| \\ \gamma_c &= -atan\,2(z_c - z_I, x_c - x_I) \end{aligned}$$

Equation 117

where k_v is used to adjust what point on the LOS vector between the launch platform and threat that the interceptor will aim at.

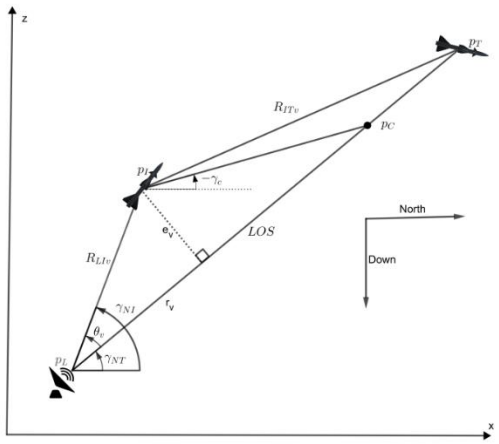

Figure 39 The guidance system decomposed in the vertical plane.

3. Horizontal Guidance Systems

In the horizontal plane, the angles between north, threat, and interceptor are derived as

$$\begin{aligned} \chi_{NT} &= tan^{-1}\left(\frac{y_T - y_L}{x_T - x_L}\right) \\ \chi_{NI} &= tan^{-1}\left(\frac{y_I - y_L}{x_I - x_L}\right) \\ \psi_h &= \chi_{NT} - \chi_{NI} \end{aligned}$$

Equation 118

where $p_c = (x_c, y_c, z_c)$ is the vertical reference location in the vertical plane from which the commanded flight path angle is calculated. The horizontal distance between the launch platform and the interceptor is

$$R_{LIh} = cos(\gamma_{NI}) R_{LI}$$

Equation 119

while the distance between the interceptor and threat is

$$R_{ITh} = cos(\gamma_{NI})\sqrt{(x_T - x_I)^2 + (y_T - y_I)^2}$$

Equation 120

Furthermore, e_h, r_h and ultimately the necessary commanding flight path angle χ_c is determined as

$$\begin{aligned} e_h &= sin(\psi_h)R_{LIh} \\ r_h &= \sqrt{R_{LIh}^2 - e_h^2} \\ |p_c - p_L| &= r_h + k_h\sqrt{R_{ITh}^2 - e_h^2} \\ z_c &= sin(\chi_{NT})|p_c - p_L| \\ \chi_c &= atan\,2(y_c - y_I, x_c - x_I) \end{aligned}$$

Equation 121

where k_h is used to adjust what point on the LOS vector between the launch platform and threat that the interceptor will aim at.

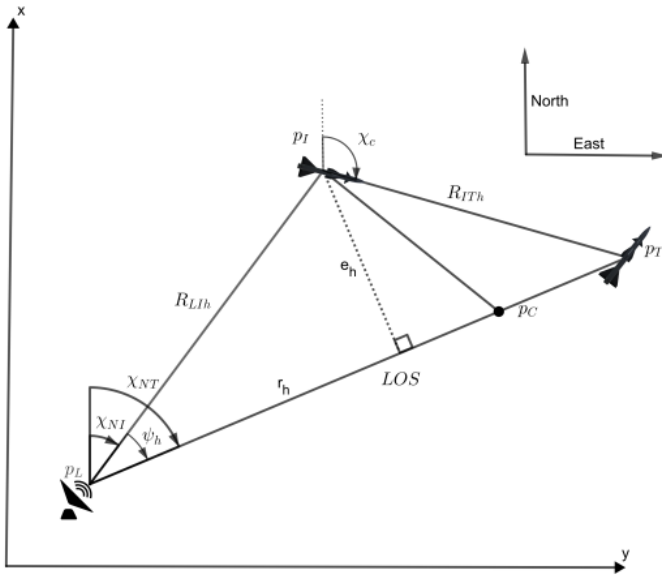

Figure 40 The guidance system decomposed in the horizontal plane.

4. Future Target Position Estimation

As mentioned above, the guidance system directs the missile in a straight path between the launch platform and the target. As long as the target has a velocity greater than zero, the missile will follow a plainly non-optimal trajectory in terms of total distance traveled.

If the target location is to be estimated in the future, the guiding law may be modified to follow a point ahead of the target. By defining $\Delta t := t^* - t$ where t denotes the present time and t^*denotes a future time, the target's location at time t^*may be approximated as

$$p_T(t^*) = p_T(t) + v_T(t)\Delta t$$

Equation 122

Δt will be selected as the amount of time required for the missile to intercept the target or reach the Closest Point of Approach (CPA). This is referred to in literature as time-to-go t go (Palumbo et al., 2010" " b). The engagement geometry between the missile and the target is shown in Figure 40.

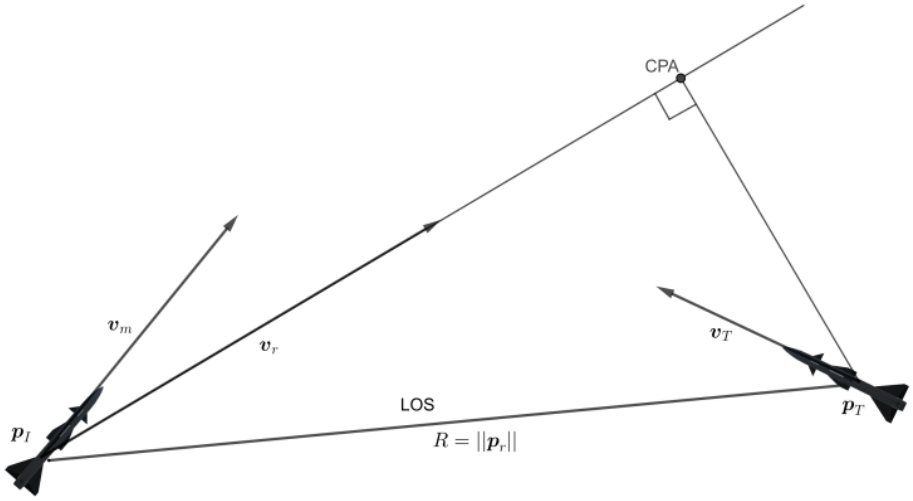

Figure 41 Geometry of missile-target engagement.

By specifying the relative position as $\boldsymbol{p}_r := p_T - p_I$ and the relative velocity as $\boldsymbol{v}_r := v_T - v_I$, the future target-missile relative position at time t^*can be expressed as follows (Palumbo et al., 2010" " b):

$$\bar{\boldsymbol{r}}(t^*) = \bar{\boldsymbol{r}}(t) + \bar{\boldsymbol{v}}(t)\Delta t$$

Equation 123

By inspecting figure 41, illustrated by the parpendicual line between the target and CPA, it is easy to see that the following condition holds:

$$\bar{\boldsymbol{r}}(t^*) \cdot \bar{\boldsymbol{v}}(t^*) = 0$$

Equation 124

By combining (0equation 123) and (equation 124), and by assuming constant velocity, the expression for $t_{go} := \Delta t$ yields

$$t_{go} = -\frac{\boldsymbol{p}_r(t) \cdot \boldsymbol{v}_r(t)}{\boldsymbol{v}_r(t) \cdot \boldsymbol{v}_r(t)}$$

Equation 125

After obtaining an estimate of t_{go}, the expected location of the target at may be calculated using (equation 122) as

$$\tilde{p}_T = p_T(t) + v_T(t)t_{go}$$

Equation 126

where $\tilde{p}_T$ denotes the expected location of the target at the time of closest approach, assuming that both the missile and the target are travelling at the same velocity.

While the prediction makes use of relative velocity information, the calculation of $t_{go}$is only used as a rough reference for the future estimation of the target's position.

This alleviates the requirement for exact measurements. As a result, it is assumed that the KF calculated in Target- Tracking filter Section from on-ground measurements provides a reasonable approximation of the relative velocity. On the other hand, the decreased precision could result in the interceptor missing the target during the terminal phase. The PN law places a higher premium on accuracy of estimates because it is directly involved in calculating the commanded acceleration, necessitating the use of on-board sensors.

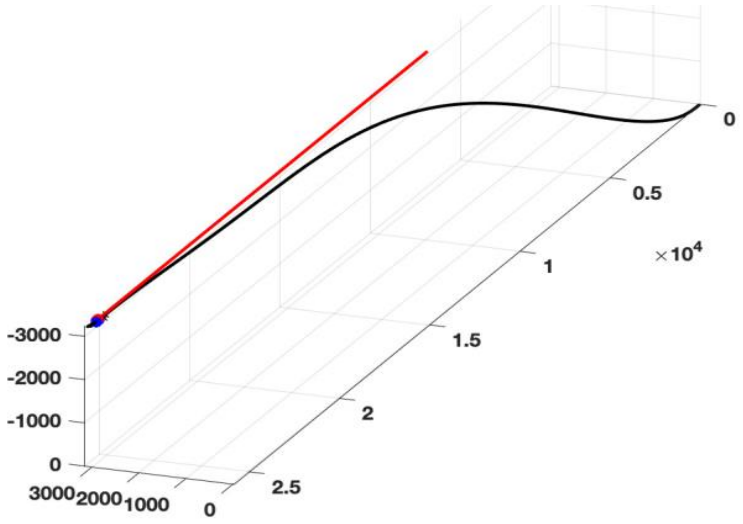

Figure 42 Missile detecting the current target position, p_T. Interception time: 8.725 sec.

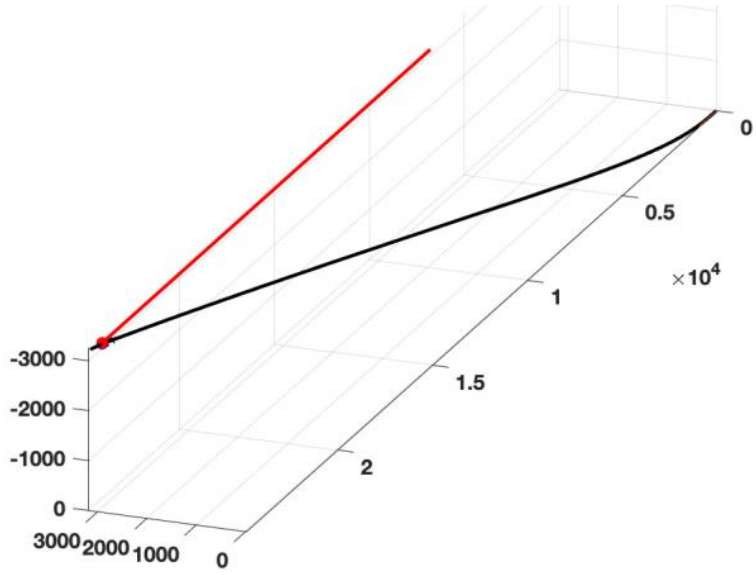

Figure 43 Missile tracking an expected target location in the future, $\tilde{p}_T$. Time of interception: 8.250 seconds.

Figure 42 and 43 shows how the interceptor is tracking and intercepting a target. The initial position of the threat in NED is $\boldsymbol{p}_T(0) = [7000 \quad 3100 \quad -3200]^T$ while it is moving at a constant velocity of $\boldsymbol{v}_T = [2100 \quad 0 \quad 0]^T$. The target is modeled as a point mass. The interceptor has the initial position $\boldsymbol{p}_I(0) = [0 \quad 0 \quad 0]^T$, initial attitude $\boldsymbol{\Theta}(0) = [0 \quad 0 \quad 0]^T$ and is traveling with a constant velocity magnitude of $V_m = 1000 \text{ m/s}$. In figure 42, the guidance algorithm is following the LOS vector between the launch platform at $\boldsymbol{p}_L = [0 \quad 0 \quad 0]^T$ and the targets position p_T. In figure 43, the LOS vector is pointing from the launch platform towards the predicted location of the target $\tilde{p}_T$, as given in (equation 126). While the missile is able to successfully intercept in both simulations, the result in figure 42 gives a reduction of 0.475 seconds (or 5.5%) in the total time from launch to interception.

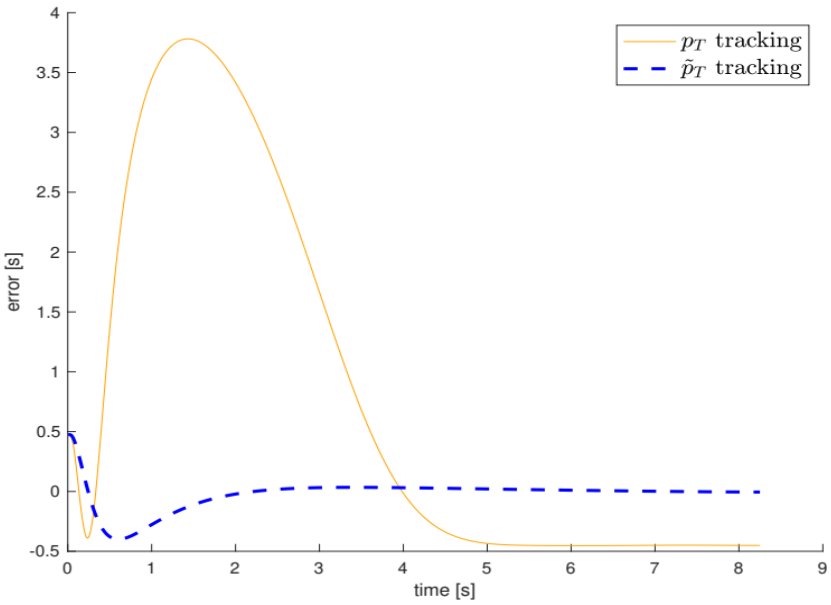

Figure 44 Time-to-go estimation error.

The discrepancy between the estimated t_{go} from (equation 125) and the actual time left till interception is seen in Figure 44. When $\tilde{p}_T$ is employed, the time error is visibly closer to zero throughout the experiment.

Given that t_{go}calculates using CPA, the departure from zero may be taken as a measure of the trajectory's optimality. After 1.4 seconds, the peak with an amplitude of 3.8 for p_T indicates that p_T is not the ideal option. This may be proved intuitively by anticipating the start of the trajectory seen in figure 42.

X. IMPLEMENTATION

A. Introduction

The whole GNC system, including all subsystems described in this thesis have been implemented in a MATLAB/Simulink environment. This chapter will examine several significant features and elements relating the implementation.

In order to accomplish the mission goal mentioned an asset and danger have to be present in the simulation environment in addition to the interceptor.

Figure 45 demonstrates the connection between asset, threat and interceptor. The dark square in 45 may be substituted with the bright squares in The picture, and vice versa.

The bullet points in 45 discusses the many maneouvers, control and navigation technologies that are available.

Transition blocks are implemented to conveniently switch between utilizing the genuine states and the estimated states from INS and tracking KF. The three-loop autopilot and PN law is put in a single subsystem, while the course/flight-path angle autopilot and the LOS guidance is placed in another. This makes it easier to switch between the multiple GNC systems, simply providing another switch block.

B. Environment of Simulation

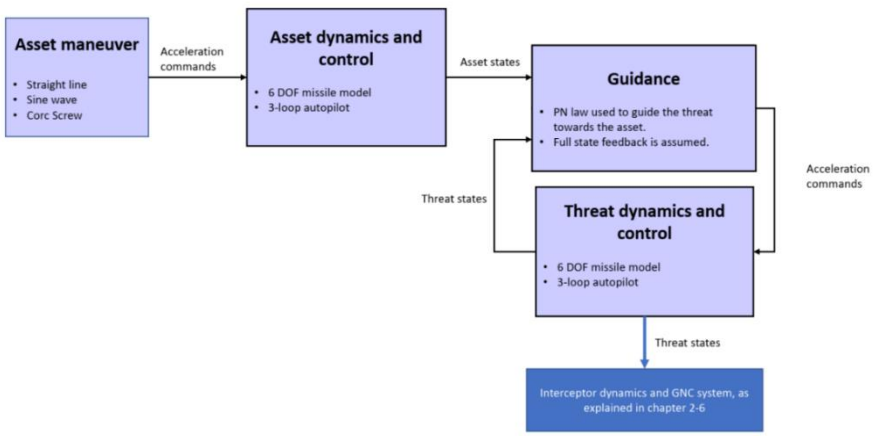

Figure 45 The three rigid bodies' control mechanisms and their relationship.

1. Interceptor

The interceptor's purpose is to neutralize a danger before it can reach the asset. The three-loop autopilot with PN law and the course/flight-path-angle autopilot with LOS guidance are developed and compared in the next chapter for various circumstances. Additionally, the interceptor will make use of sensor models; MEKF and target-tracking filters will be constructed and evaluated under a variety of conditions. The interceptor will monitor the threat independently of the asset movement and will be unaware of the threat's guidance system or trajectory in advance.

2. Threat

The threat's purpose is to strike the asset before it can be destroyed by the interceptor. It is assumed that the threat receives full-state input, which eliminates the need for state estimate and asset tracking filters. The danger is monitoring and calculating the trajectory by using the three-loop autopilot in conjunction with the PN law. Because the threat is unaware of the interceptor, the guiding law will not optimize its trajectory in order to avoid being destroyed by it.

3. Asset

Both the threat and the interceptor are unaware of the asset's movement. The assumption is that full-state feedback is present, and the trajectory is determined using the straightforward operations outlined in Section 10.4. Because no information about the threat or interceptor is available, the asset's movements are not determined by the threat's or interceptor's trajectory.

C. Missile Animation

To aid in visualizing the missile's attitude and trajectory, an animation of the missile's body is shown. While a simple marker on a 3D plot will enough to illustrate the trajectory, an animation of the missile's body will enhance the capacity to study the missile's attitude. It is plausible to suppose that the missile's route and flight path angle will vary from its attitude, since sideslip and angle of attack cannot be assumed to be equal. By modifying Riley's (2003) code, the verticies and faces of a CAD file are extracted into a.mat file (see cad2mat.m). Additionally, by changing the code from Scordamaglia (2016), the.mat file's 3D body is shown in the orientation of the missile's

attitude. Finally, this is shown as a three-dimensional animation that depicts the interceptor's and threat's trajectory. The illustration in Figure 46 illustrates how an interceptor monitoring a point mass might be displayed. The black line indicates the trajectory of the missile, while the red line indicates the point mass. This simulation was conducted using the guidance law deduced in LOS guidance with course and flight-path-angle commands Section in mind.

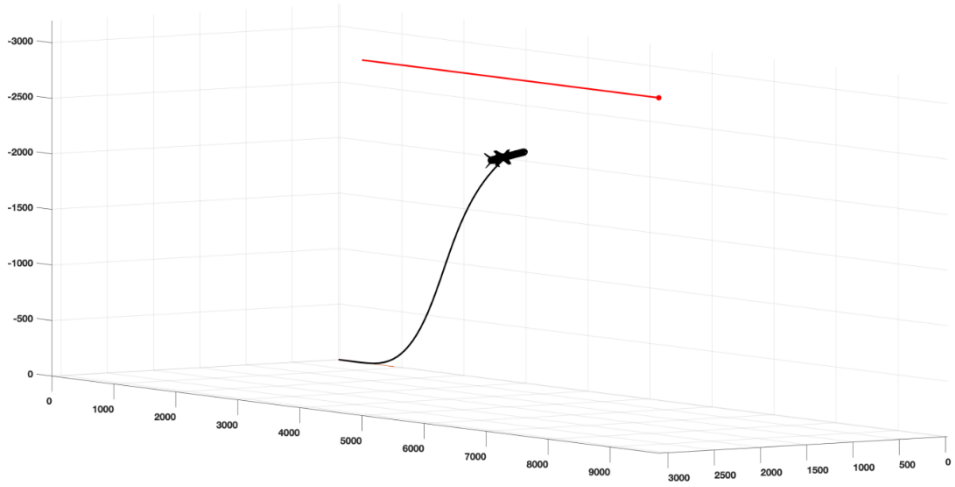

Figure 46 Pursuit of a moving point mass by a missile.

D. Maneuvers

Rather of tracking a target using one of the suggested guiding rules, certain basic maneuvers may be used to generate the required trajectory. These moves are used to simulate assets and, in certain situations, threats. The various motions detailed in this section generate acceleration orders that are sent to the three-loop autopilot described in Chapter 7. The rigid body is supposed to be initialized with a specified starting location $\boldsymbol{p}_0$, velocity $\boldsymbol{v}_0$, and attitude Θ_0.

1. Straight-line

The simplest maneuver is the straight line maneouver. Simply set the acceleration command to zero to obtain the straight-line trajectory.

$$a_c = [0 \quad 0 \quad 0]$$

Equation 127

The three-loop autopilot will next attempt to maintain a straight course for the rigid body.

2. Sine Wave in Yaw

The acceleration instruction, when used to generate a sine wave, produces.

$$a_c = [0 \quad 0 \quad a_\psi]$$

Equation 128

where

$$a_\psi = 1.5sin(2\pi t)$$

Equation 129

3. Corc Screw

The acceleration command that is used to perform the corkscrew maneuver is computed as

$$a_c = [0 \quad a_\theta \quad a_\psi]$$

Equation 130

where

$$a_\theta = 1.5sin(2\pi t + \pi/2)$$

Equation 131

and

$$a_\psi = 1.5sin(2\pi t)$$

Equation 132

Figure 46 demonstrates the asset's corc screw maneuver.

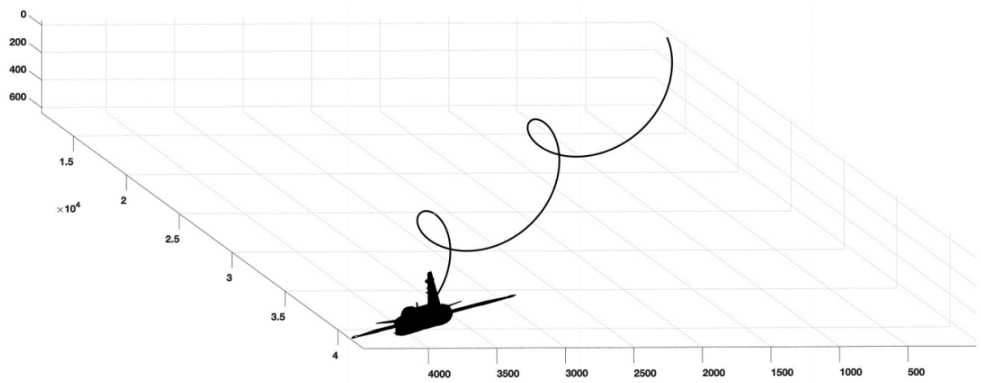

Figure 47 Execution of the corc screw maneouver by an asset.

E. Quaternion Normalization

Numerical round-off mistakes may occur, resulting in a violation of the quaternion's unit constraint. This is avoided by using the following normalization.

$$\boldsymbol{q}[k+1] = \frac{\boldsymbol{q}[k+1]}{|\boldsymbol{q}[k+1]|}$$

Equation 133

XI. THE OUTCOME OF THE SIMULATION

A. Case Studies Are Described

As a performance indicator, the result is expressed as Root Mean Square (RMS) errors, which are determined using the following formula.

$$RMS = \sqrt{\frac{1}{N}\sum_{i=1}^{N}\left(\hat{x}(i) - x_{true}(i)\right)^2}$$

Equation 134

1. Stop Condition

If the missile misses or intercepts the target, the simulation will immediately end. To mimic an interception, the missile must pass within a preset distance of the target. The range is set at "6 m" since it is thought that an explosion within this distance is sufficient to kill the target effectively. If there is a miss between the interceptor and the danger, the distance between them will begin to increase rather than decrease. In other words, the range rate $\dot{R}$ will degenerate towards a negative value.

Following that, the following stop criteria are determined:

if $R < 6$ then print 'interception sucessfull'; return true; else if $R > 6$ and $\dot{R} < 0$ then print 'interception unsucessfull'; return true; else return false;

Naturally, these requirements hold true for both the interceptor and the threat, as well as the threat and the asset. If one of the interceptions is successful, the other is declared unsuccessful.

B. Initial Circumstances and Parameters

With a constant sample step size of h=0.005 seconds, the system is sampled, equivalent to the 200 Hz sampling rate of the (IMU).

1. Parameters for Kalman Filters

The MEKF was tuned using the following discrete KF tuning matrices.

$$Q_{k,\,\text{mekf}} = \text{diag}(1\text{e}-10_{1\times3} \quad 1\text{e}-14_{1\times2} \quad 1\text{e}-13 \quad 1\text{e}-8_{1\times2} \quad 1\text{e}-7 \quad 1\text{e}-12_{1\times3})$$
$$R_{k,\,\text{mekf}} = \frac{1}{t_{\text{mekf}}}\text{diag}(10_{1\times3} \quad 1\text{e}-3_{1\times3} \quad 5_{1\times3} \quad 1\text{e}-2_{1\times3})$$
$$\hat{P}_{0,\,\text{mekf}} = \text{diag}(1\text{e}-1_{1\times3} \quad 1\text{e}-2_{1\times3} \quad 1\text{e}-10_{1\times3} \quad 2\text{e}-6_{1\times3} \quad 5\text{e}-2_{1\times3})$$

Equation 135

The Kalman filter tuning matrices provide results for target tracking.

$$Q_{k,tkf} = \text{diag}(1\text{e}-6_{1\times3}\ 1\text{e}-5_{1\times3}\ 1\text{e}-8_{1\times3})$$
$$R_{k,tkf} = \frac{1}{t_{tkf}}\text{diag}(1_{1\times3})$$
$$\hat{P}_{0,tkf} = \text{diag}(1\text{e}-2_{1\times3}\ 2.25_{1\times3}\ 20_{1\times3})$$

Equation 136

The Kalman filter used to estimate $\boldsymbol{f}_{\text{ins}}^{n}$ is initialized as follows:

$$Q_{k,fkf} = \text{diag}(1\text{e}9_{1\times3}\ 1\text{e}8_{1\times3}\ 1\text{e}11)$$
$$R_{k,fkf} = \frac{1}{t_{fkf}}\text{diag}(10_{1\times3}\ 1\text{e}-3_{1\times3})$$
$$\hat{P}_{0,fkf} = \text{diag}(1\text{e}-5_{1\times9})$$

Equation 137

2. Parameters for the autopilot and the reference model

The autopilot feed gains are selected as follows:

$$K_{\dot{\alpha}} = 0.1$$
$$K_{\dot{\beta}} = 0.1$$

Equation 138

The flight-path-angle controller's tracking and input weight matrices are selected as follows:

$$Q_{\gamma} = \text{diag}(1 \quad 1.5)\ R_{\gamma} = 2$$

Equation 139

whereas the course controller's tracking and inputs weight matrices are

$$Q_{\chi} = \text{diag}(1 \quad 1.5)\ R_{\chi} = 2$$

Equation 140

For the reference model, both the lateral and longitudinal autopilots are set to $\omega_n = 100$ and $\gamma = 1$.

3. Guidance law Parameters

$k_h = 0.9$ and $k_v = 0.9$ are utilized for LOS guiding. Additionally, the guidance controller is set up to intercept at the projected target location $\tilde{p}$.

N=5 is used as the proportional navigation constant for the PN law.

4. Initial Circumstances for The Interceptor

The interceptor is modelled as a rigid body with the following properties:

Initial position:

$$p_I^n(0) = (-2000m - 100m\ 0)^T$$

Equation 141

Initial velocity:

$$v_I^n(0) = (3000\ \mathrm{m/s} \quad 0 \quad 0)^T$$

Equation 142

Initial attitude:

$$\Theta_I^n(0) = (0 \quad 0 \quad 0)^T$$

Equation 143

The interceptor is utilizing the proportional navigation algorithm to intercept the threat. The Interceptor employs filters from Chapter 5 to estimate INS and track threats.

5. Threatening Initial Circumstances

The threat is modeled as a rigid body that exhibits the following characteristics:

Initial position:

$$p_T^n(0) = (6000m\ 6000m\ -6000m)^T$$

Equation 144

Initial velocity:

$$v_T^n(0) = (2600\ \mathrm{m/s} \quad 0 \quad 0)^T$$

Equation 145

Initial attitude:

$$\Theta_T^n(0) = (0 \quad 0 \quad 0)^T$$

Equation 146

The danger is that the asset will be intercepted by the proportionate navigation algorithm. The threat is believed to have complete awareness of its own and the assets' states, i.e., complete state feedback.

6. Initial Circumstances of The Asset

The asset is represented as a rigid body that exhibits the following properties:

Initial position:

$$p_A^n(0) = (12000m \quad 0 \quad 0)^T$$

Equation 147

Initial velocity:

$$v_A^n(0) = (2000m/s \quad 0 \quad 0)^T$$

Equation 148

Initial attitude:

$$\Theta_A^n(0) = (0 \quad 0 \quad 0)^T$$

Equation 149

The asset is evading the threat by using the Cork-screw technique.

The simulations are conducted using a gyro measurement bias specified as follows:

$$b_{acc}^b := \left[b_{acc,x}^b \quad b_{acc,y}^b \quad b_{acc,z}^b\right]^T$$

Equation 150

Wiener process is modeled. Initialize the bias as follows:

$$b_{ars,0}^b = (1.3\text{e} - 2\text{rad/s}\ 1.6\text{e} - 2\text{rad/s}\ 1.9\text{e} - 2\text{rad/s})^T$$

Equation 151

where

$$\dot{b}_{ars}^b = \omega_{b,ars}$$

Equation 152

and $\omega_{b,ars}$ is white noise. The bias is saturated such that

$$-1.4b_{ars,0}^{b} \leq |b_{ars}^{b}| \leq 1.4b_{ars,0}^{b}$$

Equation 153

to prevent the tendency for the value to expand out of proportion to the beginning value. Gyro bias is defined as

$$\hat{b}_{ars}^{b} := \begin{bmatrix} b_{ars,\phi}^{b} & \hat{b}_{ars,\theta}^{b} & \hat{b}_{ars,\psi}^{b} \end{bmatrix}^{T}$$

Equation 154

The simulations are run using an acceleration measurement bias established as follows:

$$b_{acc}^{b} := \begin{bmatrix} b_{acc,x}^{b} & b_{acc,y}^{b} & b_{acc,z}^{b} \end{bmatrix}^{T}$$

Equation 155

Wiener process is modeled. Initialize the bias as follows:

$$b_{acc,0}^{b} = (1.3\ \mathrm{m/s^2} \quad 1.6\ \mathrm{m/s^2} \quad 1.9\ \mathrm{m/s^2})^{T}$$

Equation 156

where

$$\dot{b}_{acc}^{b} = \omega_{b,acc}$$

Equation 157

and $\omega_{b,acc}$ is white noise. The bias is saturated such that

$$-1.4b_{acc,0}^{b} \leq |b_{acc}^{b}| \leq 1.4b_{acc,0}^{b}$$

Equation 158

The term "estimated acceleration bias" refers to the following:

$$\hat{b}_{acc}^{b} := \begin{bmatrix} \hat{b}_{acc,x}^{b} & \hat{b}_{acc,y}^{b} & \hat{b}_{acc,z}^{b} \end{bmatrix}^{T}$$

Equation 159

C. State Estimation

The first case study examines the performance of the MEKF in the error condition.

The first case study employs three distinct INS sampling rates. Simulink's time step is always $h = 0.005$ seconds.

Both IMU and GNSS data are acquired in the first simulation at a sampling rate of $t_{gnss} = t_{imu} = 200$ H. This is an implausible simulation scenario, as GNSS receivers are incapable of maintaining such a high rate of aiding, as discussed in subsection (8.3.3) GNSS. The purpose of this case study is to examine the MEKF's ability to provide exact state estimates at more realistic sampling rates, in comparison to the ideal but unrealistic situation described in this instance.

The second scenario involves the acquisition of GNSS data at a decreased frequency of $t_{gnss} = \frac{t_{imu}}{20} = 10$ Hz This implies that although the INS equations will continue to be updated at the same rate as the high-frequency IMU observations, the corrections will be calculated at a lower rate.

The third scenario will have the aiding updates reduced to $t_{gnss} = \frac{t_{imu}}{100} = 2$ Hz. For all three simulations, the target tracking data are assumed to be taken at a rate of $t_{tkf} = 200$ Hz.

Case 1:	Case 2:	Case 3:
$t_{imu} = 200$ Hz	$t_{imu} = 200$ Hz	$t_{imu} = 200$ Hz
$t_{tkf} = 200$ Hz	$t_{tkf} = 200$ Hz	$t_{tkf} = 200$ Hz
$t_{gnss} = 200$ Hz	$t_{gnss} = 10$ Hz	$t_{gnss} = 2$ Hz
$t_{mekf} = 200$ Hz	$t_{mekf} = 10$ Hz	$t_{mekf} = 2$ Hz

Equation 160

1. The Outcome of The Simulation

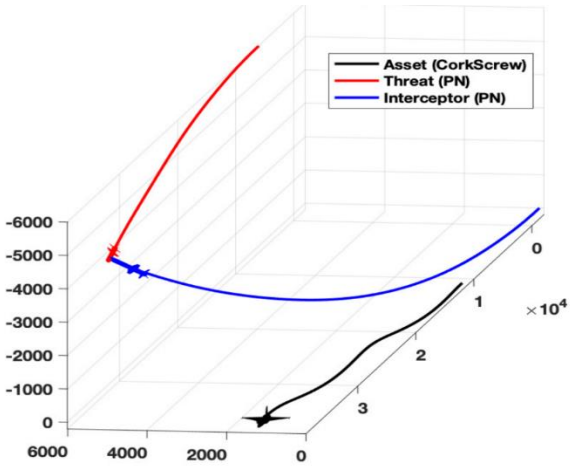

Figure 48 Case 2: Trajectory.

The trajectories of the asset, threat, and interceptor are depicted in Figure 48. The interceptor and threat both use PN, while the asset makes use of a corc screw maneuver.

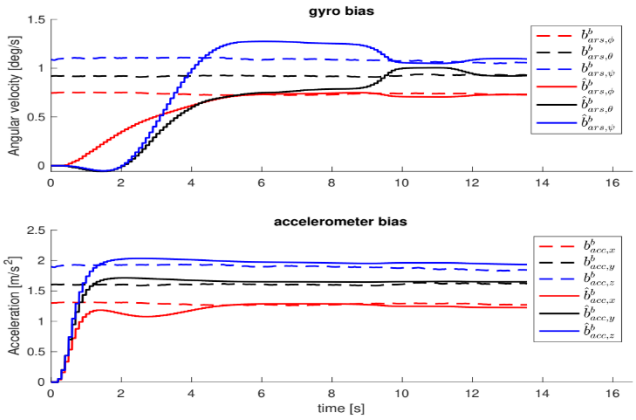

Figure 49 bias estimation.

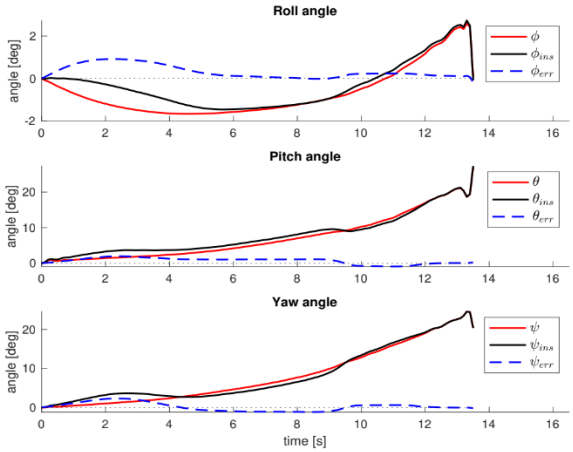

Figure 50 Case 2: Atittude estimate.

As seen in Figure 49, the system is capable of estimating all gyro and accelerometer biases. The graphic explains how to estimate bias in Simulation 2 by varying the sample rate. This demonstrates reasonable approximations for situations in which the IMU and GNSS data are acquired at different sample rates. Figure 50 illustrates the interceptor's attitude estimates and estimation mistakes. Take note that the attitude problem is most noticeable during the simulation's first six seconds. This is an anticipated outcome, since it corresponds to the time required for bias estimation to reach convergence, as seen in Figure 49.

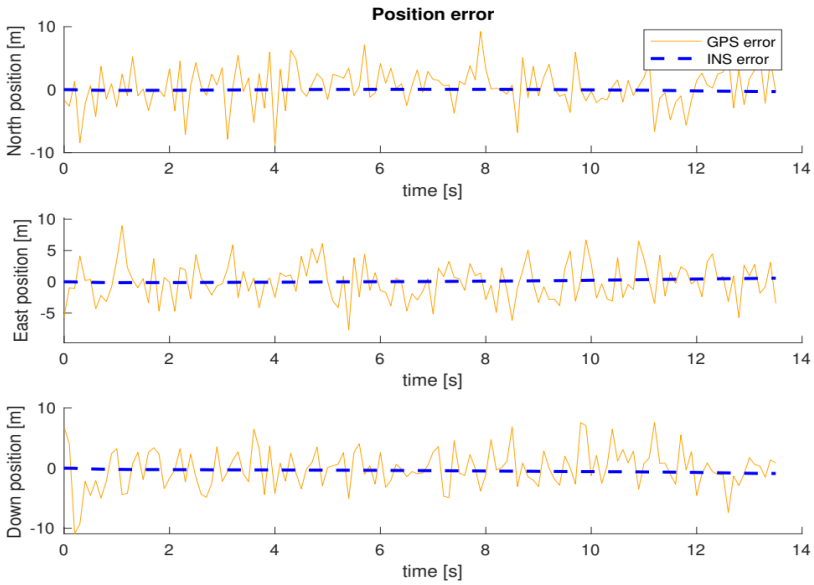

Figure 51 Case 2: Estimation of position error.

Figure 51 illustrates how GNSS noise is effectively filtered out of position measurements.

The errors in state estimate are shown in Table 3. for three separate simulations. The greatest error is the difference between the real and estimated states at any point in time throughout the simulation. The final error is the difference between the real and estimated states at the simulation's conclusion. RMS is the root mean square of the RMS value as defined in Described case studies Section

Table 3 Shows the estimate errors for the INS at various sampling rates.

	Attitude (deg)			Position (m)			Velocity (m/s)		
	roll	pitch	yaw	north	east	down	north	east	down
Case 1									
Max error	-0.86	-2.0	-2.4	-0.39	0.75	-0.72	0.29	-0.32	0.86
Final error	0.081	-0.31	0.26	-0.39	0.73	-0.72	0.29	0.29	0.86
RMS	0.32	1.0	0.99	0.13	0.33	0.31	0.092	0.089	0.1
Case 2									
Max error	-0.93	-2.0	-2.3	-0.33	0.57	-0.88	-0.29	-0.38	-0.45
Final error	0.17	-0.28	0.12	-0.33	0.57	-0.88	0.087	0.14	0.43
RMS	0.44	1.1	1.1	0.12	0.23	0.48	0.11	0.1	0.11
Case 3									
Max error	-2.1	-4.9	5.3	-1.9	-2.8	-3.7	1.1	-1.3	-1.4
Final error	0.048	0.65	-0.77	-1.9	-1.5	-3.1	0.33	0.86	0.99
RMS	1.0	2.3	2.7	1.0	1.8	2.6	0.6	0.6	0.57

Take note that cases 1 and 2 provide almost identical RMS values. This demonstrates that a sampling rate of $t_{gnss} = 10$ Hz and $t_{imu} = 200$ Hz is enough for obtaining promising state estimates. When the sample settings specified in Case 3 are used, the accuracy of state estimate is marginally reduced.

2. Targets Tracking

The error between the true and estimated relative positions, relative velocity, and threat acceleration is depicted in Figure 52. Figure 52 illustrates the linear KF performance in three distinct directions: north, east, and down. In this case, relative position measurements with a standard deviation of $\_\sigma_r = 2$ m are obtained.

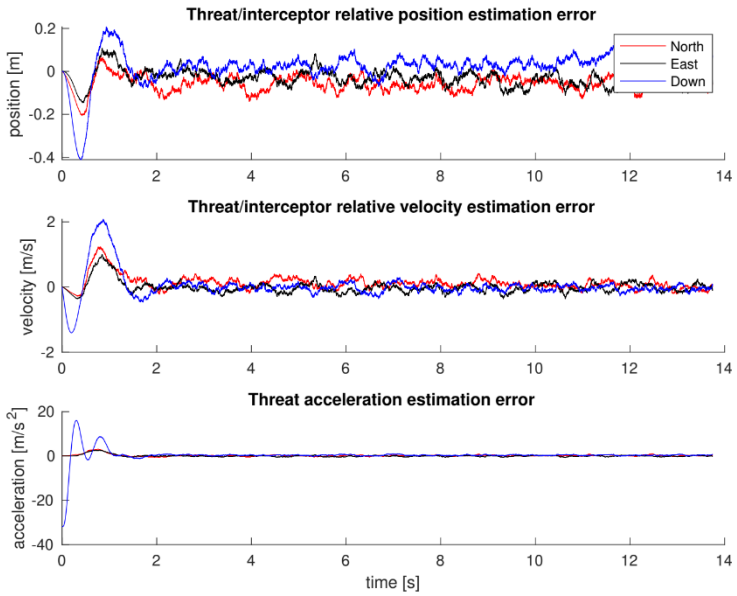

Figure 52 Errors in target tracking estimate.

Figure 53 The comparison of estimated position errors to measurement errors, which gives demonstrates that the results are satisfactory.

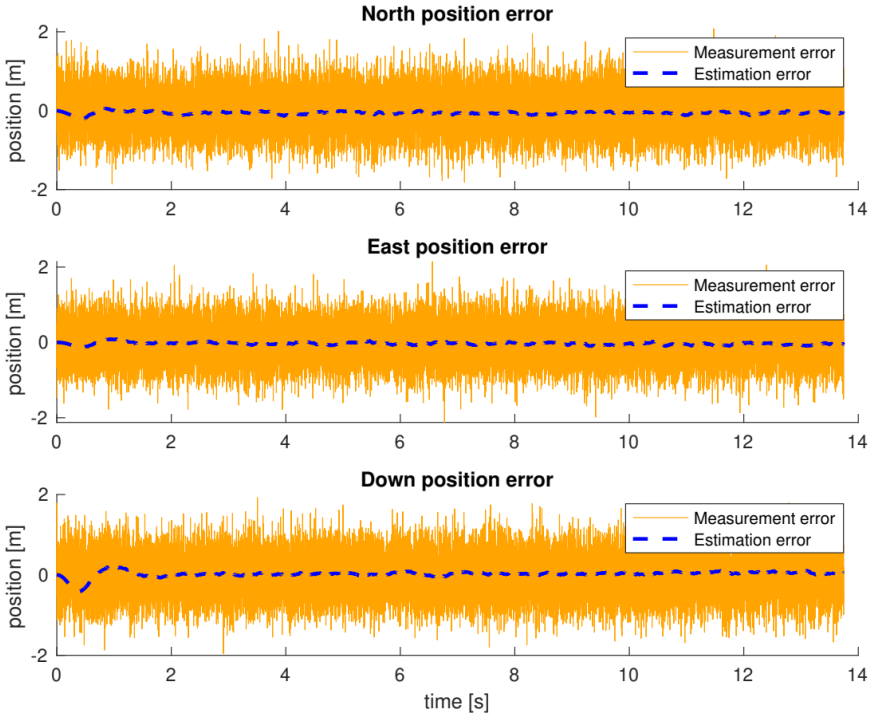

Figure 53 Estimated vs. measured relative location error for target tracking.

The filter employs its state estimations to linearize the state equations on the fly. It may soon diverge if the estimate error gets too big or if the process is described wrongly. That is, the efficiency of the target-tracking KF is closely tied to the estimate accuracy of

the MEKF, since information regarding the interceptor's acceleration in inertial frame has to be precise.

D. Comparative Analysis of Guidance Laws

This section will compare the major distinctions, disadvantages, and advantages of two distinct guidance laws.

1. Interceptor's Force of Action

The specific force L2-norm acting on the interceptor's body is illustrated in figure 54 under the same conditions as in the previous section.

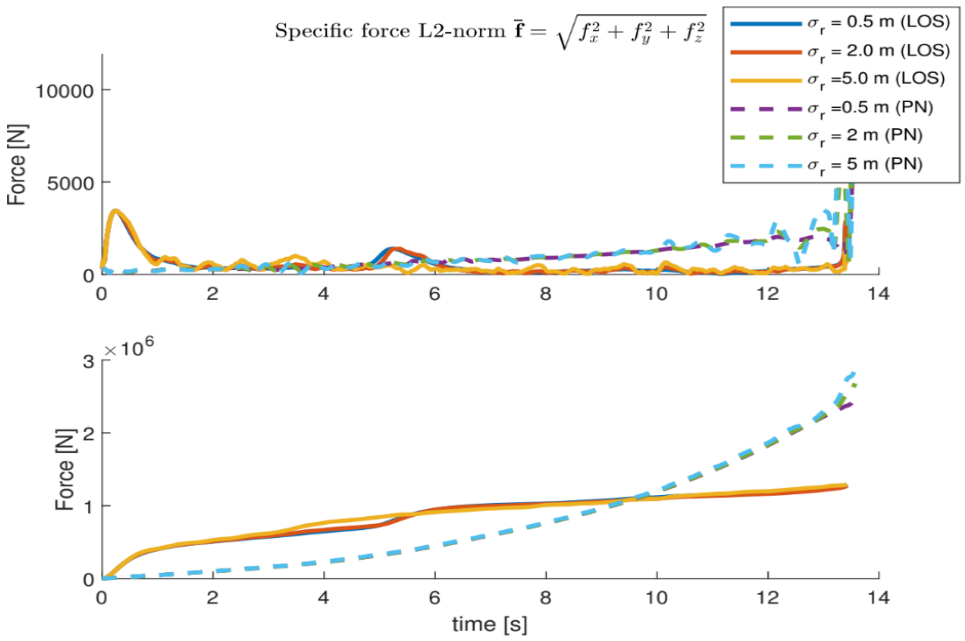

Figure 54 The interceptor is subjected to a certain force in response to a threat. $\sigma_r$denotes the standard deviation of the noise in the relative position measurement. The subplot at the bottom depicts the cumulative force over time.

Figure 54 demonstrates that after a period, the PN law will begin to acquire a bigger cumulative force operating on the projectile than the LOS law. As the LOS law is forecasting the future location of target at interception time, one may anticipate that the force acting on the interceptor will be greater during the first phase of the launch. The PN legislation on the other hand, would apply the most agressive fin deflections while closing up upon the target. This may be confirmed by glancing at the figure. How much influence this has in a practical situation is impossible to determine, although it is directly tied to gasoline use. If fuel consumption is a concern, there could be instances

where the LOS rule will make the missile capable to traverse a wider distance even before fuel runs out.

This may also be taken as a technique to demonstrate the two guidance laws' noise sensitivity. Given that _r has an effect on both the relative position and velocity estimations employed in the PN law, it is logical to assume that the PN law is more susceptible to erroneous measurements than the LOS legislation.

Additionally, three distinct case studies were conducted to determine the difference in simulation duration, L2-norm specific force, ultimate distance, and interception verification. Videos of the simulations are included in the.zip file's "animation" section.

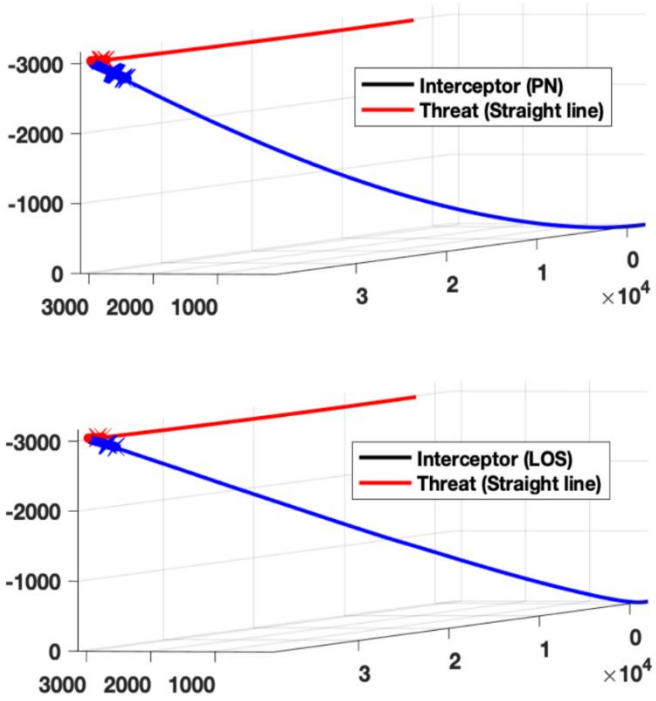

Figure 55 Interceptor tracking a threat traveling on a straight path. The LOS law is determining the best trajectory towards to the location of intercept, that is on a striaght line from the launch platform. See "StraightLine LOS.avi" and "StraightLine PN.avi" i.

2. Scenario 1: Threat Moving on A Straight Line

In the first scenario, the threat is simulated to travel on a straight line, so that the acceleration inputs to the threat becomes a $a_c = [0 \quad 0 \quad 0]$. This is a predictale trajectory, and the LOS guidance must therefore be able to predict the location of interception effectively.

3. Scenario 2: Threat Doing Sine Wave

In the second scenario, the threat is subjected to a sine wave input via the yaw channel $a_c = [0 \quad 0 \quad a_\psi]$, where $a_\psi = 1.5\sin(2\pi t)$. This is a more uncertain trajectory, as (equation 126) provides inaccurate estimates when the velocity changes rapidly. As a result, the interceptor's trajectory will continuously change. The interceptor's behavior under two distinct guidance laws is illustrated in Figure 56. Notably, the PN law is capable of guiding the interceptor in a more direct path towards to the threat than the LOS law, which is consistent with the preceding reasoning.

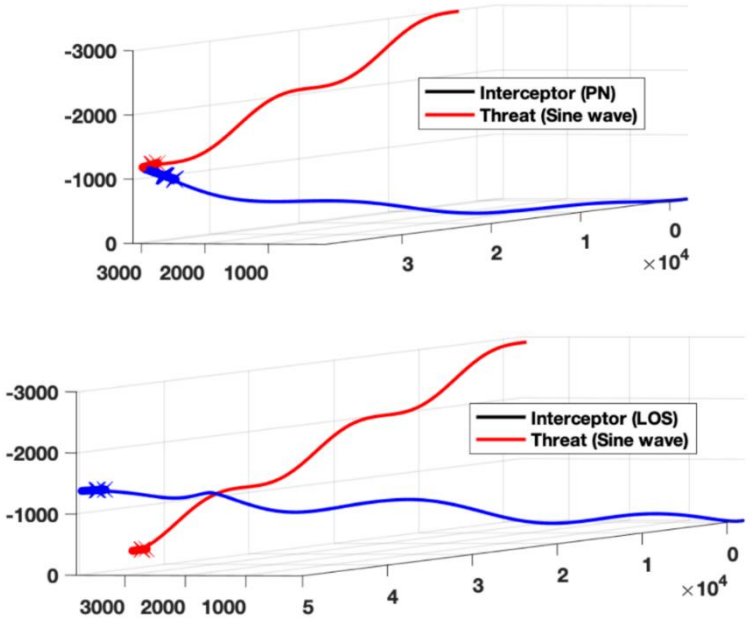

Figure 56 Interceptor doing the sine wave maneuver in pursuit of a danger. When a danger employs an unanticipated move, the LOS law fails miserably. For video of the simulation, see "Sine LOS.avi" and "Sine PN.avi" in the.zip file.

4. Scenario 3: Threat Intercepting an Asset

This scenario study is similar with the one in section 11.3, where the asset utilizes the PN law to intercept an asset, employing the corc screw maneuver.

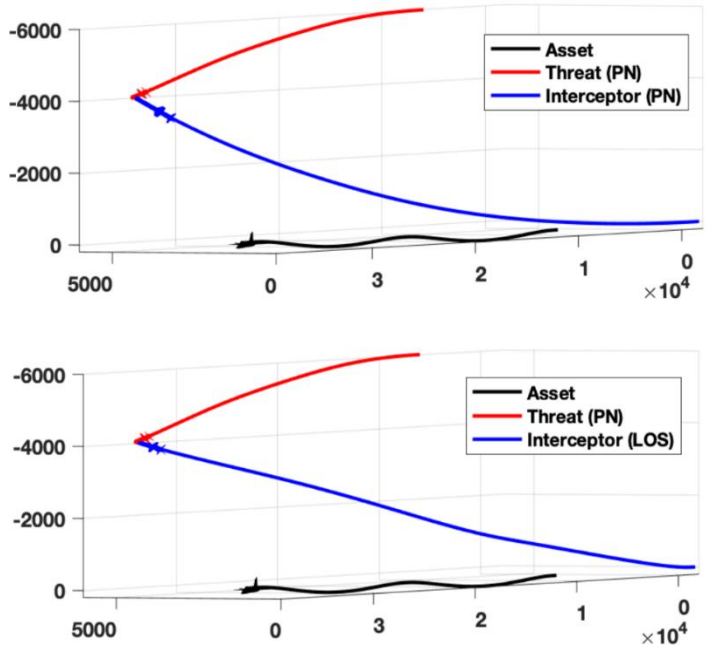

Figure 57 Interceptor acting in response to a threat uses the PN law to intercept an asset. As with the sine wave maneuver, this results in an unpredictable target maneuver. For video of the simulation, see "Intercept LOS.avi" and "Intercept PN.avi" in the.zip fi.

5. The Outcome of The Simulation

The simulation results for all three situations are shown in Figure 58. The simulation time is calculated from the moment the missile is fired until it is intercepted successfully or unsuccessfully. Force is the L2-norm of the summation of the missile's individual forces during simulation. The interceptor's ultimate distance from the danger. Interception is a Boolean variable that indicates whether or not the interception was successful. FSF is an abbreviation for full state feedback, which implies that all states are known in advance. This is equivalent to disabling the INS system and directly feeding the guidance and control blocks depicted in Figures which we mentioned before with the missile states from the airframe.

Scenario 1, in which the threat travels straight ahead, results in successful interceptions using both the LOS and PN for complete state feedback, and $\sigma_r = 0.5$. This is to be anticipated, given the threat's direction is predictable and straightforward for both laws to follow. Take note that the LOS law is still capable of intercepting the target when $\sigma_r = 5$. This is understandable, given that the LOS law is less susceptible to measurement noise than the PN law.

Table 4 Interception time, cumulative specific force, and information about interception for various simulation scenarios including PN and LOS guidance rules.

	LOS			PN		
	FSF	$\sigma_r = 0.5$	$\sigma_r = 5$	FSF	$\sigma_r = 0.5$	$\sigma_r = 5$
Case 1						
Time [s]	14.0	14.0	14.1	13.7	13.8	13.9
Force [N]	5.7e5	7.3e5	1.1e6	8.9e5	1.3e6	2.2e6
Distance [m]	5.3	5.0	4.4	5.3	4.2	8.7
Interception	✓	✓	✓	✓	✓	✗
Case 2						
Time [s]	17.8	17.8	17.8	13.6	13.6	13.6
Force [N]	3.6e6	3.4e6	3.7e6	1.4e6	1.7e6	2.3e6
Distance [m]	10.0	9.8.0	11.7	5.4	4.6	5.8
Interception	✗	✗	✗	✓	✓	✓
Case 3						
Time [s]	13.4	13.4	13.4	13.5	13.5	13.6
Force [N]	1.1e6	1.3e6	1.4e6	2.1e6	2.4e6	2.9e6
Distance [m]	11.5	12.1	11.4	4.8	2.6	8.3
Interception	✗	✗	✗	✓	✓	✗

*Scenario 2, i*n which the threat moves in a sine wave, demonstrates the LOS law's poor performance. The LOS legislation derives its trajectory from a prediction of the threat's location at the time of closest approach. Due to the threat's extremely time-varying attitude as a result of the sine wave, this location will fluctuate significantly. As seen in Figure 57, the interceptor's trajectory for LOS results in a wave with a substantially larger amplitude than the PN law's wave. According to Figure 58, the simulation duration, force, and end distance are all much greater for LOS than for PN.

Scenario 3, in which the threat attempts to intercept an asset, results in comparable simulation times for both methodologies, although the end distance is often greater for LOS than for PN. Take note that in both this situation and the straight-line tracking provided in Scenario 1, the particular force norm for PN is much greater than the specific force standard for LOS.

XII. CONCLUSION

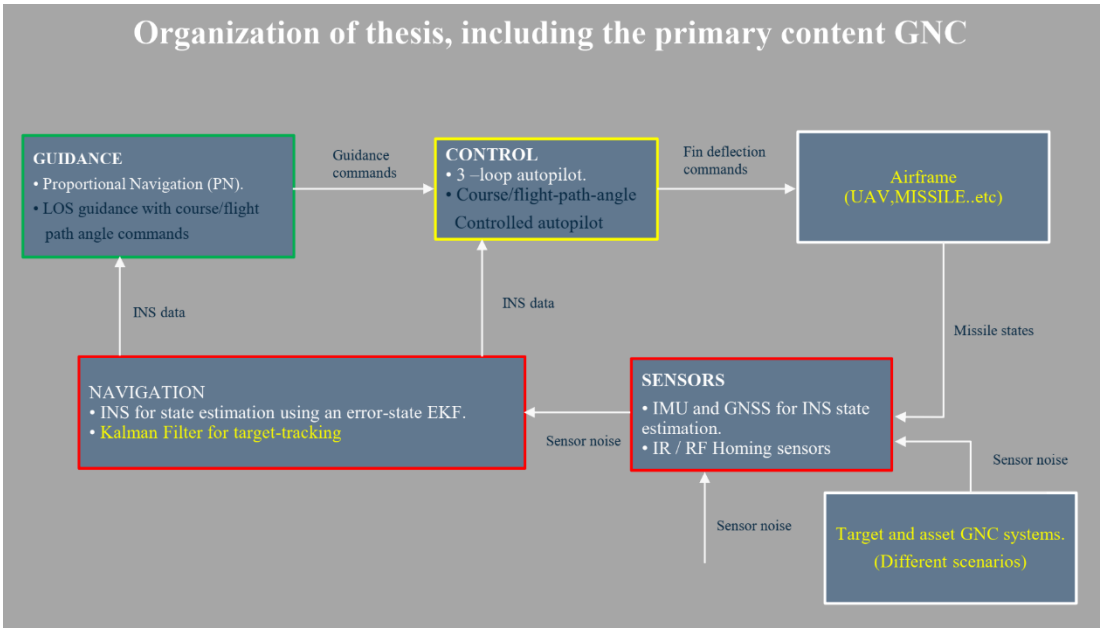

Figure 58 Organization of thesis, including the primary content Guidance, Navigation and Control (GNC)

Numerous GNC designs have been developed and evaluated for missile-target engagements:

Autopilot with three loops and PN guiding law.

Autopilot for course / flight path angle using LOS guiding legislation.

MEKF based on quaternions with GNSS assistance.

In comparison to another approach that relies on INS pseudo-measurements, the KF differentiator was used to estimate the MEKF measurement reference.

Three-body simulation environment with six-degree-of-freedom asset, threat, and interceptor models.

Different situations were simulated to determine the influence on state estimates and the overall performance of the two GNC systems. The three-body simulation environment is used to provide more realistic outcomes when both the threat and interceptor have defined goals.

The simulation findings provide good results for estimating missile states, even at sampling rates as low as 2 Hz.The KF differentiator is used to calculate the $\boldsymbol{f}_{\text{ins}}$ reference, but the pseudo-measurement technique, which employs yaw angle estimation, achieves a higher degree of precision, with a final error as low as 9.3e-3 for the simulation in section 8.7. Both strategies provide simulations in which the interceptor successfully completes the mission goal.

We examined and compared two distinct navigation and control systems. The computed trajectories for the two approaches are somewhat different, and their relative strengths and weaknesses are shown to be depending on the threat's trajectory.

When the threat travels in a predictable manner, such as in a straight line, the LOS guidance law performs well. Because the LOS guidance is based on the expected threat's location at CPA, straight line maneuvers result in an apparent ideal trajectory for the missile. Due to the fact that the LOS guidance law relies on course and flight-path angle commands, it is demonstrated that it has difficulty intercepting a threat that makes evasive or unpredictable movements just before interception, despite the fact that it is capable of guiding the missile to a point near the threat. Additionally, it is shown that the LOS rule has a smaller magnitude of specific force acting on the projectile. This is because the missile calculates the threat's location and the guiding orders do not need quick attitude adjustments.

The PN law performs well in terms of tracking and intercepting the target, both straight-line tracking and sine wave tracking, as well as in the three-body case. However, the PN law performs poorly when the size of the relative position estimate for the target-tracking filter is large. Simulations demonstrate that when the requirement for interception $R \leq 6$ m, a relative position standard deviation of $\_\sigma_r = 5$ m leads in an unsuccessfull interception for the straight-line and three-body cases. The PN law also exhibits exponential development in the total specific force exerted on the rigid body as the standard deviation of the relative position noise is increased. This seems not to be an issue with the LOS guideline statute.

XIII. REFERENCES

BOOKS

BALCHEN, J. G., ANDRESEN, T., FOSS, B. A., (2004). **Regulerings Teknikk. NTNU**, Institutt for Teknisk Kybernetikk.

BEARD, R. W., MCLAIN, T. W., (2013). **Small Unmanned Aircraft: Theory and Practice,** Princeton, NJ. No.1, Princeton University Press.

BRYNE, T. H., FOSSEN, T. I., (Aug 2016). **Introductory Lecture Notes on Aided Inertial Navigation Systems.** Tech. Rep., NTNU, Trondheim.

BRYSON, A. E. J., (2015). **Control of Spacecraft and Aircraft**. Vol. 3. Princeton University Press.

FOSSEN, T. I., (2011). **Handbook of Marine Craft Hydrodynamics and Motion Control**. John Wiley & Sons Ltd.

INNOCENTI, M., FRAGOPOULOS, D. (2004). **Stability considerations in quaternion attitude control using discontinuous Lyapunov functions**. Control Theory & Applications Iee Proceedings.

JAY, F., (2008). **Aided Navigation: GPS with High Rate Sensors**. The McGraw-Hill Companies. URL http://www.amazon.com/Aided-Navigation-High-Rate Sensors/dp/0071493298

NPTEL, (2012). **Missile Guidance Laws**, 100–109.

ONR, (2001). Broad Agency Announcement (BAA) for the Office of Naval Research (ONR) Navy and Marine Corps FY2018 Basic Research Challenge (BRC) Program.

PALUMBO, N. F., (2010). **Guest Editor's Introduction: Homing Missile Guidance and Control.**

RILEY, D., (2003). **CAD2MATDEMO.M.**

TRIMBLE, (2012). **Serial Embedded GPS Receiver (SEGR) Solution for RF and DAE Embedded Applications.**

UTC Aerospace Systems, (2017). **TITAN ® Tactical Grade Inertial Measurement Unit (IMU) Product Benefits**. URL www.utcaerospacesystems.com/gnc

ARTICLES

CIMEN, T., (2011). A generic approach to missile autopilot design using state-dependent nonlinear control. **IFAC Proceedings Volumes (IFAC-PapersOnline)** 18 (PART 1), 9587–9600.

CRASSIDIS, J. L., MARKLEY, F. L., CHENG, Y., (2007). Survey of Nonlinear Attitude Estimation Methods. **Journal of Guidance, Control, and Dynamics** 30 (1), 12–28. URL http://arc.aiaa.org/doi/10.2514/1.22452

HORTON, M. P., (1995). Autopilots for tactical missiles: an overview. Proceedings of the Institution of Mechanical Engineers. Part I, **Journal of Systems and Control Engineering,** 209 (2), 127–139.

MALEY, J. M., (2013). quaternion multiplicative extended kalman filter for nonspinning guided projectiles. **Army Research Labratory,** ARL 2016-Augus (July), 8043–8048.

MARKLEY, F. L., 2008. Attitude Error Representations for Kalman Filtering. **Journal of Guidance, Control and Dynamics,** 26 (2), 311–317.

MRACEK, C., RIDGELY, D., (2005). Missile Longitudinal Autopilots: Comparison of Multiple Three Loop Topologies. **AIAA Guidance, Navigation, and Control Conference and Exhibit.**

PALUMBO, N. F., BLAUWKAMP, R. A., LLOYD, J. M., (2010a). Basic Principles of Homing Guidance, 25–41. **Johns Hopkins APL Technical Digest (Applied Physics Laboratory),** 29 (1), 2–8.

PALUMBO, N. F., BLAUWKAMP, R. A., LLOYD, J. M., (2010b). Modern homing missile guidance theory and techniques. **Johns Hopkins APL Technical Digest (Applied Physics Laboratory),** 29 (1), 42–59.

PALUMBO, N. F., HARRISON, G. A., BLAUWKAMP, R. A., MARQUART, J. K., (2010c). Guidance filter fundamentals. **Johns Hopkins APL Technical Digest (Applied Physics Laboratory),** 29 (1), 60–70.

QI, H., MOORE, J. B., (2002). Direct Kalman filtering approach for GPS/INS integration. **IEEE Transactions on Aerospace and Electronic Systems** 38 (2), 687–693.

SALIH, A. A. A.-A., LIYANA, N., CHE, A., ZAINI, A., ZHAHIR, A., (2013). The Suitability of GPS Receivers Update Rates for Navigation Applications 7 (6), 1012–1019.

SCORDAMAGLIA, V., (2016). **Trajectory and Attitude Plot Version 3**.

SIOURIS, G. M., (2004). Missile Guidance and Control Systems. **Applied Mechanics Reviews,** 57 (6), B32. URL http://appliedmechanicsreviews.asmedigitalcollection.asme.org/article.aspx?articleid=1398173

SOLA, J., (2017). Quaternion kinematics for the error-state Kalman filter. **CoRR**, vol.
abs/1711.02508, 2017. [Online]. URL http://arxiv.org/abs/1711.02508.

WEEHONG TAN, PACKARD, A., BALAS, G., (2000). Quasi-LPV modeling and LPV control of a generic missile. Proceedings of the 2000 American Control Conference. **ACC (IEEE Cat. No.00CH36334)** (June), 3692–3696 vol.5. URL http://ieeexplore.ieee.org/document/879259/

ZHANG, C., LI, X., GAO, S., LIN, T., WANG, L., (2017). Performance analysis of global navigation satellite system signal acquisition aided by different grade inertial navigation system under highly dynamic conditions. **Sensors (Switzerland)** 17 (5).

DISSERTATIONS

SEFASTSSON, U., (2016). Evaluation of Missile Guidance and Autopilot through a 6 DOF Simulation Mode. (Ph.D. thesis), KTH Royal Institute of Technology.

APPENDIX

Appendix-1: MEKF

Appendix-2: INS equations

Appendix-3: *fins* Estimation

Appendix-4: Target tracking KF

Appendix-5: LOS guidance law

Appendix-1: MEKF

```
function err = MEKF(fnins,GPS,yimu,yins,MEKFinit)
% ------------------------------------------------------------------------
% Multiplicate extended Kalman filter
%
% Input:
% fnins - specific force reference from KF differentiator
% GPS - GPS measurements
% yimu - IMU sensor measurements (accelerometer, gyro, magnetometer)
% yins - measurements from INS
% qins - quaternion measurement
% binsars - biasestimation for gyro
% wbnb - angular velocity
% h - sampling rate
%
% Output:
% err - error-state from MEKF, injection term for INS
%
% Notes:
% comment / uncomment fbins 2 and the 4th line in H matrix to switch
between
% method 1 and 2 for fbins reference computation
%

% Author: Henning Ward
% Date: June 2019
% ------------------------------------------------------------------------

%%

Z3 = zeros(3);
I3 = eye(3);
err = zeros(16,1);
h = MEKFinit.h;

mned = [22494.35 5372.67 42301.72]'; %magnetic field (UC Berkeley
, USA) [nT]
persistent RQPhat


if isempty(R)
R = MEKFinit.R;
Q = MEKFinit.Q;
Phat = MEKFinit.Phat;

end
Tars = MEKFinit.Tars;
Tacc = MEKFinit.Tacc;

epsins = yins(7:9);
qins = eps2q(epsins);
%qinsnormalizationtopreventnumericalerrors
qins = qins/norm(qins);
Rins = Rquat(qins);

pnnb = GPS(1:3);
vnnb = GPS(4:6);
fbimu = yimu(1:3);
mbimu = yimu(7:9)/norm(yimu(7:9));
y = [pnnb;vnnb;fbimu;mbimu];

pins = yins(1:3);
vins = yins(4:6);

binsars = yins(10:12);
binsacc = yins(13:15);

wbnb = yimu(4:6);

fbins = Rins'*fnins;

%uncomment for method 2
```

```
%f b i n s = Smtrx ( w b nb - b i n s a r s ) * R ins ' * v i n s ;

m b i n s = R ins ' * ( m ned / norm ( m ned ) ) ;


y i n s = [ p i n s ; v i n s ; f b i n s ; m b i n s ] ;

ag param = 2 ; %gi b b s p a r a m e t r i z a t i o n
a g = ag param * q i n s ( 2 : 4 ) / q i n s ( 1 ) ;

A = [ Z3 I3 Z3 Z3 Z3
Z3 Z3 -R i n s * Smtrx ( f b im u - b i n s a c c ) Z3 -R i n s
Z3 Z3 -Smtrx ( w b nb - b i n s a r s ) -I3 Z3
Z3 Z3 Z3 -I3 / T ars Z3
Z3 Z3 Z3 Z3 -I3 / Tacc ] ;

E = [ Z3 Z3 Z3 Z3
-R i n s Z3 Z3 Z3 %w acc
Z3 -I3 Z3 Z3 %w ars
Z3 Z3 I3 Z3 %a r s b i a s ( n o i s e )
Z3 Z3 Z3 I3 ] ; %a c c b i a s ( n o i s e


H = [ I3 Z3 Z3 Z3 Z3
Z3 I3 Z3 Z3 Z3
Z3 Z3 Smtrx ( f b i n s ) Z3 Z3
Z3 Z3 Smtrx ( m b i n s ) Z3 Z3 ] ;


%uncomment f o r method 2
% H = [ I3 Z3 Z3 Z3 Z3
% Z3 I3 Z3 Z3 Z3
% Z3 Z3 Smtrx ( Smtrx ( w b nb - b i n s a r s ) * R ins ' * v n n b ) Z3 Z3
% Z3 Z3 Smtrx ( m b i n s ) Z3 Z3 ] ;

% D i s cr e t e -tim e model
Ad = eye ( 1 5) + h * A;
Ed = h * E ;

dy = y - y i n s ;


%% KF u p d at e
% KF g ai n
K = P h a t * H' / (H * P h a t * H' + R) ;

% new x h a t
x e s t = K * dy ;
% ----------
p e s t = x e s t ( 1 : 3 ) ;
v e s t = x e s t ( 4 : 6 ) ;
a g e s t = x e s t ( 7 : 9 ) ;
q e s t = 1 / s q r t ( ag param ^2 + a g e s t '* a g e s t ) *[ ag param a g e s t ' ] ' ;

b i n s a r s e s t = x e s t ( 1 0 : 1 2 ) ;
b i n s a c c e s t = x e s t ( 1 3 : 1 5 ) ;
% ----------

% C o v ari a n c e u p d at e
P h a t = ( eye ( 1 5)-K*H) * P h a t * ( eye ( 1 5) - K*H) ' + K*R*K' ;
P h a t = ( P h a t + P h at ' ) / 2 ;


% C o v ari a n c e p r e d i c t o r ( k +1)
P h a t = Ad * P h a t * Ad' + Ed * Q * Ed ' ;


e r r = [ p e s t ; v e s t ; q e s t ; b i n s a r s e s t ; b i n s a c c e s t ] ;
```

Appendix-2: INS equations

```
function yins = INSequations(yins, yimu, err, INSinit)
% ------------------------------------------------------------------------
% Inertial Navigation System (INS) equations
%
% Input:
% yins - INS estimates
% yimu - IMU measurements
% err - error from MEKF
% yins - measurements from INS
% INSinit - INS initialization
%
% Output:
% yins - INS estimates
%
% Author: Henning Ward
% Date: May 2019
% ------------------------------------------------------------------------

%%

vb = zeros(3,1);
yinit = zeros(15,1);
yins = yins + yinit;
errinit = zeros(16,1);
err = err + errinit;
h = INSinit.h;

persistent insinitprevErr

%initialization
if isempty(insinit)

newMeasurement = false;
insinit = yins;
vb = insinit(4:6);
err = zeros(16,1);
err(7) = 1;
yins = INSinit.xins;
yins(10:15) = 0.000001;
prevErr = err;

else
newMeasurement = false;
if err(7) < 0.001
err(7) = 1; %quaternioninitializationq0 = [1000]
end

if(prevErr ~= err)
newMeasurement = true;
end
prevErr = err;

fbimu = yimu(1:3);
wbnb = yimu(4:6);

xdotins = zeros(15,1);

pins = yins(1:3);
vins = yins(4:6);
epsins = yins(7:9);
qins = eps2q(epsins);
%qinsnormalizationtopreventnumericalerrors
qins = qins/norm(qins);
binsars = yins(10:12);
binsacc = yins(13:15);
Rins = Rquat(qins);


fnimu = Rins*fbimu;

```

```
if(newMeasurement)
%% Move error and reset
pins=pins+err(1:3);
vins=vins+err(4:6);
qins=quatmultiply(qins',err(7:10)')';
qins=qins/norm(qins);
binsars=binsars+err(11:13);
binsacc=binsacc+err(14:16);
yins=[pins;vins;qins(2:4);binsars;binsacc];
end

%% Strapdown INS equations
xdotins(1:3)=yins(4:6);
xdotins(4:6)=fnimu-Rins*binsacc;
qinsdot=0.5*quatmultiply(qins',[0;wbnb-binsars]');
xdotins(7:9)=qinsdot(2:4);
xdotins(10:12)=0;
xdotins(13:15)=0;

yins=yins+h*xdotins;
end

yins=yins;
```

Appendix-3: *fins* Estimation

```
function fnins = KFfins(GPS, KFfinit)
% ------------------------------------------------
% KF differentiator for fins reference calculatio
%
% Input:
% GPS - GPS measurements
% KFinit - Initparameters
%
% Output:
% fnins - finsestimation
%
%
% Author : Henning Ward
% Date : May 2019
% ------------------------------------------------

%%

m2feet = 1/0.3048;
persistent RQPhatI3Z3xhatg

fnins = zeros(3,1); %memory allocation

p_meas = GPS(1:3);
v_meas = GPS(4:6);
h = KFfinit.h;

%initialization
if isempty(R)
Z3 = zeros(3);
I3 = eye(3);
g = 9.81 * m2feet;
x_hat = KFfinit.x_hat;

P_hat = KFfinit.P_hat;
Q = KFfinit.Q;
R = KFfinit.R;

else


% Error model
A = [ Z3 I3 Z3
Z3 Z3 I3
Z3 Z3 Z3 ];

B = [zeros(1,5) ones(1,1) zeros(1,3)]'

E = [ I3 Z3 Z3
Z3 I3 Z3
Z3 Z3 I3 ];

C = [ I3 Z3 Z3

Z3 I3 Z3 ];
%%

% Discrete-time model
Ad = eye(9) + h*A;
Ed = h*E;

% Measurements
y = [p_meas; v_meas];

% KF gain
K = P_hat*C'/(C*P_hat*C' + R);

% corrector
x_hat = x_hat + K*(y - C*x_hat);
P_hat = (eye(9)-K*C)*P_hat*(eye(9) - K*C)' + K*R*K';
P_hat = (P_hat + P_hat')/2;

```

```
73 x h at = Ad * x h at + h * B * g ;
74
75 P h a t = Ad * P h a t * Ad' + Ed * Q * Ed ' ;
76
77 end
78 f n i n s = x h at ( 7 : 9 ) ;
```

Appendix-4: Target tracking KF

```
function xhat = targettrackingKF(dP, aI, TKF)
% ------------------------------------------------------------------------
% KF for target tracking
%
% Input:
% dp - relative position measurement
% aI - Intercept or acceleration measurement from INS
% TKF - TKF init
% T - Threat/Target states
%
% Output:
% xhat - Threat/Target estimated states
%
% Notes:
% Because of high values for acceleration, the position estimate tends to
% drift if sample time is too low.
%
% Author: Henning Ward
% Date: May 2019
% ------------------------------------------------------------------------

%%

h = TKF.h;
Z3 = zeros(3);
I3 = eye(3);

persistent R Q Phat xhat

% initialization
if isempty(R)
xhat = TKF.xhat;
P hat = TKF.Phat;
Q = TKF.Q;
R = TKF.R;

else

% Error model
A = [Z3 I3 Z3
Z3 Z3 I3
Z3 Z3 Z3];

B = [zeros(3,3) -eye(3) zeros(3,3)]';

E = [Z3 Z3 I3]';

C = [I3 Z3 Z3];

% Discrete-time model
Ad = eye(9) + h*A;
Ad(1,3) = 0.5*h^2;
Ed = h*E;

% Measurements
y = dP;

% KF gain
K = Phat*C'/(C*Phat*C' + R);

% corrector
xhat = xhat + K*(y - C*xhat);
Phat = (eye(9)-K*C)*Phat*(eye(9) - K*C)' + K*R*K';
Phat = (Phat + Phat')/2;

xhat = Ad*xhat + h*B*aI;

Phat = Ad*Phat*Ad' + Ed*Q*Ed';

end

xhat = xhat;
```

Appendix-5: LOS guidance law

```
function [chi, gamma, tgo] = LOSGuidance(xhat, T, yrb)
% ------------------------------------------------------------------------
% LOS guidance law
%
% Input:
% xhat - Interceptor/Threat relative state estimates
% T - Threat position, velocity and acceleration
% yrb - Rigid body states
%
% Output:
% chi - Course angle
% gamma - flight path angle
% tgo - time-to-go
%
% Author: Henning Ward
% Date: May 2019
% ------------------------------------------------------------------------

%%

persistent initfunc

%initialization
if isempty(initfunc)
initfunc = true;
chi = 0;
gamma = 0;
tgo = 0;
else

%position threat
pT = T(1:3);
vT = T(4:6);

%position interceptor
pI = yrb(19:21);
vI = yrb(16:18);

%position Launcher
pL = [0 0 0]';

pR = xhat(1:3);
vR = xhat(4:6);
tgo = -(pR'*vR)/(vR'*vR);

vT = vI + vR;
pT = pT + vT*tgo;

%distance between launch platform and interceptor
RLI = norm(pI - pL);

%angle between horizontal plane and interceptor
gammaNI = asin(pI(3)/RLI);

%angle between NORTH and interceptor
chiNI = atan2(pI(2) - pL(2), pI(1) - pL(1));
%angEM = atan2(pM(2) - pL(2), pM(1) - pL(1));

%distance between launch platform and threat
RLT = norm(pT - pL);

%angle between horizontal plane and threat
gammaNT = asin((pT(3) -pL(3))/RLT);

%angle between NORTH and threat
chiNT = atan2(pT(2) - pL(2), pT(1) - pL(1));
%theta = atan2(pT(2) - pL(2), pT(1) - pL(1));

%% COURSE (horizontal)
%angle between interceptor and threat horizontal plane
thetah = chiNT - chiNI;
%distance between launch platform and interceptor in horizontal plane
```

```
RLIh = cos ( gammaNI ) * RLI ;
eh = s i n ( t h e t a h ) * RLIh ;
rh = s q r t ( RLIh^2-eh ^ 2 ) ;
Rit h = cos ( gammaNI ) * abs ( norm ( pT ( 1 : 2 )-pI ( 1 : 2 ) ) ) ;
kh = 0 . 9 ;

ahdh = s q r t ( abs ( Rit h ^2-eh ^ 2 ) ) ;
d i s t h = rh + kh * ahdh ;
xc = cos ( chiNT ) * d i s t h ;
yc = s i n ( chiNT ) * d i s t h ;
c h i = at a n 2 ( yc - pI ( 2 ) , xc - pI ( 1 ) ) ;

%% AoA ( v e r t i c a l , North /-Down)
aITv = gammaNI - gammaNT ;
%d i s t a n c e between l a u n c h p l a t f o rm and i n t e r c e p t o r i n v e r i c a l pl a n e
RLIv = cos ( chiNI ) * RLI ;
ev = s i n ( aITv ) * RLIv ;
rv = s q r t ( RLIv^2-ev ^ 2 ) ;
Rit v = abs ( norm ( pT ( 1 : 2 : 3 )-pI ( 1 : 2 : 3 ) ) ) ;
kv = 0 . 9 ;

ahdv = s q r t ( abs ( Rit v ^2-ev ^ 2 ) ) ;
d i s t v = rv + kv * ahdv ;
zc = s i n (gammaNT) * d i s t v ;
gamma = -at a n 2 ( zc - pI ( 3 ) , xc - pI ( 1 ) ) ;
end
```

RESUME

Alfateh MOKHTAR AHMED

EDUCATION:

Bachelor Degree

- PHYSICS SCIENCE – Omdurman Islamic University, Sudan (2009-2011).
- International University of Sarajevo, BACHELOR OF SCIENCE IN ELECTRICAL AND ELECTRONICS ENGINEERING – 2017.

MASTER Degree

- İstanbul aydin University, MASTER OF SCIENCE IN ELECTRICAL AND ELECTRONICS ENGINEERING – Aydin University-2022.

CERTIFICATES:

- FUTURE PROTECTORS PROGRAM – Dubai Police General Command,WHO,UN&Right Start Foundation 2006.
- PR AND PROTOCO – Ministry of Interior Sudan, Sudan Police - 2009.
- ENGLISH LANGUAGE SCHOOL ELS – International University of Sarajevo -2014.
- CERTIFICATE IN ENTREPRENEURSHIP – USAID (Sarajevo)- 2015.
- LEADERSHIP – Scouting and Guiding Federation of Turkey (Sarajevo)- 2015.
- LEADERSHIP TRAINING CAMP – Federation of International Student Associations UDEF (Sarajevo) -2017.
- TURKISH LANGUAGE – Fatih Sultan Mehmet Vakıf Üniversitesi – 2018.

PROFESSIONAL EXPERIENCE AND AWARDS:

- DIRECTOR OF TRAINING, IN PUBLIC RELATIONS AND MEDIA OFFICE – LIFE MAKERS ORGANIZATION – 2010, Khartoum, Sudan.
- DIRECTOR OF IR OFFICE – ENVIRONMENT AND SOCIETY SAFETY ORGANIZATION – 2011 , Khartoum, Sudan.
- ELECTRICAL ENGINEERING INTERN – BH TELECOM – 2016.
- ELECTRICAL ENGINEERING INTERN – YESARI GROUP SARAJEVO – 2016.
- COMPUTER EQUIPMENT OPERATOR,COMPUTER PROGRAMBLE – HASSANEIN GROUP – 2016 Khartoum, Sudan.

LANGUAGES:

- **Arabic native.**
- **Turkish.**
- **English.**
- **Bosnian.**
- **Serbian.**